

Molecular and Functional Changes of Dorsal Root Ganglion Neurons in a Rodent Model
of Intervertebral Disc Degeneration

by

Elizabeth Marie Leimer

Department of Biomedical Engineering
Duke University

Date: November 10, 2017

Approved:

Lori A. Setton, Supervisor

Cameron R. 'Dale' Bass, Chair

Jun Chen

Farshid Guilak

Samuel B. Adams

Dissertation submitted in partial fulfillment of
the requirements for the degree of Doctor
of Philosophy in the Department of
Biomedical Engineering in the Graduate School
of Duke University

2017

ABSTRACT

Molecular and Functional Changes of Dorsal Root Ganglion Neurons in a Rodent Model
of Intervertebral Disc Degeneration

by

Elizabeth Marie Leimer

Department of Biomedical Engineering
Duke University

Date: November 10, 2017

Approved:

Lori A. Setton, Supervisor

Cameron R. 'Dale' Bass, Chair

Jun Chen

Farshid Guilak

Samuel B. Adams

Dissertation submitted in partial fulfillment of
the requirements for the degree of Doctor
of Philosophy in the Department of
Biomedical Engineering in the Graduate School
of Duke University

2017

Copyright by
Elizabeth Marie Leimer
2017

Abstract

Low back pain affects up to 85% of the population in their lifetime and is strongly associated with degeneration of the intervertebral disc (IVD). Surgical lumbar disc puncture (LDP) in rodents is a widely used model of IVD degeneration due to the development of morphologic changes and evidence of altered pain-related functional measures. LDP models of IVD degeneration also show molecular changes in the dorsal root ganglia (DRGs) at less than 9 weeks post-injury, including alterations to markers of nerve growth factor (NGF)-dependent neurons. Lumbar disc puncture-induced inflammation can lead to local release of NGF, which acts on NGF receptors (TrkA, p75NTR) on the central terminals of DRG neurons innervating the IVD to play a role in pain development. TRPV1 function can be potentiated through NGF binding to these receptors, a mechanism often assessed in vitro via capsaicin challenge. The goal of this dissertation was to develop and characterize a surgical model of painful IVD degeneration in the rat, including a behavioral phenotype as well as NGF-related molecular and functional DRG neuron changes.

In the first part of this dissertation, the L5-L6 IVD in rats was surgically punctured and the behavioral phenotype was characterized until post-operative week 20 to assess development of discogenic pain. Secondly, capsaicin challenge experiments were performed in vitro to examine the functional implications of an NGF-related

mechanism in discogenic pain. Finally, IVD degeneration was confirmed and immunostaining for NGF receptors was done to further investigate the involvement of NGF-related molecular mechanisms in painful IVD degeneration.

Findings revealed a timeline of pain-related behavioral changes, with evidence of LDP-related behavioral and gait changes at 16-18 weeks post-surgery. Additionally, this model produced a phenotype of clinically relevant, bilateral behavioral changes, including decreased overall activity as well as decreased hind limb stride frequency. Finally, DRG neurons showed NGF-related molecular and functional differences 20 weeks post-surgery. Ipsilateral DRG neurons showed impaired functionality of TRPV1 receptors and impaired TRPV1 receptor insertion into the cell membrane, as well as increased p75NTR expression. Contralateral neurons showed impaired TRPV1 functionality only.

The studies in this dissertation support involvement of an NGF-related mechanism in painful IVD degeneration and establish the importance of utilizing a clinically relevant and longer-term model of IVD degeneration to investigate the specific mechanisms of pain generation.

Contents

Abstract	iv
List of Tables	xi
List of Figures	xiii
List of Equations.....	iv
List of Acronyms	v
Acknowledgements	iv
1. Introduction	1
1.1 Intervertebral Disc Neuroanatomy and Physiology	4
1.1.1 Innervation of the Healthy Rat Intervertebral Disc	5
1.1.1.1 Dual Innervation	5
1.1.1.2 Bilateral and Multisegmental Innervation.....	6
1.1.1.3 Innervation of Ventral, Lateral, and Dorsal Aspects of the IVD	7
1.2 Nociceptive Afferent DRG Neurons.....	9
1.2.1 Electrophysiological Differences	11
1.3 Intervertebral Disc Degeneration	12
1.3.1 Morphologic and Biochemical Changes.....	12
1.3.2 Inflammation.....	13
1.3.2.1 Nerve Growth Factor and Inflammation.....	15
1.3.2.2 Brain-Derived Neurotrophic Factor and Inflammation	18
1.3.2.3 Neurotrophins in Degenerate Intervertebral Discs.....	18

1.3.3 Nerve Ingrowth	18
2. In Vivo IVD Degeneration Model Development and Characterization.....	20
2.1 Introduction.....	20
2.1.1 Pain-Related Functional and Behavioral Measures.....	23
2.1.1.1 Operant Activities.....	23
2.1.1.2 Weight-Bearing and Gait	26
2.1.1.3 Mechanical Sensitivity.....	28
2.1.1.4 Pressure Hyperalgesia.....	29
2.1.1.5 Thermal Sensitivity	29
2.1.2 Objective	30
2.2 Materials and Methods	30
2.2.1 Baseline Behavioral and Functional Measures.....	30
2.2.1.1 Open Field Arena.....	31
2.2.1.2 Burrowing	34
2.2.1.3 Static Weight-Bearing/Incapacitance.....	35
2.2.1.4 Pressure Hyperalgesia (SMALGO)	35
2.2.1.5 Treadmill Gait.....	36
2.2.1.6 Pain Tolerance on Lateral Bending Maze	36
2.2.2 Surgical Model to Induce IVD Degeneration	37
2.2.3 Post-Surgical Functional and Behavioral Assessments.....	38
2.2.4 Data Analysis	39
2.2.4.1 Timeline of Model Development.....	39

2.2.4.2	Longitudinal Behavioral Differences in Naïve Animals	39
2.2.4.3	Differences Between Sham and LDP Groups	39
2.3	Results	40
2.3.1	Timeline of Model Development	40
2.3.2	Longitudinal Behavioral Differences in Naïve Animals.....	43
2.3.3	Differences Between Sham and LDP Groups.....	44
2.3.4	Effect Size Calculation	47
2.4	Discussion.....	47
2.5	Conclusion.....	50
3.	Effects of IVD Degeneration on DRG Neuron Function In Vitro.....	51
3.1	Introduction.....	51
3.1.1	Objective	54
3.2	Materials and Methods.....	54
3.2.1	Euthanasia, Exsanguination, and Perfusion.....	54
3.2.2	Tissue Harvesting and Processing	54
3.2.2.1	Tissue Harvesting	54
3.2.3	DRG Cell Isolation.....	57
3.2.4	Calcium Imaging	57
3.2.4.1	Experimental Set-Up.....	57
3.2.4.2	Experimental Protocol.....	60
3.2.5	Data Analysis	61
3.2.5.1	Determination of Responsive Neurons.....	61

3.2.5.2	Neurons Responsive to Both CAP1 and CAP2.....	63
3.2.5.3	Positive Responses to Only the Second Application of Capsaicin.....	63
3.2.5.4	CAP2/CAP1 Ratio	64
3.3	Results	65
3.3.1	Effect Size Calculation.....	74
3.4	Discussion.....	74
3.5	Conclusion.....	78
4.	Characterization of IVD and DRG Changes in IVD Degeneration Model	79
4.1	Introduction.....	79
4.1.1	Objective	81
4.2	Materials and Methods	81
4.2.1	Euthanasia, Exsanguination, and Perfusion.....	81
4.2.2	Tissue Harvesting and Processing	82
4.2.2.1	Tissue Harvesting	82
4.2.2.2	Tissue Processing	82
4.2.3	Histology & Immunohistochemistry	83
4.2.3.1	L5-L6 IVD Histology	83
4.2.3.2	DRG Immunohistochemistry	83
4.2.4	Data Analysis	85
4.2.4.1	L5-L6 IVD Histology	85
4.2.4.2	Correlations Between Pain-Related Behavioral Changes and Histology ..	86
4.2.4.3	DRG Immunohistochemistry	87

4.3 Results	92
4.3.1 L5-L6 IVD Histology	92
4.3.1.1 Effect Size Calculation.....	93
4.3.2 Correlations of Histology and Immunohistochemistry Parameters to Pain-Related Assessments.....	93
4.3.3 DRG Immunohistochemistry.....	94
4.3.3.1 Bilateral L1 DRGs.....	94
4.3.3.2 Bilateral L2 DRGs.....	99
4.4 Discussion.....	113
4.5 Conclusion.....	120
5. Conclusion and Future Directions.....	122
5.1 Conclusion.....	122
5.2 Future Directions.....	124
References	129
Biography.....	147

List of Tables

Table 1: Acclimatation to Investigator Handling.....	31
Table 2: Equipment Acclimation Protocol.....	33
Table 3: Left versus Right-Independent Functional and Behavioral Assessments.....	34
Table 4: Left versus Right Functional and Behavioral Assessments.....	34
Table 5: Behavioral Assessment Effect Sizes.....	47
Table 6: Calcium Imaging Results.....	67
Table 7: Comparison of CAP1-Responsive Neurons to that of Prior Studies.....	69
Table 8: CAP2/CAP1 Ratio Effect Size.....	74
Table 9: IHC Targets for L1 DRGs.....	84
Table 10: IHC Targets for L2 DRGs.....	85
Table 11: IVD Histology Grading Criteria. Modified from Tam and co-workers [174]....	86
Table 12: Assessments and Critical Values Used for Correlation Analysis.....	87
Table 13: Grade of IVD Degeneration Effect Size.....	93
Table 14: Spearman’s Correlation Coefficients for Comparisons Between Behavioral and Histologic Changes.....	94
Table 15: TrkA CTCF Z-Statistic and Effect Size.....	96
Table 16: p75NTR CTCF Z-Statistic and Effect Size.....	99
Table 17: Number of TRPV1+ cells.....	102
Table 18: TRPV1 CTCF Z-Statistic and Effect Size.....	105
Table 19: Maximum Diameter for PGP9.5+ Cells.....	107
Table 20: Effect Size of Maximum Diameter for PGP9.5+ Cells.....	107

Table 21: Maximum Diameter for TRPV1+ Cells.....	110
Table 22: Effect Size of Maximum Diameter for TRPV1+ Cells.....	110
Table 23: Percentage of TRPV1+ Area with Effect Sizes.....	113

List of Figures

Figure 1: An anterior-posterior schematic of spinal neuroanatomy.....	5
Figure 2: Dual innervation of the sensory pathways from the dorsal portion of the rat L5-L6 IVD.....	8
Figure 3: Nociceptive afferent small myelinated A δ and unmyelinated C fibers innervate the outer AF in non-pathologic IVDs.....	10
Figure 4: A schematic depicting possible mechanisms of discogenic pain.	14
Figure 5: NGF binding to TrkA activates many pathways related to cell survival (left). NGF binding to p75NTR can activate pathways associated with cell survival or apoptosis (right).	17
Figure 6: Pain Tolerance on Lateral Bending Maze.	26
Figure 7: An in vivo model of lumbar radiculopathy showed decreased unilateral weight-bearing on the affected limb compared to the contralateral limb.	27
Figure 8: Surgical procedure to visualize the L5-L6 IVD.	38
Figure 9: Timeline of functional and behavioral measures from baseline to post-operative week 20, including pressure hyperalgesia (A), burrowing (B), and treadmill gait (C,D).	42
Figure 10: Functional and behavioral measures for Naïve rats over 20 weeks, including open field arena (A), static weight-bearing (B), burrowing (C), pressure hyperalgesia (D), and treadmill gait (E,F).	44
Figure 11: Percent time spent traveling in 30 minutes over 20 weeks for Sham and LDP rats.....	45
Figure 12: Functional and behavioral measures for Sham and LDP rats over 20 weeks, including treadmill gait (A,E,F), static weight-bearing (B), burrowing (C), and pressure hyperalgesia (D).	46
Figure 13: Pain tolerance on lateral bending maze for Naïve rats (A) and Sham and LDP rats (B) over 20 weeks.....	47

Figure 14: Selected mechanisms of NGF-mediated activation of TRPV1 via TrkA.	53
Figure 15: Dorsal view of spine during tissue harvest procedure.	56
Figure 16: Calcium imaging recording view.	59
Figure 17: A recording of 1 individual neuron that returned to baseline after every stimulus.	61
Figure 18: Percentage of neurons responsive to application of CAP1.	66
Figure 19: Percentage of L1 and L2 DRG neurons responsive to both applications of capsaicin (A, B) and CAP2 only (C, D) during the low capsaicin dose (100 nM) NGF potentiation protocol.	71
Figure 20: L1 and L2 DRG neuron CAP2/CAP1 ratios (A, B) and the percentage of neurons with a CAP2/CAP1 ratio greater than 1 (C, D) during the low capsaicin dose (100 nM) NGF potentiation protocol.	73
Figure 21: Image processing using ImageJ.	88
Figure 22: Safranin-O/Fast Green histology stain for IVD grade of degeneration 20 weeks post-surgery.	92
Figure 23: Histologic grades of L5-L6 IVD degeneration at 20 weeks post-surgery.	93
Figure 24: Bilateral L1 DRG sections immunostained for TrkA.	95
Figure 25: Corrected total cell fluorescence z-scores of TrkA staining for ipsilateral (A) and contralateral (B) L1 DRG neurons.	96
Figure 26: Bilateral L1 DRG sections immunostained for p75NTR.	98
Figure 27: Corrected total cell fluorescence z-scores of p75NTR staining for ipsilateral (A) and contralateral (B) L1 DRG neurons.	99
Figure 28: DRG neuron counts.	101
Figure 29: Ipsilateral L2 DRG neurons co-stained for PGP9.5 and TRPV1.	103
Figure 30: Contralateral L2 DRG neurons co-stained for PGP9.5 and TRPV1.	104

Figure 31: Corrected total cell fluorescence z-scores of TRPV1 staining for ipsilateral (A) and contralateral (B) L2 DRG neurons.....	105
Figure 32: Maximum diameter of PGP9.5+ cells of the ipsilateral (A) and contralateral (B) L2 DRGs.	106
Figure 33: Maximum diameter of the ipsilateral (A) and contralateral (B) TRPV1+ cells. Neuronal size distribution of ipsilateral and contralateral Sham (C, E) and LDP (D, F) TRPV1+ and TRPV1- cells.....	109
Figure 34: Percentage of TRPV1+ Area in L2 DRG neurons.	112

List of Equations

Equation 1: $d = (x_1 - x_2)/\sigma$	40
Equation 2: $[(Maximum\ response / Average\ Baseline) - 1] * 100 = PR$	61
Equation 3: $PR_{CAP2} / PR_{CAP1} = CAP2 / CAP1\ Ratio$	64
Equation 4: $CTCF = (I_{cytoplasm} - I_{background}) * (area_{cytoplasm})$	89
Equation 5: $Z = (CTCF - Mean\ CTCF) / SD$	89

List of Acronyms

AF: anulus fibrosis

ALL: anterior longitudinal ligament

AP: action potential

BDNF: brain-derived neurotrophic factor

BSA: bovine serum albumin

CAP1: first application of capsaicin in NGF potentiation protocol

CAP2: second application of capsaicin in NGF potentiation protocol

CGRP: calcitonin gene-related peptide

CSF1: macrophage colony-stimulating factor 1

CTCF: corrected total cell fluorescence

DEG/ENaC: degenerin/epithelial sodium channel

DiI: 1,1'-Diocadecyl-3,3',3'-Tetramethylindocarbocyanine Perchlorate (DiIC₁₈(3))

DRG: dorsal root ganglion

ERK: extracellular signal-regulated kinase

FG: fluoro-gold

FGFR3: fibroblast growth factor receptor 3

FLU: fluorescence unit

GAP43: growth-associated protein 43

GDNF: glial cell line-derived neurotrophic factor

GFR α 1: GDNF family receptor alpha-1

GFR α 3: GDNF family receptor alpha-3

HBSS: Hank's buffered saline solution

HEPES: 4-(2-hydroxyethyl)-1-piperazineethanesulfonic acid

IB4: isolectin B4

IGF1: insulin-like growth factor 1

IL-1 β : interleukin 1 beta

IL-6: interleukin 6

IP3: phosphoinositide-3 kinase

IVD: intervertebral disc

LDP: lumbar disc puncture

MAPK: mitogen-activated protein kinase

NF- κ B: nuclear factor kappa beta

NGF: nerve growth factor

NP: nucleus pulposus

NPY: neuropeptide Y

OA: osteoarthritis

P2X3: P2 purinoceptor 3

p75NTR: p75 neurotrophin receptor

PBS: phosphate buffered saline

PFA: paraformaldehyde

PGP9.5: protein gene product 9.5

PI: propidium iodide

PIP₂: phosphatidylinositol-4,5-bisphosphate

PKA: protein kinase A

PKC γ : protein kinase C gamma

PLC γ : phospholipase C gamma

PLL: posterior longitudinal ligament

PR: percentage response

PST: paravertebral sympathetic trunk

RC: ramus communicans

Ret: receptor tyrosine kinase

ROI: region of interest

SD: standard deviation

SEM: standard error of the mean

SMALGO: small animal algometer

SP: substance P

sTNFR_{II}: soluble tumor necrosis factor receptor type II

SVN: sinuvertebral nerve

TNF- α : tumor necrosis factor-alpha

TrkA: tyrosine kinase A

TrkB: tyrosine kinase B

TrkC: tyrosine kinase C

TRPV1: transient receptor potential cation channel subfamily vanilloid member 1

VB: vertebral body

VR1: vanilloid receptor 1

Acknowledgements

This dissertation would not have been possible without help from mentors, students, and staff at Washington University in St. Louis, where this work was completed. I would like to thank Lori Setton, PhD for her mentorship and guidance during my time in the lab, and for the unique opportunity to help her set up a new research program and laboratory. I appreciate all the time and energy she has spent challenging me to become a better scientist and researcher, for her unwavering support, and for allowing me to follow the data and delve into new areas of research for the laboratory.

I would also like to thank my committee members, Cameron 'Dale' Bass, PhD, Jun Chen, PhD, Farshid Guilak, PhD, and Samuel Adams, MD, for their guidance and encouragement. I would especially like to thank Dr. Adams for allowing me to help with his research, which has given me a strong background in both statistics and metabolomics, as well as his support during my final semester at Duke University. I would also like to thank Dr. Bass for agreeing to chair my dissertation committee, and especially for providing a surrogate laboratory during my final semester at Duke University.

I am also very grateful for the people who made scientific contributions to this dissertation, including Munish Gupta, MD, Liufang Jing, MS, Matthew Gayoso, and Simon Tang, PhD. I would especially like to thank Dr. Gupta in the Department of

Orthopaedic Surgery for his substantial contributions to developing the surgical model and for ensuring that this research maintained translational value. I am very thankful for all of the hard work and support provided by Liufang, including immunostaining and microscopy, without which this dissertation would not have been possible. Matthew was a wonderful undergraduate student on this project and I am grateful for his curious attitude and motivation to learn, as well as all the hard work he has put into this research from the very beginning.

I would also like to acknowledge Lisa McIlvried, PhD in the Department of Anesthesia for taking the time to teach me neuron cell culture and calcium imaging techniques, as well as for experimental suggestions and challenging me to investigate further. Nisha Iyer, PhD in the Department of Biomedical Engineering taught me many techniques that I used to preserve neuronal architecture for work included in this dissertation, for which I am grateful. I have also had the privilege to work with wonderful personnel in the Department of Comparative Medicine. None of this work would have been possible without the veterinary support and guidance provided by Tammie Keadle, DVM, PhD, Jenny Kalishman, DVM, MS, Nicole Semanik, RVT, and Daniel Piatchek.

Many additional current and former Setton Lab members also provided encouragement and support throughout this process, including Bailey Fearing, PhD,

Laura Tanenbaum, PhD, Priscilla Hwang, PhD, Devin Bridgen, PhD, Timothy Mwangi, PhD, and Jing Han, MD, who provided ample expertise, support, and advice.

Finally, I would like to thank my friends and family for their support and encouragement throughout this process, especially my parents, Paul and Joy, my brother and sister, Brian and Andrea, and my husband, Nate.

1. Introduction

The estimated annual occurrence of chronic low back pain in the United States is 5-20% [1] and low back pain affects up to 85% of the population in their lifetime [2]. Low back pain is the leading cause of disability worldwide and accounts for nearly 50% of the musculoskeletal burden of disease [3]. Patients living with low back pain experience a decreased ability to perform activities of daily living and a deteriorating quality of life [1]. Low back pain contributes to a substantial portion of the cost of health care in the United States and worldwide [4], with estimated direct costs of \$12 to \$90 billion [5, 6] and indirect costs of \$7 to \$28 billion [7, 8] in the United States annually. The etiology of low back pain remains unclear, but it is associated with degeneration of the intervertebral disc (IVD) in 40% of cases [9, 10]. Degenerative changes result in altered disc height and biomechanics of the entire spinal column, possibly leading to low back pain and may occur over time either due to an injury or naturally increasing age. The incidence of IVD degeneration and associated pathologies such as spinal stenosis continue to rise as the aged population increases in the United States and worldwide [11].

Clinical low back pain can be divided into three categories based on the timeline of symptoms: acute (less than 4 weeks), subacute (4-12 weeks), and chronic (longer than 12 weeks) [12]. Available treatments for IVD degeneration and low back pain overall

continue to be aimed at managing symptoms such as pain, and include conservative pharmacotherapy such as muscle relaxants, local delivery of corticosteroids, local anesthetics, manipulation therapy, and surgical treatments such as discectomy and spinal fusion [11]. These solutions may provide short-term relief from acute pain, but all fall short of managing chronic low back pain and in some cases lead to further complications. A better understanding of the key mediators of painful IVD degeneration will lead to more targeted and effective therapeutic treatments to help this category of patients better manage their low back pain.

IVD degeneration is characterized by decreased water content, decreased cellularity, loss of proteoglycans, and increased matrix fibrosis [11, 13-16] (section 1.3.1). These changes also occur with natural aging, yet many people are asymptomatic. Painful IVD degeneration can be due to loss of disc height or osteophyte formation, which can cause nerve root impingement and subsequent unilateral or bilateral radiating pain. Another cause of painful disc degeneration could be sensory afferent nerve fiber growth into the IVD after injury-induced inflammation (section 1.3.3). As healthy IVDs are both avascular and aneural, the latter etiology could result in discogenic pain, defined as pain originating from chemically or mechanically damaged IVDs due to irritation of innervating nerves [17].

Inflammation after IVD injury increases expression of nerve growth factor (NGF), which promotes axonal growth of small nociceptive NGF-sensitive dorsal root ganglia (DRG) neurons [18] (section 1.3.3). NGF binding to the high-affinity NGF receptor tyrosine kinase A (TrkA) or the low-affinity NGF receptor p75 neurotrophin receptor (p75NTR) on sensory afferent neurons initiates signal transduction pathways which promote survival or lead to expression of additional pro-inflammatory cytokines [19, 20] (section 1.3.2; Figure 6), providing a possible mechanism for progression toward chronic low back pain.

This objective of this work was to determine the role of elevated NGF in painful IVD degeneration through molecular and functional changes to the DRG neurons over long periods of exposure to degenerative changes in the IVD. Our central hypothesis was that upregulation of NGF in the degenerate IVD leads to elevated expression of TrkA and p75NTR in neurons of innervating DRGs, which is associated with pain-related behaviors. In the studies presented here, an *in vivo* surgical model of painful IVD degeneration was developed and characterized (Chapter 2). Female Sprague-Dawley rats were chosen because of the vast number of functional and behavioral assessments available for rats, and also for their size, which facilitated the surgical procedure and satisfied limitations on use of behavioral testing equipment. It was important for the rats to be skeletally mature at the beginning of the study and still fit

the size limitations of the behavioral equipment 22 weeks later at the end of the study. After this time period, studies were done to determine grade of IVD degeneration and molecular changes to DRG neurons (Chapter 3). Additionally, studies were conducted with primary DRG cell isolates to determine changes in sensitization to NGF after long periods of exposure to degenerative changes in the IVD (Chapter 4).

1.1 Intervertebral Disc Neuroanatomy and Physiology

The adult human IVD is largely aneural. In the non-pathologic disc, innervation is limited to the outer three to four lamellae of the anulus fibrosus (AF) [21, 22] via branches from the sinuvertebral nerves [23, 24], ventral rami, or gray rami communicantes [23], which transmit neuronal signals between the DRGs of the peripheral nervous system and sympathetic chain ganglia of the autonomic nervous system as shown in Figure 1. The DRG contains cell bodies of sensory afferent neurons, which transmit sensory information from terminal organ sensory receptors such as proprioceptors and nociceptors to the dorsal horn of the spinal cord [25]. The sympathetic trunk lies retroperitoneally on the anterolateral surface of the vertebrae and transmits information between levels of the spine. It stretches from the T1 to L2 vertebral levels in humans, and the rat sympathetic trunk stretches from the superior cervical ganglion near the common carotid artery to the sacral level of the spine [26, 27].

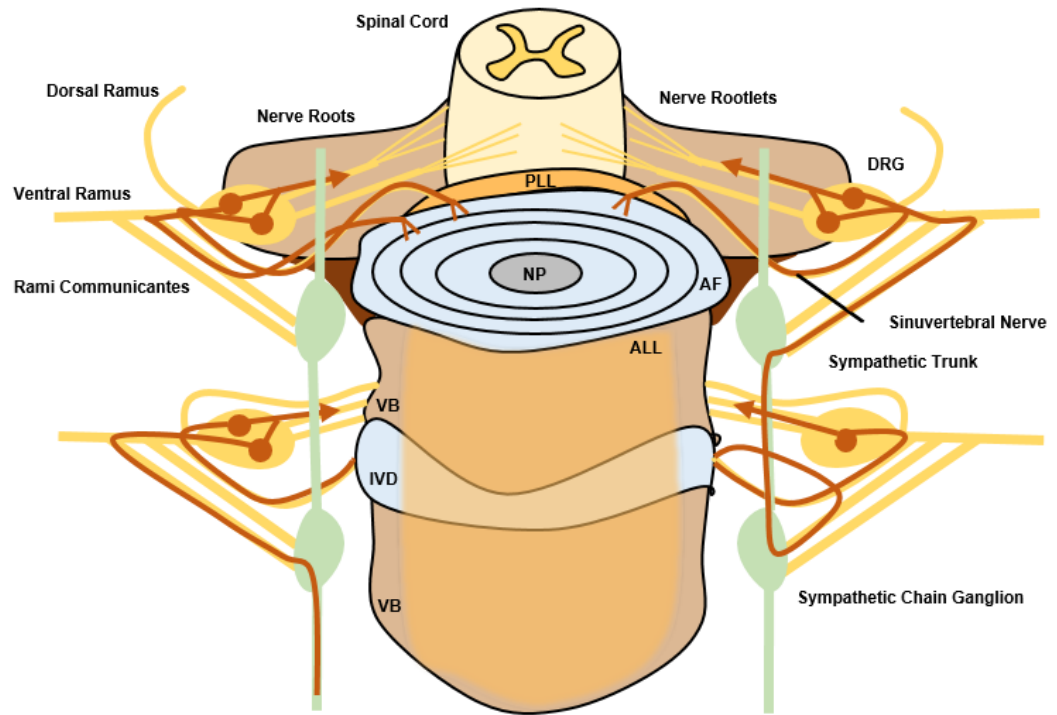


Figure 1: An anterior-posterior schematic of spinal neuroanatomy. This schematic shows the spinal cord, dorsal and ventral rootlets and roots, dorsal root ganglia (DRG), rami communicantes, sinuvertebral nerves, and sympathetic chain ganglia (green). Potential pathways of IVD sensory innervation are also depicted (red). Nucleus pulposus (NP), Anulus fibrosus (AF), Intervertebral disc (IVD), Vertebral body (VB), Anterior longitudinal ligament (ALL; orange overlay), Posterior longitudinal ligament (PLL).

1.1.1 Innervation of the Healthy Rat Intervertebral Disc

1.1.1.1 Dual Innervation

The posterior longitudinal ligament (PLL), which overlies the vertebral column, and connective tissue around the IVD are also innervated [28, 29] as demonstrated previously [30]. In this study, Kojima and co-workers used an acetylcholinesterase

histochemical method to determine the neural innervation of the IVD and PLL in a rat model, and found that nerve fibers directly innervating the IVD are derived from a branch of the gray ramus, and nerve fibers innervating the IVD via the PLL are derived from a second source. This became the first study to suggest dual innervation of the IVD and also polysegmental innervation by DRGs of multiple levels [30].

1.1.1.2 Bilateral and Multisegmental Innervation

Adult humans most frequently injure the posterior portion of the L4-L5 IVD [27, 31], which corresponds to the rat L5-L6 IVD anatomically [32]. In order to understand the process for neo-innervation of the pathological IVD, it is important to verify the neural innervation of the non-pathologic IVD. To determine the origin of nerves supplying the posterior portion of the lumbar IVD, a study by Nakamura and co-workers stained whole rat lumbar spines using an acetylcholinesterase histochemical method after resecting different bilateral levels of the sympathetic trunk. This study showed that the IVD is innervated by branches from the autonomic nervous system and the dorsal portion of the IVD is innervated bilaterally and multisegmentally [27], which challenged the conventional belief that each IVD is innervated by the corresponding DRG [30, 31].

1.1.1.3 Innervation of Ventral, Lateral, and Dorsal Aspects of the IVD

These results led to more interest in the sensory innervation of each portion of the IVD. A study by Morinaga and co-workers showed that bilateral L1 and L2 DRGs innervate the anterior, or ventral, portion of the L5-L6 IVD in rats using anterior labeling of horseradish peroxidase or cholera toxin B as a retrograde labeling agent [33]. A similar study by Ohtori and co-workers used Fluoro-Gold (FG) labeling to show that the posterior, or dorsal, portion of the L5-L6 IVD in rats is innervated in two ways: segmentally by adjacent segments L3 to L6 via the sinuvertebral nerves and PLL, and non-segmentally by distant segments T13 to L2 via the paravertebral sympathetic trunks through the L5 rami communicantes as shown in Figure 2. Bilateral L1 and L2 DRGs were found to be the main contributors to sensory innervation of the dorsal portion of the L5-L6 rat IVD [34]. A study by Aoki and co-workers showed that sensory innervation is predominantly supplied by the L1, L2, and L3 DRGs ipsilateral to FG placement on the lateral portion of the L5-L6 IVD [35]. Together, these findings from the ventral, dorsal, and lateral sensory innervation studies of the L5-L6 rat IVD show that nociceptive information from all portions of this IVD is transmitted mainly by the L1 and L2 DRG neurons [35, 36].

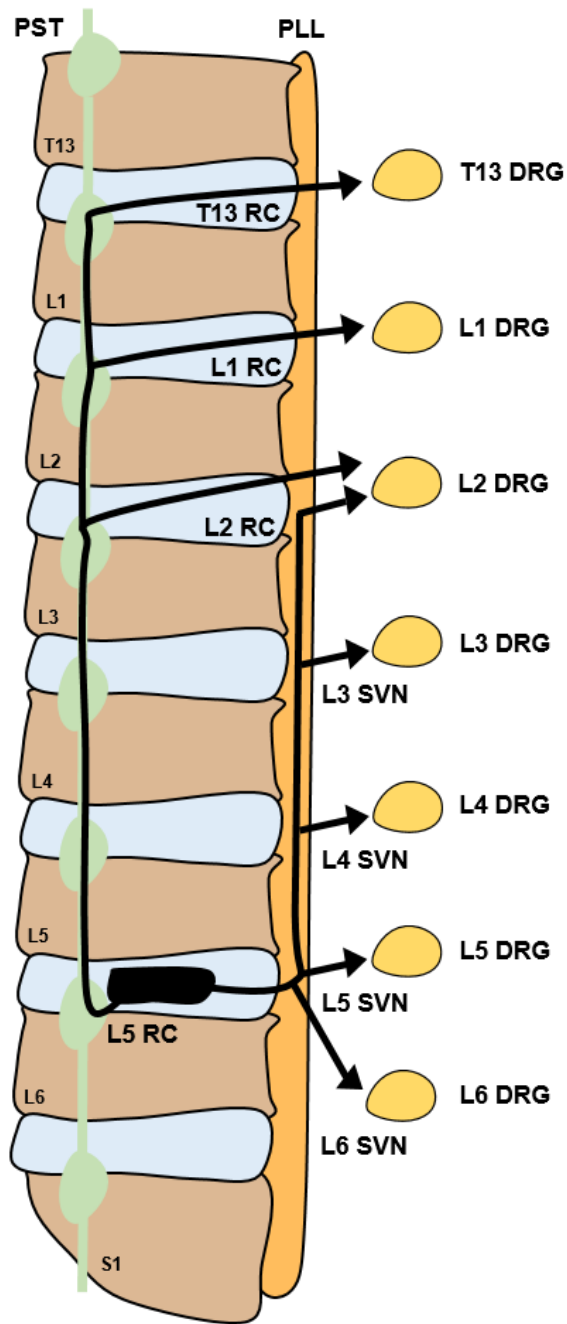


Figure 2: Dual innervation of the sensory pathways from the dorsal portion of the rat L5-L6 IVD. Dorsal root ganglion (DRG), Paravertebral sympathetic trunk (PST), Posterior longitudinal ligament (PLL), Ramus communicans (RC), Sinuvertebral nerve (SVN).

1.2 Nociceptive Afferent DRG Neurons

Nociceptive information from the lumbar IVD is transmitted to the DRGs via free nerve endings of small, nociceptive afferent small myelinated A δ and unmyelinated C fibers, which innervate the outer AF. The A δ fibers carry information from mechanical or mechanothermal nociceptors, and the C fibers, which comprise about 70% of all fibers carrying noxious input, are activated by a variety of high-intensity mechanical, chemical and thermal stimulation [37]. These neurons can be classified into two distinct groups [38]: nerve growth factor (NGF)-dependent neurons and glial cell line-derived neurotrophic factor (GDNF)-dependent neurons. NGF-dependent neurons account for about half of the DRG neurons innervating the IVD and express the high-affinity NGF receptor tyrosine kinase A (TrkA) [39] and the low-affinity NGF receptor p75 neurotrophin receptor (p75NTR). GDNF-dependent neurons express the GDNF receptor, Ret [40, 41]. In normal conditions, 8-24% of NGF-dependent DRG neurons will also express brain-derived neurotrophic factor (BDNF) and its receptor tyrosine kinase B (TrkB), which participate in nociceptive signal transmission [42]. NGF-dependent neurons are also positive for calcitonin gene-related peptide (CGRP) and substance P (SP), neuropeptides associated with inflammation and pain [43, 44] as well as transient receptor potential cation channel subfamily vanilloid member 1 (TRPV1), a pain-related receptor (Figure 3). Because of the strong correlation between expression of CGRP and

the NGF receptor [39], and isolectin B4 (IB4) and the GDNF receptor [41], CGRP and IB4-binding glycoprotein are recognized as standard neuronal markers for NGF- and GDNF-dependent neurons, respectively [18].

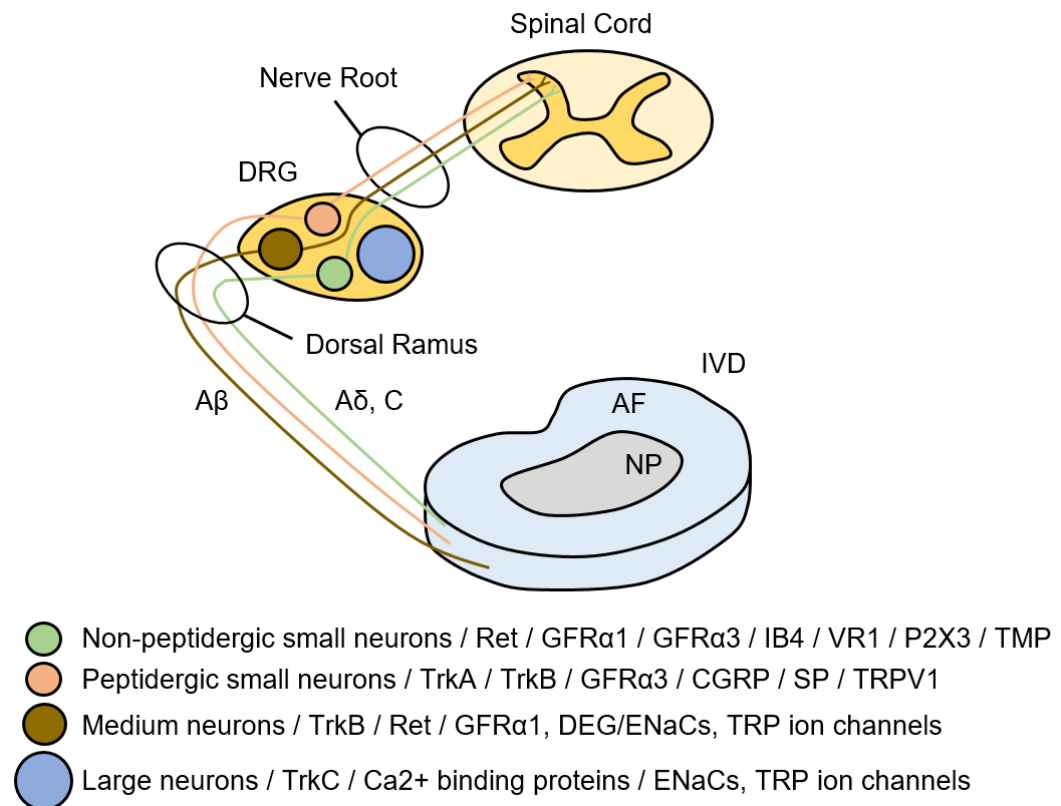


Figure 3: Nociceptive afferent small myelinated A δ and unmyelinated C fibers innervate the outer AF in non-pathologic IVDs. Each A δ or C fiber corresponds to either a peptidergic or non-peptidergic neuron. Peptidergic small neurons are NGF-dependent and express TrkA, TrkB, CGRP, SP, and TRPV1. Non-peptidergic small neurons are GDNF-dependent and express Ret and IB4.

GDNF-dependent neurons project predominantly to lamina II of the dorsal horn of the spinal cord where interneurons containing protein kinase C gamma (PKC γ) are

present [45]. Because PKC γ -containing neurons are associated with neuropathic pain produced by nerve injury [46], GDNF-dependent neurons are considered to be important in neuropathic pain [36]. Studies of IVD neuronal innervation show that only 0.6-1% of innervating nerve fibers are positive for the GDNF-dependent neuronal marker, IB4 [47,48]. These findings indicate that nociceptive information from the lumbar IVD is transmitted mainly by CGRP-immunoreactive NGF-dependent neurons [47].

1.2.1 Electrophysiological Differences

A study by Stucky and Lewin found that these two types of neurons also exhibit electrophysiological differences, suggesting that they are functionally different [49]. Action potentials (APs) in NGF-dependent neurons have a lower threshold and are shorter in duration than GDNF-dependent neurons, and small diameter sensory neurons ($\leq 26 \mu\text{m}$) with an inflection in the falling phase of the action potential are more likely to be nociceptors [50]. GDNF-dependent neurons express 2.1-fold larger voltage-gated tetrodotoxin-resistant sodium currents than NGF-dependent neurons [49], which supports longer AP duration in GDNF-dependent neurons as increased concentrations of tetrodotoxin-resistant sodium channels are responsible for larger duration APs [50]. In addition, NGF-dependent neurons display larger heat-activated currents than GDNF-dependent neurons. These larger NGF heat-induced currents correlate with C fibers that

respond with a large burst of APs, suggesting that NGF-dependent neurons are more involved with acute responses to noxious heat stimuli than GDNF-dependent neurons [49]. Functional differences between these DRG neurons have also been demonstrated via *in vitro* application of the pro-inflammatory cytokine IL-6, histamine, or capsaicin, followed by calcium imaging [51, 52]. Functional differences between these neuronal populations have been investigated in pathologic states such as surgically-induced IVD herniation [53, 54]. However, functional differences in nociceptive afferent DRG neurons have not yet been investigated in a model of painful IVD degeneration.

1.3 Intervertebral Disc Degeneration

1.3.1 Morphologic and Biochemical Changes

IVD degeneration is a complex and multi-factorial process, and can be linked to nutritional, environmental, and genetic factors. IVD degeneration is characterized by changes in morphology. The boundary between the AF and nucleus pulposus (NP) becomes less distinct as the NP becomes more fibrotic [14-17]. Structural changes occur which lead to an increasing degree of disorganization [15, 51, 56], and cell apoptosis and necrosis is increased with more than 50% of cells showing evidence of necrosis [57].

The most significant biochemical change which occurs in IVD degeneration is the loss of hydration in parallel with loss of proteoglycans and glycosaminoglycans. This leads to a loss of osmotic pressure and consequent loss of IVD height, and is associated

with altered mechanisms of load support in the AF and endplate [58], increased penetration of proteins and cytokines into the IVD [59], and neural ingrowth into the degenerate IVD [60, 61], which potentially drive IVD degeneration and have been associated with discogenic pain [58, 62].

1.3.2 Inflammation

Levels of pro-inflammatory mediators in painful IVDs are elevated compared to asymptomatic IVDs [36, 63, 64]. Elevated levels of cytokines including tumor necrosis factor- α (TNF- α) and interleukin-1 β (IL-1 β) are present in herniated IVDs [63, 65-69], which the IVD cells locally synthesize and secrete [65]. Macrophages, a source of pro-inflammatory mediators and NGF [70] are also present in painful IVDs [69] as shown in Figure 4.

Elevation of TNF- α and IL-1 β in painful IVDs induces NGF [36, 71-73] and SP [74] mRNA expression and protein secretion as shown in Figure 4. Miyagi and co-workers found that the local inflammatory response (TNF- α , IL-6, NGF) to induced IVD injury returned to normal levels within 2 weeks, but elevated levels of painful neuropeptides such as NGF in DRG neurons innervating punctured IVDs continued until the end of the study at 8 weeks [75].

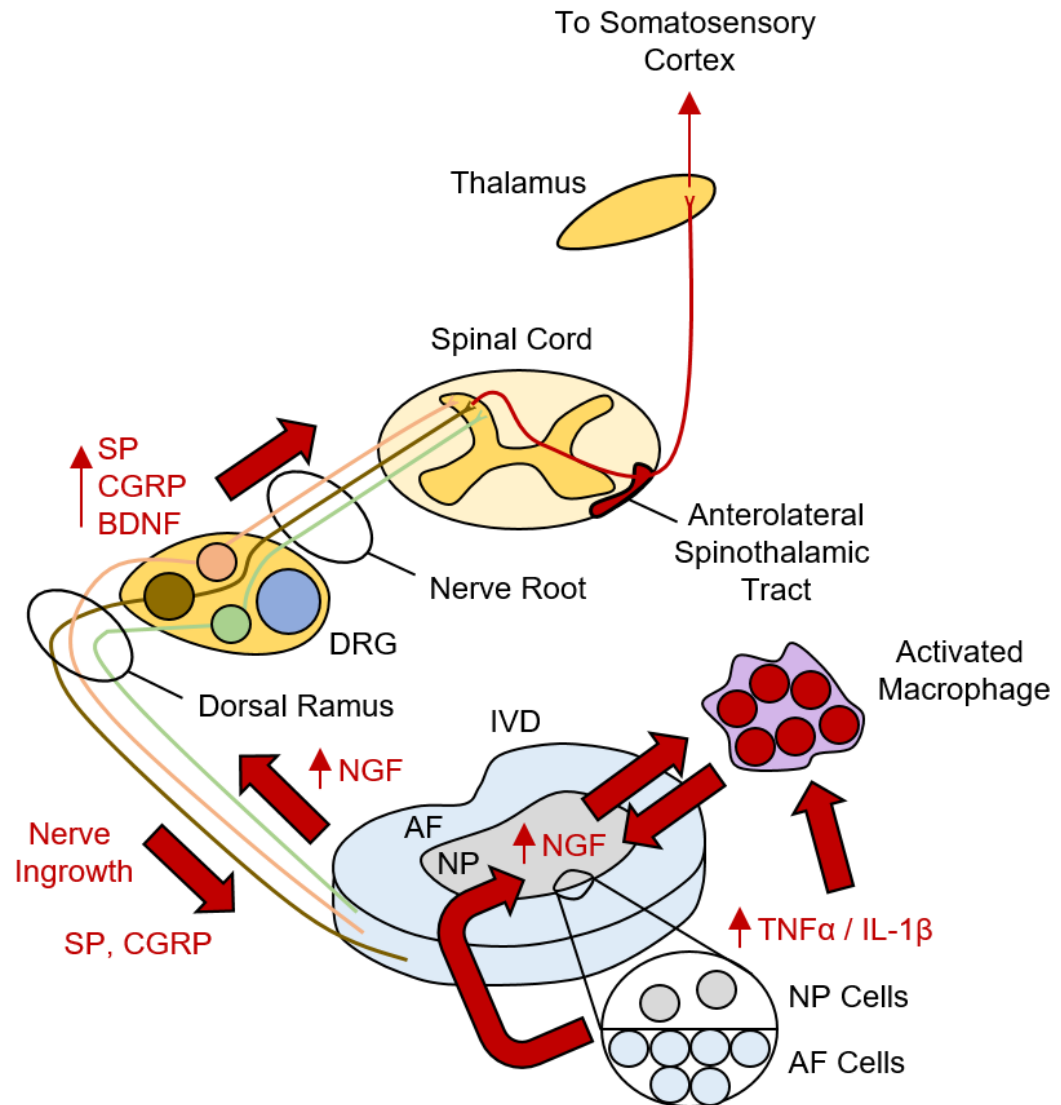


Figure 4: A schematic depicting possible mechanisms of discogenic pain. Inflammation leads to pro-inflammatory cytokine release by IVD cells, which act on macrophages to trigger NGF secretion. IVD cells increase expression of NGF and SP. NGF can stimulate inflammatory cells locally or act on TrkA-expressing neurons to induce expression of CGRP and SP, which mediate pain. Increased NGF also results in nociceptive nerve fiber ingrowth, which maintains pain. CGRP and SP mediate synaptic transmission in the dorsal horn of the spinal cord and BDNF produced in the DRG neurons projects to the spinal cord and modulates pain transmission.

1.3.2.1 Nerve Growth Factor and Inflammation

NGF contributes to inflammatory hyperalgesia via TrkA in small DRG neurons due to upregulation of NGF synthesis by the inflamed tissue [76] and upregulation of TrkA in DRG neurons [77]. NGF sensitizes the primary afferent neurons to produce hyperalgesia [71, 78, 79] by regulating the expression of SP, CGRP, TRPV1, and other molecules associated with pain in NGF-dependent neurons [47, 80]. NGF binding to TrkA or p75NTR initiates signal transduction pathways such as Ras/ERK/MAPK or NF- κ B to activate transcription factors which promote survival or lead to expression of additional pro-inflammatory cytokines, respectively [20, 81] as shown in Figure 5. These findings identify NGF as a key mediator in inflammatory pain [36]. NGF also regulates collateral sprouting of sympathetic fibers to DRG neurons [20], which is related to maintenance of chronic pain [82, 83]. Therefore, NGF synthesized in the IVD may act on TrkA receptors on the central terminals of DRG neurons innervating the IVD to play a role in chronic pain development [36, 84].

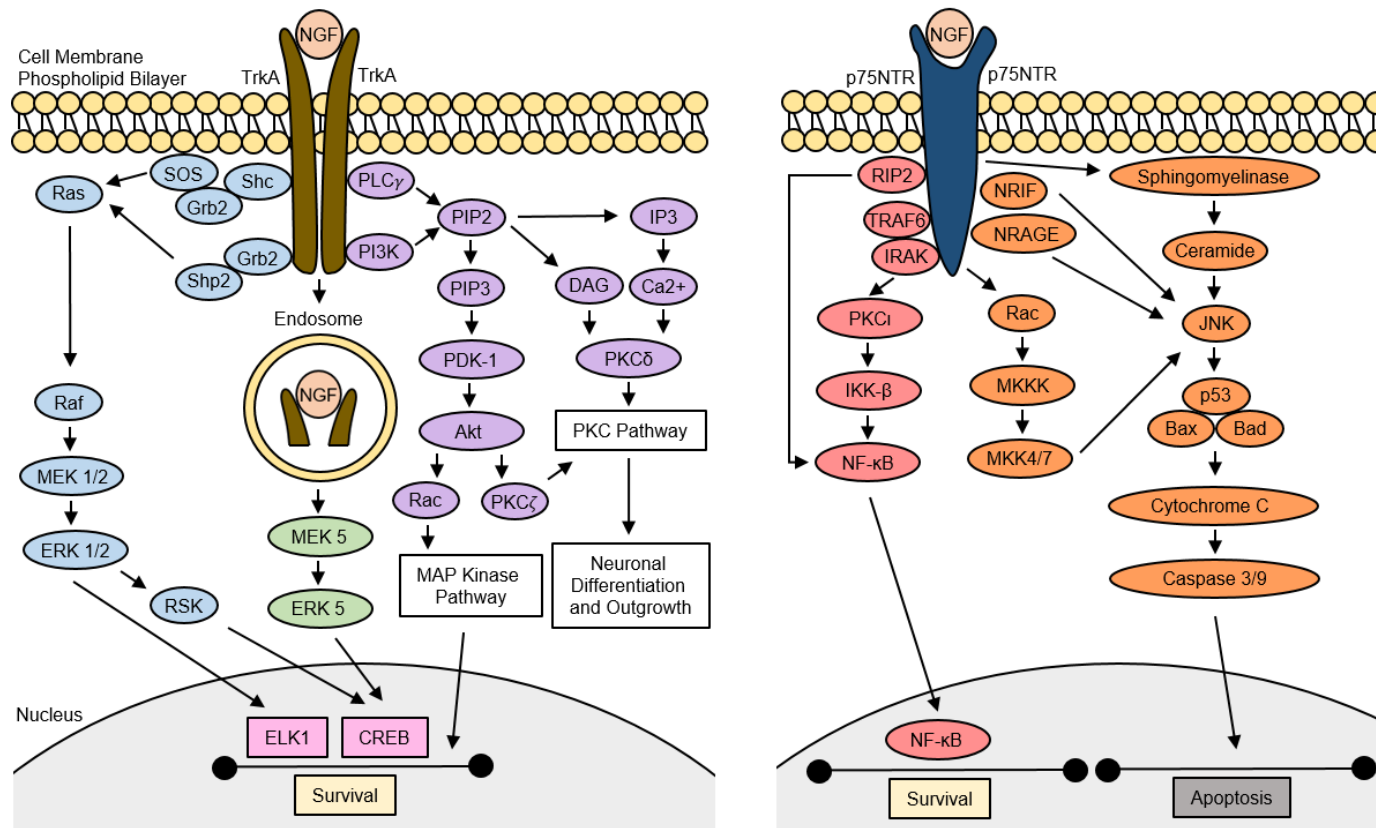


Figure 5: NGF binding to TrkA activates many pathways related to cell survival (left). NGF binding to p75NTR can activate pathways associated with cell survival or apoptosis (right). Each color represents a different biochemical pathway.

1.3.2.2 Brain-Derived Neurotrophic Factor and Inflammation

Peripheral inflammation also results in BDNF upregulation in the DRG neurons (Figure 4), which is associated with increased BDNF release in the central nociceptive terminals located in the dorsal horn of the spinal cord [85, 86]. BDNF acts to modulate neuronal signaling and is co-localized in vesicles with SP [87]. BDNF expression is also upregulated in TrkA-positive DRG neurons after NGF treatment [80, 88]. These findings suggest that BDNF modulates functions mediated by small diameter sensory neurons and regulates the integration and processing of nociceptive information in the dorsal horn of the spinal cord [89-91]. BDNF could be a key mediator in the signaling and processing of discogenic pain.

1.3.2.3 Neurotrophins in Degenerate Intervertebral Discs

NGF, TrkA, and p75NTR show increased expression in painful IVDs [66, 84], and immunostaining shows that NGF, TrkA, and BDNF and its receptor tyrosine kinase B (TrkB) are expressed in the IVD at every stage of degeneration [92]. NGF may regulate receptors such as TRPV1, bradykinin receptors, and sodium channels to potentiate long term effects on nociceptors [80].

1.3.3 Nerve Ingrowth

Nerve fibers have frequently been found in degenerate IVDs as evidenced by elevated immunohistochemical staining for growth-associated protein 43 (GAP43) [18,

84], a marker of axonal growth and synaptic plasticity [93-95], suggesting new nerve ingrowth as a possible mechanism of discogenic pain [62, 96, 97]. A study by Aoki and co-workers used co-labeling of GAP43 and CGRP to show that IVD inflammation induced by Freund's adjuvant promotes axonal growth of NGF-sensitive DRG neurons innervating the affected IVD [50]. This is supported by work from Freemont and co-workers which co-labeled human IVD specimens from patients with chronic low back pain with GAP43 and TrkA to show that increased NGF expression leads to actively growing nerve fibers which express an increased concentration of NGF receptors. They also noted an absence of these NGF-receptor expressing nerve fibers in asymptomatic human IVD specimens [84]. These results suggest that NGF is induced by pro-inflammatory mediators in human IVD and promotes axonal growth of small nociceptive NGF-sensitive DRG neurons [18]. This is also supported by an in vitro study from Aoki and co-workers which showed that TNF- α more effectively induces GAP43 expression in NGF-sensitive DRG neurons than in GDNF-sensitive neurons [98]. Together, these findings illustrate the importance of injury-induced inflammation and sensory afferent innervation in painful IVD degeneration.

2. In Vivo IVD Degeneration Model Development and Characterization

2.1 Introduction

The in vivo environment is crucial for understanding complex multifactorial pathologies such as IVD degeneration and mechanisms of pain generation, as well as determining the efficacy of potential regenerative and therapeutic strategies. Many different species have been used as pre-clinical models of IVD degeneration, including mouse [99, 100], rat [101-103], rabbit [104, 105], sheep [106, 107], goat [108, 109], and primates [110-112]. These models can be divided into experimentally induced (mechanical compression, instability, structural injury, chemical) or spontaneous IVD degeneration [113]. For this study, it was important to have a model of IVD degeneration in rats that would be clinically relevant, tunable, and reproducible. Therefore, we chose to induce a structural injury by puncturing a single lumbar IVD.

Prior studies have accessed the rat lumbar IVD through a variety of approaches. Most commonly, midline abdominal incisions [46, 116] have been done to access the ventral [75, 115, 102, 103, 116-120], lateral [35, 47, 121], or ventrolateral [18, 122] portions of the lumbar IVDs. However, accessing the rat lumbar IVD via a ventral abdominal approach introduces sizable trauma to the animal and may slow surgical recovery. Also, humans most frequently injure the posterior or posterolateral aspect of an IVD [27, 31], possibly making a ventral IVD injury less clinically relevant.

Dorsal approaches with the animal in a prone position have also been reported in conjunction with facetectomy [101, 122-125], hemifacetectomy [126], or fluoroscopic guidance around the facet joint [127] to access the dorsolateral portion of the lumbar IVDs. However, modifying these vertebral connections alters spinal stability and could lead to additional complications, making this a poor model for studying IVD degeneration resulting from an isolated IVD injury. A dorsal approach using fluoroscopic guidance to access the IVD is a promising model for studying IVD degeneration resulting from an isolated IVD injury, as it is less invasive than other approaches and spinal stability remains intact, but it is limited by the size of the space around the facet joint and surgical and technological proficiency.

As injury to the dorsal portion of the IVD may be more clinically relevant, it is important to consider the main contributors to sensory innervation of that portion of the rat L5-L6 IVD, the bilateral L1 and L2 DRGs [33]. However, the lateral portion of the rat L5-L6 IVD is mainly innervated by the ipsilateral L1, L2, and L3 DRGs [34]. Due to the biomechanical and technical limitations of a dorsal surgical approach, accessing the lateral aspect of the IVD may be the most feasible option while inducing the least amount of surgical trauma and still allowing the L1 and L2 DRG neuronal response to be studied.

A study by Onda and co-workers investigated the role of NGF and pain-related behavioral changes following surgical herniation of a rat lumbar IVD [123]. Rats were

placed in a prone position and the dorsolateral aspect of the IVD was exposed via paravertebral muscle dissection and facetectomy, followed by puncture with a 27G needle and slow injection of 0.3 mL of air. Mechanical and thermal sensitivity tests showed no differences between this experimental group and the sham control group out to 3 weeks post-surgery. However, NGF levels were significantly elevated at day 3 post-surgery compared to the sham control group [123]. This model used a dorsolateral approach to access the rat lumbar spine, altered spinal stability via facetectomy, and monitored behavioral changes until week 3 post-surgery.

A stab incision for inducing IVD degeneration was demonstrated in a rat model by Rousseau and co-workers [115]. The lateral aspect of 3 adjacent caudal rat IVDs was exposed surgically and stabbed (number 11 blade; depth of 1.5 mm) in skeletally mature Sprague-Dawley rats. A second group of rats underwent a midline ventral abdominal incision into the peritoneum to access the retroperitoneal space, and the ventral aspect of 3 adjacent lumbar IVDs was stabbed in the same way. Injured caudal IVDs showed degenerative changes on histology at 4 weeks post-surgery, but changes consistent with degeneration were less apparent in the injured lumbar IVDs. Animals with lumbar IVD injury showed significantly decreased performance on the Rotamex rotating rod test at 2-4 weeks post-surgery [115]. This model used a lateral approach to injure multiple rat tail IVDs, as well as a ventral abdominal approach to access the rat lumbar spine to

injure multiple lumbar IVDs, and monitored behavioral changes until week 4 post-surgery.

Recently, studies have induced lumbar IVD degeneration in rats via puncture of the ventral aspect of multiple rat IVDs via a midline ventral abdominal incision with a 0.5 mm or 0.8 mm microsurgical drill (equivalent to a 25G or 21G needle, respectively) to a depth of 2 mm [103], or a 26G needle to a depth of 3 mm and subsequent injection of 2.5 μ L phosphate buffered saline (PBS) [102]. These prior pre-clinical models of IVD degeneration injured multiple IVDs per animal [115, 102, 103], which confounds the mechanism of pain generation. In addition, IVD degeneration is a chronic pathology and therefore requires a substantial amount of time to develop. However, these prior studies ended functional and behavioral assessments, as well as assessments of molecular changes, at or before 7 or 9 weeks post-injury, respectively [115, 102, 103].

2.1.1 Pain-Related Functional and Behavioral Measures

2.1.1.1 Operant Activities

Operant assessments have recently been proposed to evaluate pain in animal models of musculoskeletal pathology [128-130]. Operant assessments of pain in preclinical models may have more relevance to pain experienced by humans and also improve data reliability [131, 132]. Advantages of operant measures of general activity, such as open field assessments, burrowing and mazes, include simultaneous

measurements of multiple objective parameters related to movement in a short time-frame, as well as absence of evoked responses.

2.1.1.1.1 Running Wheel

Running wheels, with or without instrumentation, are commonly used to measure general physical activity in rodents [99, 133, 134]. A review by Novak and co-workers presented detailed relationships between wheel running and physiological or psychological outcomes and concluded that increased wheel running activity does not necessarily represent increased general activity levels in rodents [135]. Using the running wheel assessment to detect differences between groups is especially difficult with rats, as rats must be acclimated to the equipment and trained over time to run on the wheel consistently. Even with this training, rats still show decreasing running wheel activity over time. A study by Peng and co-workers investigated differences in longitudinal wheel running for male Long Evans rats from age 3-36 months. Rats showed the most running activity at age 3 months, but then demonstrated a strong negative relationship between running activity and increasing age. By age 12 months, running activity had reduced by to less than half that seen initially at 3 months [133]. Because of this dramatic decrease in running wheel activity in rats over time, it is likely that subtle models of pain would not lead to dramatic differences between treatment groups.

2.1.1.1.2 Open Field

Open field testing can yield horizontal activity measures such as distance traveled and percentage of time spent traveling, as well as rearing behavior. Automated video-tracking software such as EthoVision XT (Noldus, Leesburg, VA) has the ability to identify the animal present in the recording and compute desired parameters independent of the observer after defining an arena of interest [136]. Decreased open field activity has previously been shown in a rat model of unilateral knee osteoarthritis (OA) [137].

2.1.1.1.3 Burrowing

Burrowing behavior in rats is innate and highly conserved, and has been used previously to evaluate animal well-being [138]. Prior studies in rat models of unilateral hind paw inflammation [139] and unilateral knee arthritis [137] have demonstrated decreased burrowing activity over 2 hours as measured by the amount of gravel displaced from a hollow tube pre-filled with gravel weighing 2500 g.

2.1.1.1.4 Pain Tolerance on Lateral Bending Maze

Rodent mazes have been developed previously to study anxiety, learning and memory, and spontaneous exploration [140]. We decided to design a custom, rectangular 4-turn maze to evaluate pain tolerance on lateral bending after an injury to the low back. Successful completion of each turn through the maze requires extreme

lateral bending of the spine, and subsequent turns alternate between left and right lateral bending as depicted in Figure 6.



Figure 6: Pain Tolerance on Lateral Bending Maze.

2.1.1.2 Weight-Bearing and Gait

2.1.1.2.1 Static Weight-Bearing/Incapacitance

Changes in weight-bearing and strength characteristics are often powerful descriptors of pain. Commercially available meters of hind limb weight-bearing, known as incapacitance meters, have the ability to measure the percent of weight borne on left versus right hind limbs. Previous work in our laboratory with a rat model of surgically-induced lumbar radiculopathy showed a significant reduction in weight-bearing on the affected limb [141] as described in Figure 7.

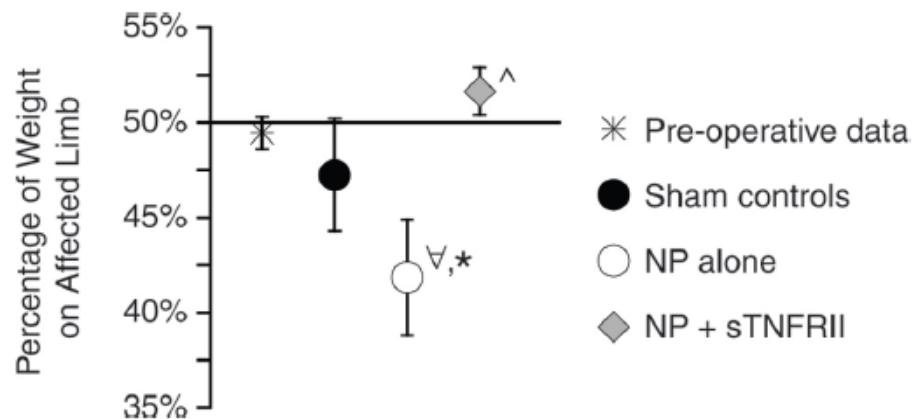


Figure 7: An in vivo model of lumbar radiculopathy showed decreased unilateral weight-bearing on the affected limb compared to the contralateral limb, and compared to animals with NP and soluble tumor necrosis factor receptor type II (sTNFRII) treatment [141]. Image courtesy of L.A. Setton.

2.1.1.2.2 Treadmill Gait

Because gait properties are correlated to velocity, a treadmill is advantageous for obtaining consistent gait descriptors across animals. In early work, a custom-designed treadmill was used [141, 142] to document gait parameters in type IX collagen knockout mice which exhibited premature onset of OA and IVD degeneration. Mutant mice were found to use elevated hind limb stance times, increased step width, and shorter stride lengths as compared to wildtype mice, showing some similarities to gait in patients seeking to reduce joint or back pain [142]. In general, locomotion with pain is characterized by slower and longer periods of approach to weight-bearing (longer stance time), increased stride width, and decreased stride length, which stabilize the affected individual. More recently, several commercially available treadmills provide a clear belt and automated software to analyze geometric measures of gait. Our laboratory

now uses a DigiGait™ treadmill (Mouse Specifics Inc, Quincy, MA) for rodent gait analysis. One prior study of surgically-induced IVD degeneration in the rat via puncture of multiple lumbar IVDs reported altered stability of the hind limbs with decreased swing duration, increased percentage of stride in stance, and an increased stance/swing ratio [102].

2.1.1.3 Mechanical Sensitivity

The most widely accepted test of mechanical sensitivity uses von Frey filaments to assess tactile allodynia (non-noxious mechanical stimulus). The von Frey method applies hand-held monofilaments of known stiffness to an affected area in human subjects with an oral response noted. In animals, the filaments are applied to the plantar surface of the paws; stiffer filaments will provoke a paw withdrawal with or without licking of the stimulated paw, and the force necessary to induce withdrawal may be reduced with pain. Multiple trials may be used over a series of monofilament applications to approximate the “50% paw withdrawal threshold”. Our laboratory has found altered paw withdrawal thresholds in many rodent models of musculoskeletal pain including the type IX collagen knockout mouse [141, 142]. Studies by Lai and co-workers as well as Kim and co-workers induced IVD degeneration in the rat via puncture of multiple lumbar IVDs and found conflicting results for mechanical allodynia: Lai and co-workers found that the withdrawal threshold of the lumbar IVD puncture group progressively decreased throughout the study [102]; in contrast, Kim

and co-workers found no mechanical allodynia in the lumbar IVD puncture group and concluded that IVD puncture injury may generate mild inflammation which is not sufficient for the development of statistically significant mechanical allodynia [103]. This is important, as clinically significant mechanical sensitization may not develop in patients with discogenic low back pain [143].

2.1.1.4 Pressure Hyperalgesia

Algometers have been developed to measure site-specific pain by applying an external pressure which elicits an increased response in human subjects. The small animal algometer applies pressure continuously to a local site while the animal is restrained and the force associated with eliciting a response is recorded. Kim and co-workers induced IVD degeneration in the rat via puncture of multiple lumbar IVDs and found that the pressure hyperalgesia threshold progressively decreased as measured by vocalization in the lumbar IVD puncture group compared to the sham control group [103]. This test is clinically relevant, as mechanical pressure on patients' IVDs is used to assess their degree of low back pain [144].

2.1.1.5 Thermal Sensitivity

Changes to heat pain thresholds have been studied in human subjects and reflect a generalized neuropathic response. In animals, thermal sensitivity can be quantified by latency to paw or tail withdrawal from a noxious heat source [145]. Lai and co-workers

induced IVD degeneration in the rat via puncture of multiple lumbar IVDs and found no significant changes in thermal hyperalgesia paw withdrawal [102].

2.1.2 Objective

The objective of this work was to develop and characterize a surgical model of IVD degeneration in the rat. We describe here a novel surgical procedure for accessing the lateral aspect of the L5-L6 IVD and the resulting behavioral and sensitivity phenotype in female Sprague-Dawley rats.

2.2 Materials and Methods

2.2.1 Baseline Behavioral and Functional Measures

A total of 37 female Sprague-Dawley rats (age 15 weeks; Envigo; Indianapolis, IN) were used for this 20 week study. Animals were first acclimated to investigator handling over a period of 7 days, followed by acclimation to the behavioral testing equipment over a period of 4 consecutive days to minimize the stress response (Tables 1, 2). Each rat was acclimated individually to the testing equipment. The day prior to surgery, animals were divided into 3 groups: naïve (n=8), lumbar disc puncture (LDP) (n=14), and Sham-operated control (n=14), and pre-operative functional and sensitivity assessments were conducted to obtain baseline values (Tables 3, 4).

Table 1: Acclimation to Investigator Handling.

Day	Acclimation to Handling (per cage)
1	Observe rats upon arrival, introduce to investigator voice, no handling
2	1. Hands in cage, suede gloves (25 mins) 2. Pet dorsal back, suede gloves (5 mins)
3	1. Hands in cage, suede gloves (5 mins) 2. Pet dorsal back, suede gloves (25 mins)
4	1. Hands in cage, normal gloves (10 mins) 2. Pet dorsal back, normal gloves (15 mins) 3. Hold each rat at least 2x (5 mins)
5	1. Pet dorsal back, normal gloves (5 mins) 2. Repeatedly hold rats until comfortable being held (25 mins)
6, 7	Observe rats, let rest

2.2.1.1 Open Field Arena

General activity was assessed by allowing each rat to freely move about a black acrylic arena (60 cm x 60 cm x 60 cm) for a total of 60 minutes during the dark portion of a 12 hour light-dark cycle, and without the presence of investigators or other personnel. The behavioral testing room was illuminated by red light, and movement was recorded by a video camera (Sony Handycam HDR-CX405, Sony Corp, New York, NY) and analyzed with video tracking software (EthoVision; Noldus Information Technology, Leesburg, VA) for total distance traveled, average velocity, and percent time spent traveling. Data for percent time spent traveling in 30 minutes was used to calculate the 95% confidence interval. Animals which fell outside of this confidence interval for $\geq 25\%$ of the described timepoints within each experimental group were labeled as outliers and

excluded from all behavioral analyses. Therefore, behavioral analyses included animals from all 3 groups including Naïve (n=8), Sham (n=11), and LDP (n=13).

Table 2: Equipment Acclimation Protocol.

Assessment (Equipment)	Day 1	Day 2	Day 3	Day 4
Open Field (Arena)	Arena (20 mins)	Arena (20 mins)	Arena (20 mins)	Arena (20 mins)
Burrowing (Tube, Cage, Individual)	Empty tube added to home cage (20 mins)	Tube with 1000g gravel added to home cage (20 mins)	Tubes with 1000g gravel given to rats in individual cages (20 mins)	Tube with 2500g gravel given to rats in individual cages (20 mins)
Static Weight-Bearing (Compartment)	In compartment (5 mins)	In compartment (5 mins)	Reposition as necessary in compartment to face forward with tail out of compartment, one hind paw on each force plate	Reposition as necessary in compartment to face forward with tail out of compartment, one hind paw on each force plate
Treadmill Gait (Compartment, Light, Belt Movement)	In compartment, no light (10 mins)	In compartment (5 mins no light, 5 mins light on)	In compartment (5 mins no light, 5 mins light on, 1 min belt on at 4-6 cm/s)	In compartment (5 mins no light, 5 mins light on, increase belt speed with rest periods until speed at 20 cm/s)
Pain Tolerance Maze (Maze)	In maze, start at entry point (5 mins)	In maze, start at entry point (5 mins)	In maze, start at entry point (5 mins)	In maze, start at entry point (5 mins)
Pressure Hyperalgesia (SMALGO)	Done last—pressure applied to dorsal skin over L5-L6 IVD	Done last—pressure applied to dorsal skin over L5-L6 IVD	Done last—pressure applied to dorsal skin over L5-L6 IVD	Done last—pressure applied to dorsal skin over L5-L6 IVD

Table 3: Left versus Right-Independent Functional and Behavioral Assessments.

Assessment	Parameters Measured	Timepoints (Weeks Post-Surgery)	Number Trials Per Animal Per Timepoint
Open Field Arena	Total distance traveled (cm) Average velocity (cm/s) % time spent traveling	0, 1, 4, 8, 12, 16, 18, 20	1
Burrowing	Weight burrowed (g)	0, 1, 4, 8, 12, 16, 18, 20	1
SMALGO	Pressure sensitivity	0, 1, 4, 8, 12, 16, 18, 20	3
Treadmill Gait	Gait symmetry	0, 1, 4, 6, 8, 12, 16, 18, 20	3

Table 4: Left versus Right Functional and Behavioral Assessments.

Assessment	Parameters Measured	Timepoints (Weeks Post-Surgery)	Number Trials Per Animal Per Timepoint
Static Weight-Bearing/ Incapacitance	% weight on left hind limb (operated side)	0, 1, 4, 8, 12, 16, 18, 20	3
Treadmill Gait	Hind limb swing duration (s)	0, 1, 4, 6, 8, 12, 16, 18, 20	3

2.2.1.2 Burrowing

Methods were adapted from Deacon [138]. Briefly, 10 cm diameter white PVC pipe was sectioned into 32 cm lengths and one end of each length was closed with a fitted black foam PVC sheet. The open end of each tube was raised 6 cm by two 8 cm bolts, each placed 2.5 cm in from the tube opening and spaced 7 cm apart. Each tube was filled with 2500 g of pea-shingle gravel (diameter < 1 cm, Rock City Sand & Gravel, Red Hook, NY) and placed into a rat cage (26.0 cm x 47.6 cm x 20.3 cm). Each animal was placed into an individual burrowing cage and allowed to burrow freely for 60 minutes

during the dark portion of a 12 hour light-dark cycle, and without the presence of investigators or other personnel, and with the behavioral testing room illuminated by red light. The weight of gravel displaced was calculated and normalized to the baseline amount of gravel displaced. Additional animals were excluded from the burrowing assessment analysis if they did not successfully burrow at least 10% of the original weight of the gravel (250g) at the baseline timepoint.

2.2.1.3 Static Weight-Bearing/Incapacitance

Static weight-bearing was tested by placing the animals in an acrylic chamber so that the hind limbs were positioned on a left and right force plate, respectively. The incapacitance meter (Model BIO-SWB M, Bioseb, Vitrolles, 13845 France) calculated the average amount of force exerted by each hind paw over a 3 second interval, and the percentage of weight-bearing on the left hind limb (operated side) was calculated. Each rat repeated this assessment for a total of 3 trials per timepoint.

2.2.1.4 Pressure Hyperalgesia (SMALGO)

Local site pressure sensitivity of the low back was assessed using an algometer (SMALGO algometer, Bioseb). This device consists of small animal a force gauge with a 5 mm diameter tip which was pressed directly on the skin over the dorsal aspect of the L5-L6 IVD at midline while the animal was held by an investigator. The force was increased until the animal produced an escape reaction or audible vocalization [103, 146, 147]. Each rat repeated this assessment for a total of 3 trials per timepoint.

2.2.1.5 Treadmill Gait

Locomotion was assessed using a DigiGait™ treadmill (Mouse Specifics) with a ventral-view camera recording video of paw placement through a transparent treadmill belt. The DigiGait Imaging System™ (Mouse Specifics) generated "digital paw prints" and dynamic gait signals, representing geometric paw placement relative to the treadmill belt. Gait parameters were measured at a speed of 20 cm/s, including the bilateral parameter of forelimb versus hind limb symmetry (forelimb step frequency/hind limb step frequency) and unilateral parameters of left and right hind limb swing duration (s). Each rat repeated this assessment for a total of 3 trials per timepoint.

2.2.1.6 Pain Tolerance on Lateral Bending Maze

Pain tolerance on lateral bending was assessed using a custom-built maze designed to evaluate pain after an injury to the low back. We designed the maze with 4 alternating left and right turns, each of which requires extreme lateral bending of the spine for successful completion. At each time point, rats were allowed 2 minutes of time in the maze and the amount of time each rat needed to complete 2, 4, and 8 progressive turns through the maze was recorded, as well as the total number of turns completed. Each rat repeated the maze for a total of 3 trials per timepoint. Additional animals were excluded from the pain tolerance on lateral bending maze analysis if they failed to complete 8 turns within 2 minutes at the baseline timepoint.

2.2.2 Surgical Model to Induce IVD Degeneration

Animals were anesthetized with 1-3% isoflurane throughout the surgical procedure and a subcutaneous injection of 2-3 mL warm saline was given to help maintain body temperature and hydration. Additionally, animals were placed on a heating pad in a prone position and shaved from the mid-thoracic to sacral regions and including the left side of the animal. Ophthalmic ointment was placed on both eyes, and oxygen saturation was monitored. The shaved area was washed 3 times with chlorhexidine solution and sterile gauze, followed by 3 alcohol wipes and 3 betadine wipes. The animals were draped and a 4-5 cm dorsal skin incision was made over the lumbar region. The animals were rotated onto their right side while maintaining the sterile field and the skin on the left side of the incision was retracted by freeing the layer of connective tissue to expose the left paraspinal muscles. Because adult humans most frequently injure the posterior aspect of the L4-L5 IVD [27, 36] which corresponds to the rat L5-L6 IVD anatomically [35], the L5-L6 IVD of the LDP group was exposed via a left dorsolateral surgical approach (Figure 8) and punctured 10 times [75] using a 27 gauge needle with injection of 0.3 mL air to induce IVD degeneration. Then the muscle layers and skin were closed with 3-0 vicryl and 4-0 nylon suture, respectively. The Sham group had the dorsolateral surgical exposure with L5-L6 IVD visualization only. One subcutaneous injection of buprenorphine-SR (1 mg/kg) was given post-operatively for pain management over the next 72 hours, hydration gels were placed in each cage, and

hind paw pinch reflex was monitored until animals demonstrated normal reflexes and ambulation.

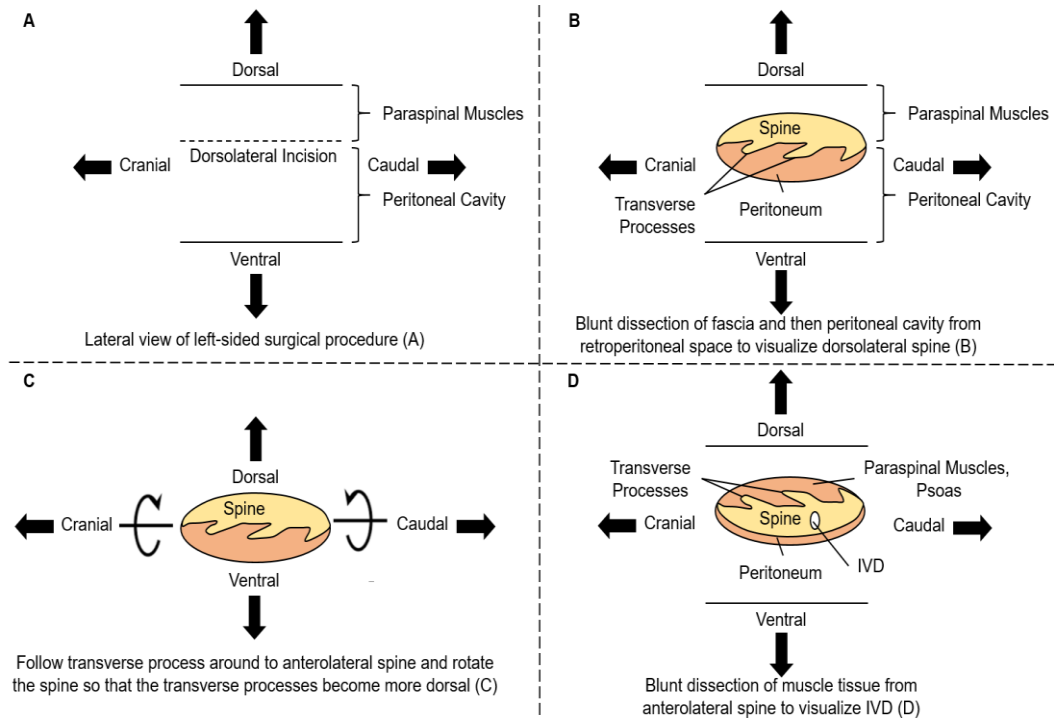


Figure 8: Surgical procedure to visualize the L5-L6 IVD. A 3 cm left-sided dorsolateral incision was made at the interface of the paraspinal muscles and peritoneal cavity (A) and a 2 cm blunt dissection of the fascia was performed until the peritoneal cavity was separated from the retroperitoneal space and the transverse processes were exposed (B). Then the transverse processes were followed anteriorly and the animal was rotated dorsally (C) for subsequent blunt dissection of 1 cm of tissue from the anterolateral aspect of the spine (D). This resulted in exposure of the L5-L6 IVD.

2.2.3 Post-Surgical Functional and Behavioral Assessments

Assessments were repeated at post-operative weeks 1, 4, 8, 12, 16, 18, and 20 for functional and behavioral assessments unrelated to treadmill gait. Treadmill gait was

repeated at post-operative weeks 1, 4, 6, 8, 12, 16, 18, and 20 (Tables 2, 3). After completion of assessments at week 20, animals were euthanized and tissues collected.

2.2.4 Data Analysis

2.2.4.1 Timeline of Model Development

Data from functional and behavioral assessments where multiple trials were obtained per rat per timepoint were averaged to obtain one data point per timepoint. These data were then analyzed via 2-factor ANOVAs with Tukey's multiple comparisons test ($\alpha < 0.05$) to determine differences between Sham and LDP groups as compared to the Naïve group (GraphPad Prism, GraphPad Software Inc, La Jolla, CA). Based on this timeline of acute changes due to surgical trauma and acute pain in this model and resolution, data were then grouped into acute (0-4 weeks), intermediate (6-16 weeks), and chronic (18-20 weeks) time bins for further analysis.

2.2.4.2 Longitudinal Behavioral Differences in Naïve Animals

Data for the Naïve group was analyzed via 1-factor ANOVAs with Tukey's multiple comparisons test ($\alpha < 0.05$) to determine changes over time (GraphPad Software).

2.2.4.3 Differences Between Sham and LDP Groups

Statistical differences between Sham and LDP groups were determined via 2-factor ANOVAs with Sidak's multiple comparisons test ($\alpha < 0.05$; GraphPad Software).

2.2.4.3.1 Effect Size Calculation

The effect size of the difference between Sham and LDP groups at the chronic timepoint was determined for the open field area assessment and also the treadmill gait parameter forelimb versus hind limb symmetry according Cohen's d using the following equation:

$$d = (x_1 - x_2)/\sigma \quad (1)$$

where x_1 and x_2 are the mean values for each group, respectively, and σ is the pooled standard deviation from both groups. Results were classified as either small (0.20-0.49), medium (0.50-0.79) or large (≥ 0.80) and were entered into G*Power 3.0.10 (Heinrich Heine University Düsseldorf, Düsseldorf, Germany) to compute the achieved power per assessment.

2.3 Results

2.3.1 Timeline of Model Development

Animals in the Sham and LDP groups showed significant deviation from the Naïve group at post-operative week 1 for parameters of pressure hyperalgesia (Naïve vs Sham: $p=0.006$; Naïve vs LDP: $p=0.006$; Figure 9A) and burrowing (Naïve vs Sham: $p=0.103$; Naïve vs LDP: $p<0.001$; Figure 9B), which resolved at post-operative week 4. Sham and LDP animals also showed significant differences at post-operative week 1 compared to the Naïve group for parameters of treadmill gait, including left hind limb swing duration (Naïve vs Sham: $p<0.001$; Naïve vs LDP: $p=0.006$; Figure 9C) and left

hind limb duty factor (Naïve vs Sham/LDP: $p < 0.001$; Figure 9D), which both resolved at post-operative week 6. Right hind limb duty factor for the LDP group also showed significance at post-operative week 1 ($p = 0.011$) and continued to trend toward significance at post-operative week 6 ($p = 0.054$).

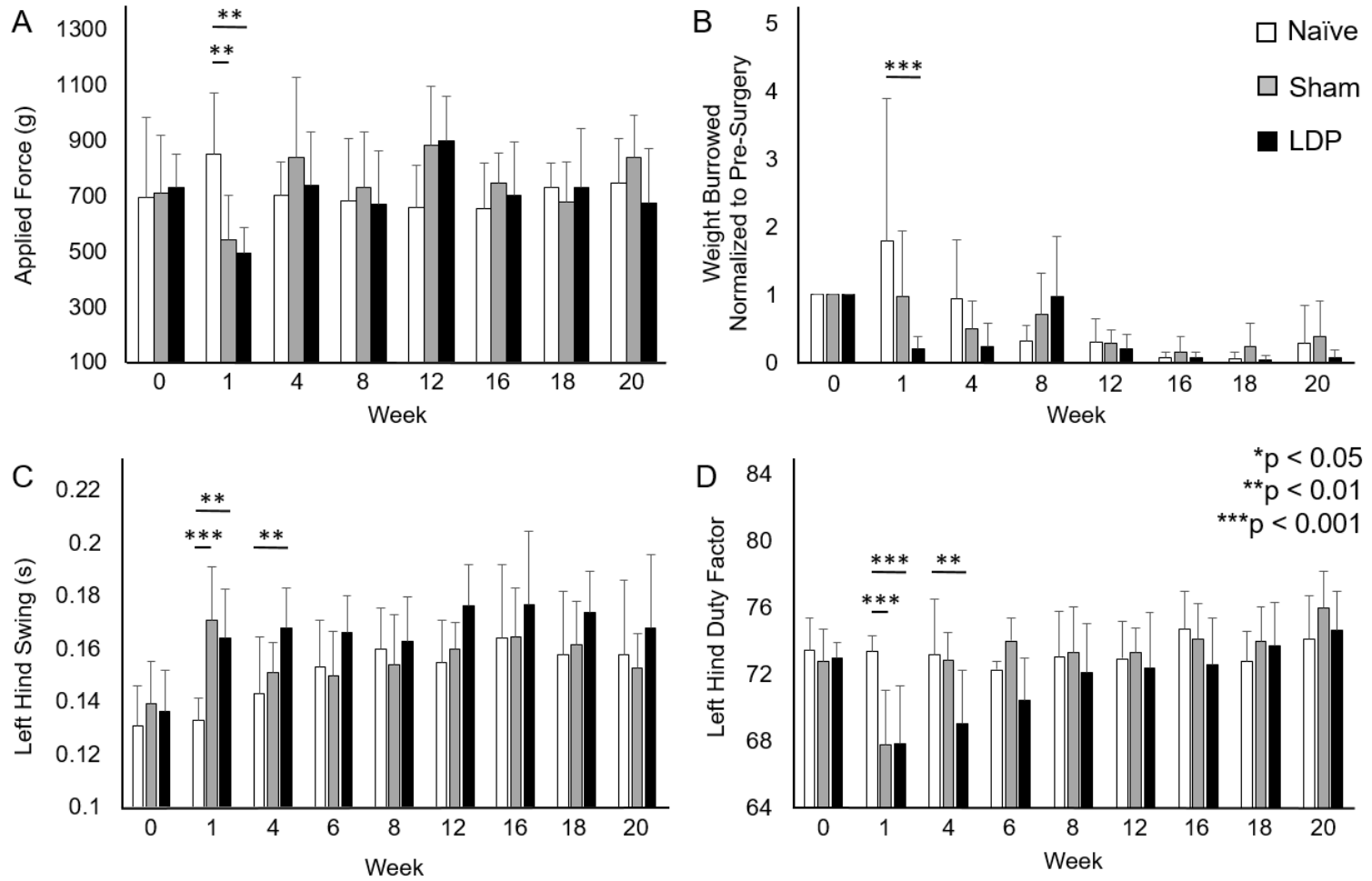


Figure 9: Timeline of functional and behavioral measures from baseline to post-operative week 20, including pressure hyperalgesia (A), burrowing (B), and treadmill gait (C,D). Error bars represent standard deviation.

2.3.2 Longitudinal Behavioral Differences in Naïve Animals

Static weight-bearing showed that Naïve animals (n=8) carried significantly more weight on the left hind limb while stationary at the chronic timepoint (p=0.033; Figure 10B). The amount of gravel displaced by Naïve rats (n=4) significantly decreased over time, achieving significance at both the intermediate (p=0.018) and chronic timepoints (p=0.020; Figure 10C). No significant differences were detected for percent time spent traveling in 30 minutes in an open field arena (n=8; Figure 10A), low back pressure hyperalgesia (n=8; Figure 10D), or treadmill gait parameters (n=5; Figure 10E, F).

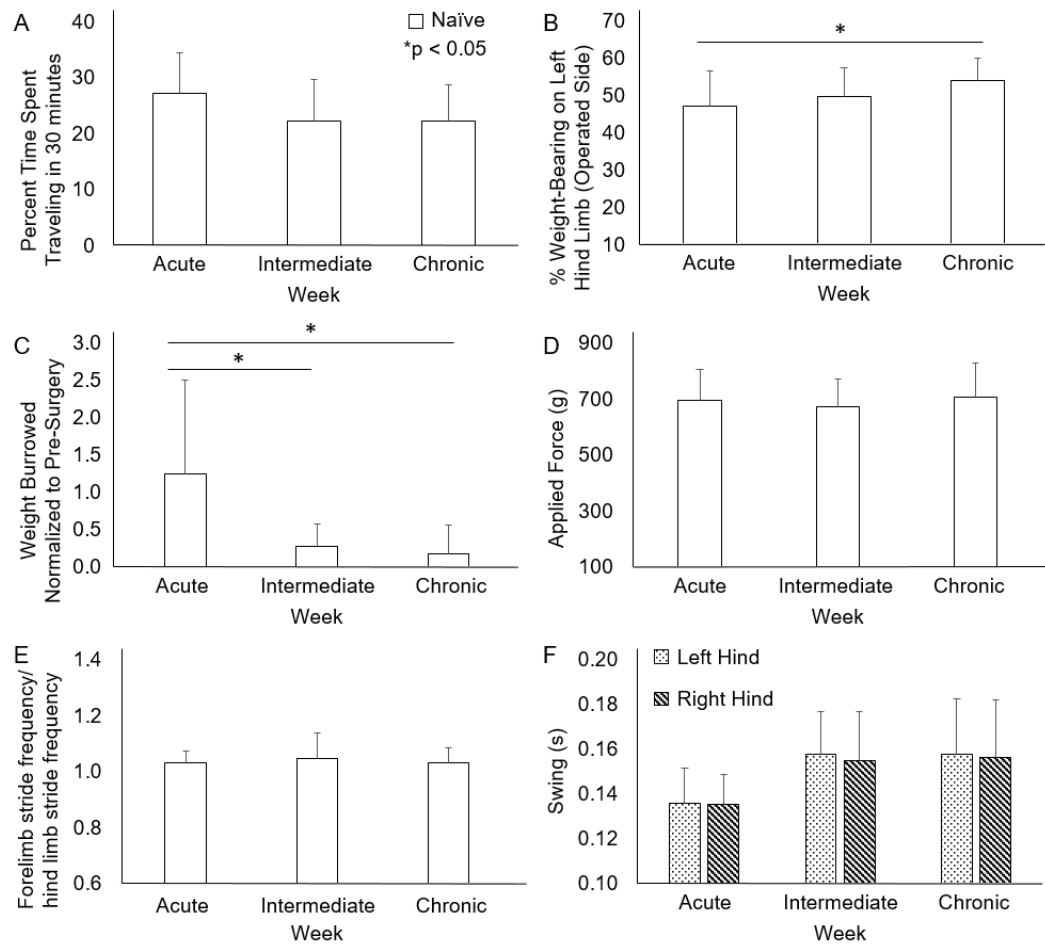


Figure 10: Functional and behavioral measures for Naïve rats over 20 weeks, including open field arena (A), static weight-bearing (B), burrowing (C), pressure hyperalgesia (D), and treadmill gait (E,F). Error bars represent standard deviation.

2.3.3 Differences Between Sham and LDP Groups

LDP rats (n=13) showed a significant decrease in percent time spent traveling over 30 minutes at the intermediate (p=0.049) and chronic (p=0.044) timepoints compared to the Sham control (n=11) as shown in Figure 11.

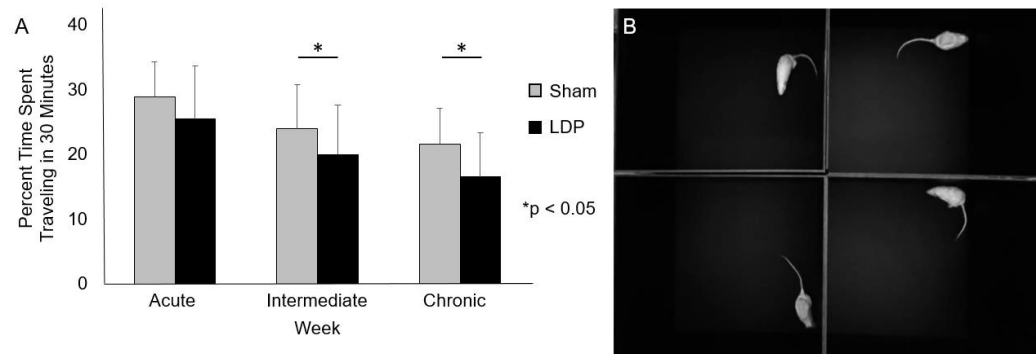


Figure 11: Percent time spent traveling in 30 minutes over 20 weeks for Sham and LDP rats (A). Error bars represent standard deviation. Recording view of rats in open field arenas (B).

LDP rats (n=12) also showed a significant deviation from forelimb versus hind limb gait symmetry at the intermediate ($p < 0.001$) and chronic time points ($p < 0.001$) compared to the Sham control (n=9; Figure 12A). LDP rats showed significantly increased left hind limb swing duration at the intermediate timepoint ($p = 0.0060$; Figure 12E) and trended toward significance at the chronic timepoint ($p = 0.075$). Right hind limb swing duration for LDP rats showed a trend toward a significant decrease at 0-4 weeks ($p = 0.051$; Figure 12F) compared to Sham animals. No significant differences were detected between Sham and LDP rats for measures of static weight-bearing or low back pressure hyperalgesia (Sham n=11, LDP n=13; Figure 12B, D), or weight burrowed (Sham n=5, LDP n=4; Figure 12C).

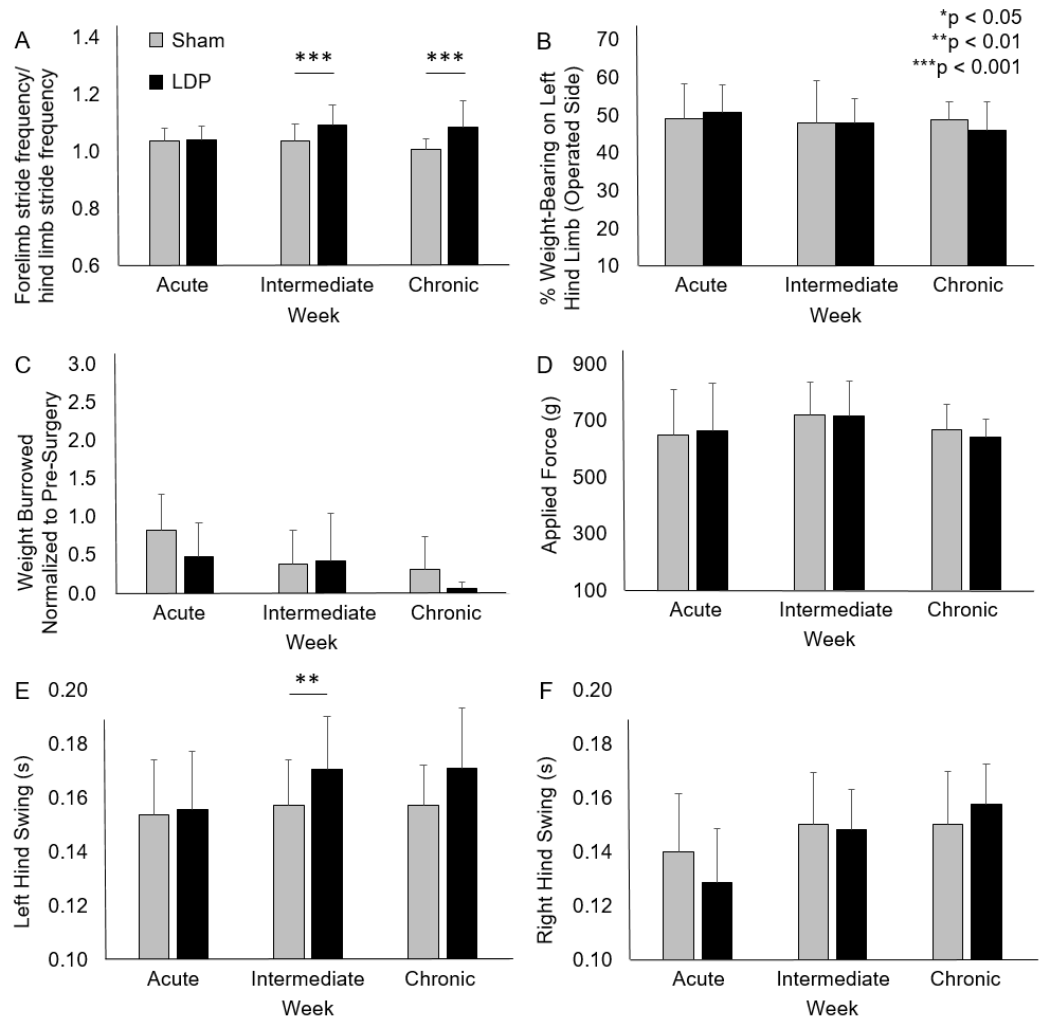


Figure 12: Functional and behavioral measures for Sham and LDP rats over 20 weeks, including treadmill gait (A,E,F), static weight-bearing (B), burrowing (C), and pressure hyperalgesia (D). Error bars represent standard deviation.

No significant differences were seen longitudinally for Naïve rats (n=3) or between Sham (n=6) and LDP (n=8) groups for the pain tolerance on lateral bending maze. Qualitatively, time to complete 2 progressive turns in 2 minutes (Figure 13) seemed to show more differences amongst groups than other tested maze parameters.

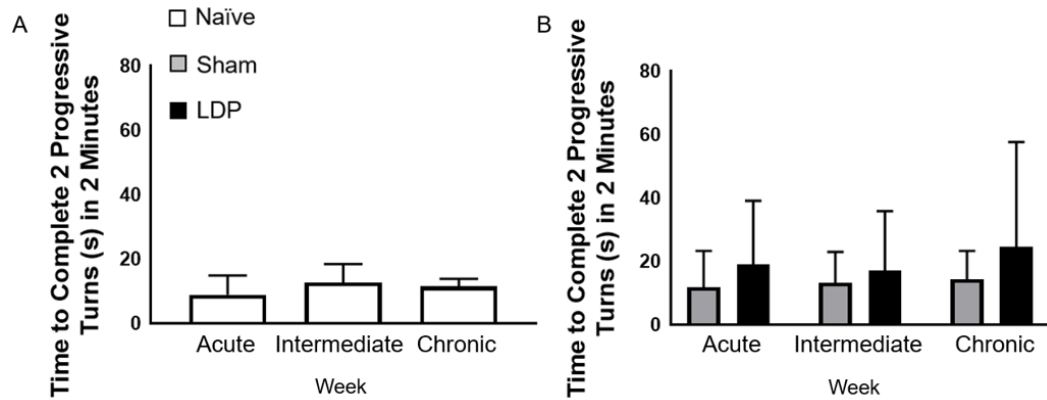


Figure 13: Pain tolerance on lateral bending maze for Naïve rats (A) and Sham and LDP rats (B) over 20 weeks. Error bars represent standard deviation.

2.3.4 Effect Size Calculation

Effect sizes and corresponding power of each assessment which demonstrated differences between the Sham and LDP groups are presented in Table 5. Both percent time spent traveling in 30 minutes and forelimb compared to hind limb gait symmetry showed large effect sizes at the chronic timepoint.

Table 5: Behavioral Assessment Effect Sizes.

Assessment	Effect Size	Power (%)
Percent Time Spent Traveling (30 minutes)	0.80	53
Forelimb versus Hind Limb vs Gait Symmetry	1.1	71

2.4 Discussion

Timeline of model development. This study was performed to characterize the functional and pain-related changes associated development of IVD degeneration following a lumbar disc puncture of one IVD in the rat. Functional and behavioral assessments out to 20 weeks post-surgery identified a distinct timeline of changes

suggestive of pain: acute changes induced by surgical trauma resolved at 4-6 weeks post-surgery, a period resembling baseline values was sustained from 6-16 weeks post-surgery, and changes were again observed at 16-20 weeks post-surgery. These results reveal that rats do not fully recover from the soft tissue trauma and acute pain induced by LDP surgery until 4-6 weeks post-surgery and develop evidence of LDP-related behavioral and gait changes at 16-18 weeks post-surgery.

Phenotypic changes. Lumbar disc puncture of one IVD revealed a functional and behavioral phenotype characterized by decreased percent time spent traveling in 30 minutes as well as decreased hind limb stride frequency compared to that of the forelimbs. Decreased open field activity has previously been shown in models of depression [148] and anxiety [149], as well as painful arthritis [138] and chronic inflammatory pain in rats [150]. However, the current study is the first to use a general activity measure via open field testing as a marker of changes post-IVD puncture and onset of IVD degeneration. This result is clinically relevant, as decreased general activity is well documented in patients with low back pain [151, 152]. Decreased hind limb stride frequency compared to forelimb stride frequency has previously been demonstrated in a spinal cord injury model [153], as the forelimbs compensate for the less functional hind limbs. Effect sizes were calculated at the chronic timepoint to remove time as a variable and focus on differences between groups due to surgical L5-L6 IVD puncture. In addition to statistically significant differences, the effect sizes for both parameters

indicate that the magnitude of the difference between the Sham and LDP groups is large at this timepoint.

This unilateral injury model may result in bilateral functional changes. This is supported by the decreased hind limb step frequency compared to that of the forelimbs as well as a lack of unilateral changes in percent hind limb weight-bearing. An increased sample size is needed to determine bilateral versus unilateral functional changes in hind limb swing duration at the chronic timepoint. Taken together, these results point to behavioral changes in our model which are consistent with those reported for other models of musculoskeletal pathology, including human clinical presentation, and suggest pain-related phenotypic changes with IVD degeneration in this model.

Comparison to literature. Previous studies of surgically-induced IVD degeneration in the rat via puncture of multiple lumbar IVDs with a 26 gauge needle [102] or 0.5 mm drill [103] have reported decreased hind limb swing duration and increased time in stance phase at post-operative week 6 [102]; importantly, this prior study also reported a significantly decreased pressure hyperalgesia threshold in the LDP rats compared to the Sham control from post-operative weeks 2-7 [103], respectively. In our study, we observed resolution of acute changes in swing duration on the operated side at post-operative week 6, significant elevation at 6-16 weeks, and a trend toward elevation at 18-20 weeks, and no significant changes in pressure hyperalgesia. Our finding of no changes in pressure hyperalgesia in this model may be related to our study

of a single degenerate IVD level, which led to a smaller surgical incision site, differences in our surgical approach, and our novel study of periods longer than 7 weeks post-surgery.

2.5 Conclusion

This study identified functional and pain-related changes associated IVD degeneration after a lumbar disc puncture of one IVD in the rat, as well as the timeline of pain development. Utilizing a clinically relevant model of IVD degeneration is critical to understanding the specific mechanisms of pain generation. Longer-term development of activity and gait changes in the LDP model of IVD degeneration may better represent the development of discogenic pain in humans.

3. Effects of IVD Degeneration on DRG Neuron Function In Vitro

3.1 Introduction

Sensory innervation of the peripheral AF of healthy IVDs, as well as the presence of infiltrating nerve fibers in degenerate IVDs has been well established [18, 84]. The absence of infiltrating nerve fibers in asymptomatic IVDs suggests involvement of innervating sensory afferent nerve fibers in nociception and pain from degenerative disc pathology [62, 96, 97] as described in section 1.3.3.

Another spinal pathology with neural involvement, IVD herniation, has also been studied as a source of low back pain. IVD herniation occurs when the AF ruptures, allowing the NP to protrude out of the IVD and onto adjacent neural structures such as DRGs or spinal nerve roots. This leads to mechanical compression of the affected structures, as well as inflammation [154]. Rat models of IVD herniation have demonstrated persistent changes in functional and behavioral assessments associated with pro-inflammatory factors, suggesting that maintenance of inflammation may play a role in chronic pain development [155]. Because of the relationship between IVD herniation and the surrounding neural structures, animal models mimicking clinical IVD herniation have also been widely used to study affected nerves for differences in neuronal nociceptive activity. A study by Shamji and co-workers investigated changes due to NP-induced inflammation in a rat model of radiculopathy where NP from a caudal IVD was placed on the right L5 DRG [156]. These animals showed changes in

gait, mechanical allodynia, and increased local expression of pro-inflammatory cytokines [156]. Allen and co-workers further characterized these behavioral changes and showed that local delivery of soluble TNF receptor type II, a TNF α antagonist, concurrent with NP placement on the right L5 DRG resolved these changes [142]. Hwang and co-workers showed that the nervous system response in this model of radiculopathy extends past the response of the local DRG neurons to include the midbrain portion the central nervous system [157]. A study by Egeland and co-workers investigated nociceptive changes in the sciatic nerve using an ex vivo rat model of IVD herniation where NP tissue from caudal IVDs was placed directly onto the L4-L5 nerve roots. The sciatic nerve was stimulated and electrophysiological recordings from the ipsilateral dorsal horn of the spinal cord were obtained. Results showed a persistent increase in C fiber activity, suggesting that NP application to the nerve roots leads to sensitization of nociceptive pathways at the spinal level [158]. Like IVD herniation, functional neuronal changes may be present in painful IVD degeneration in addition to the described behavioral changes (Chapter 2).

Inflammation induced by surgical IVD puncture can lead to local release of NGF [76], which promotes ingrowth of small, nociceptive DRG neurons with upregulated NGF receptors [18, 84]. NGF acts on TrkA, p75NTR, or TrkA-p75NTR receptor complexes [159] on the central terminals or cell bodies of these nerve fibers to play a role in pain development [84]. NGF binding to TrkA can potentiate the function of TRPV1, a

receptor present on NGF-dependent neurons which responds to chemical and thermal stimuli. This occurs via phosphorylation of TRPV1 channels by serine/threonine kinases including protein kinase C (PKC) [160], protein kinase A (PKA) [79, 161, 162], phosphoinositide-3 kinase [163, 164], and tyrosine kinase c-Src [165]. This could also occur by activation of Ras1 [166] (Figure 14). TRPV1 is inhibited by endogenous phosphatidylinositol-4,5-bisphosphate (PIP₂), but the presence of NGF activates phospholipase C_γ (PLC_γ) via TrkA and results in depleted PIP₂, allowing for activation of TRPV1 [167]. NGF-dependent sensory neurons are often challenged *in vitro* with capsaicin, a chemical stimulant, to assess TRPV1 activity.

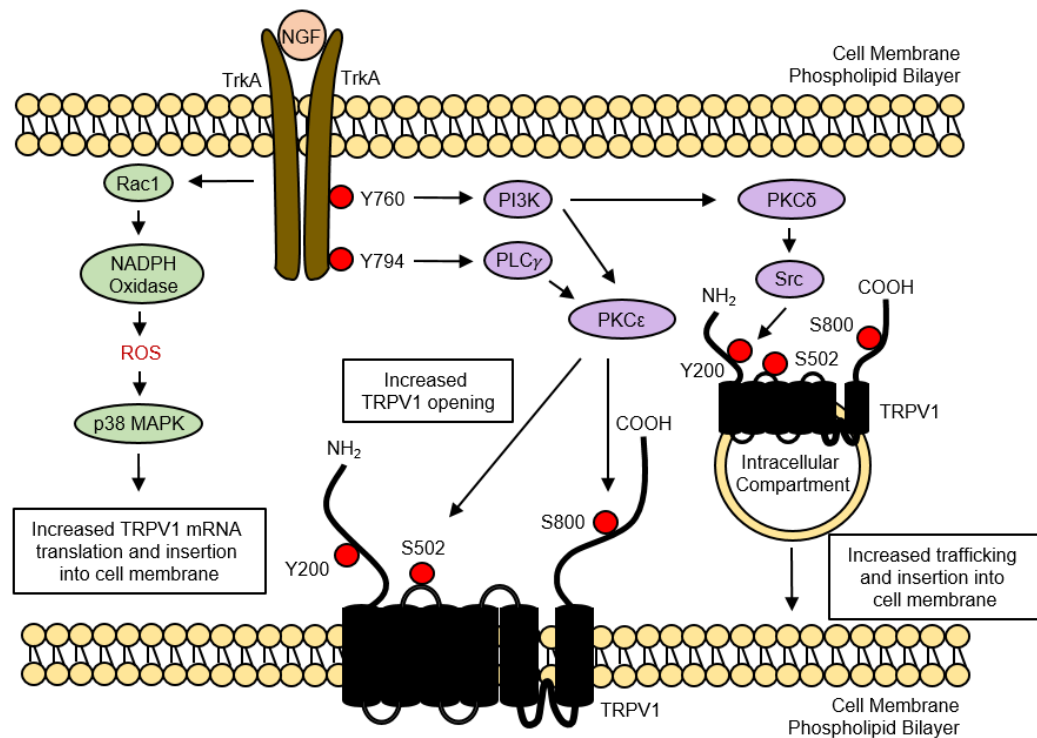


Figure 14: Selected mechanisms of NGF-mediated activation of TRPV1 via TrkA. Green and purple colors represent different biochemical pathways.

For this study, it was important to determine the effect of possible LDP-induced upregulation of NGF on TrkA expression in DRG neurons innervating the degenerate IVD. Therefore, increased expression of TrkA and TRPV1 were investigated via immunohistochemistry (described in Chapter 4) and primary DRG cell isolates were cultured and evaluated for TRPV1 function before and after acute NGF incubation via capsaicin challenge.

3.1.1 Objective

The objective of this study was to evaluate functional neuronal changes in a surgical model of painful IVD degeneration through testing of isolated DRG neurons for sensitivity to capsaicin before and after NGF incubation using calcium signaling.

3.2 *Materials and Methods*

3.2.1 Euthanasia, Exsanguination, and Perfusion

At 20-22 weeks post-surgery (age 38-40 weeks), animals were euthanized with euthanasia solution (euthanasia solution with phenytoin; 150 mg/kg; intraperitoneal) and then exsanguinated via transcardial perfusion with 1X PBS (Gibco Life Technologies, Waltham, MA) using a peristaltic pump (Naïve n=6; Sham/LDP n=9).

3.2.2 Tissue Harvesting and Processing

3.2.2.1 Tissue Harvesting

The dorsal spine was exposed, the posterior elements were removed via laminectomy to expose the spinal cord, and the spinal cord was removed. The DRGs

remained intact within the recesses of the exposed foramen after spinal cord removal due to the stronger connection between the DRGs and peripheral nerves (Figure 15). The spine was then excised, eliminating the peripheral nerve connections. Bilateral L1 and L2 DRGs were extracted from the corresponding foramen and the central and peripheral neural connections were trimmed. The L5-L6 motion segment was also harvested as described in section 4.2.2.

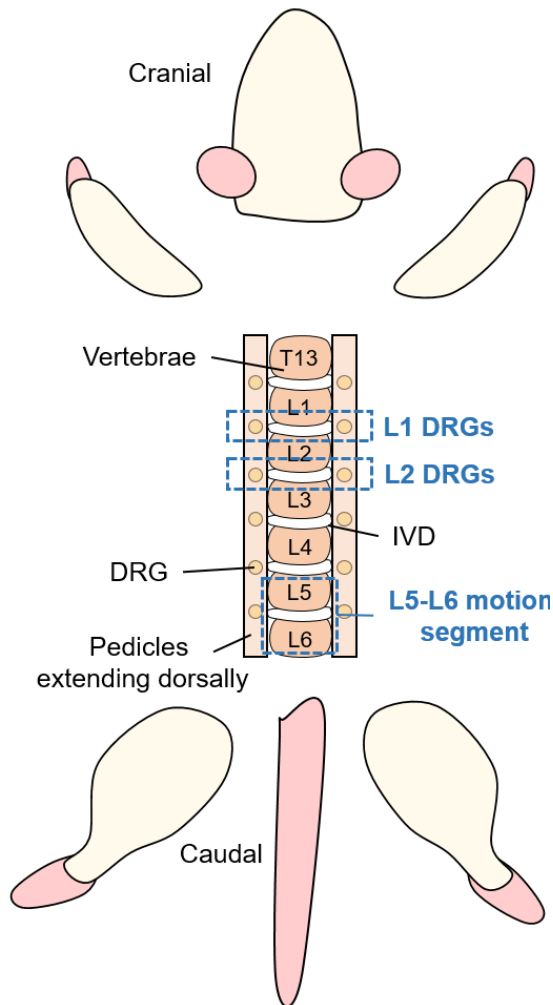


Figure 15: Dorsal view of spine during tissue harvest procedure. This schematic depicts the dorsal view after laminectomy with intact DRGs. DRGs are located within the recesses of exposed foramen, which are at the interface of the vertebrae plane and pedicles.

Bilateral L1 and L2 DRGs from each animal (Naïve n=12 L1 DRGs and n=12 L2 DRGs; Sham/LDP n=18 L1 DRGs and n=18 L2 DRGs) were separated into ipsilateral (left-sided) and contralateral (right-sided) groups and immersed in a solution of Hank's buffered saline solution (1X HBSS) without Ca^{2+} or Mg^{2+} (Gibco) plus 10 mM HEPES (stabilizing solution) and kept on ice for less than 30 minutes.

3.2.3 DRG Cell Isolation

DRGs were first incubated in 45U papain (Worthington, Lakewood, NJ)/L-cysteine (Sigma-Aldrich) in 1X HBSS without Ca²⁺ or Mg²⁺ (Gibco) plus 10 mM HEPES (Gibco) for 20 minutes. Then they were washed with stabilizing solution three times and subsequently incubated for 20 minutes in 1.5 mg/mL collagenase from clostridium histolyticum type II (Sigma-Aldrich) in stabilizing solution. DRGs were then washed three times with stabilizing solution, resuspended in culture medium consisting of Neurobasal A (Gibco) with B27 (Gibco), pen/strep (Gibco), 2 mM glutamax (Gibco), 5% fetal bovine serum (Gibco), and triturated with fire-polished Pasteur pipettes of graded diameters. The dissociated cells were filtered through a 40 µm cell strainer (Corning), plated on 804G (a laminin-rich conditioned media) [168]-coated glass coverslips (12mm diameter; Fisher Scientific, Pittsburgh, PA), and incubated overnight in culture medium. All incubations were done at 37°C and 5% CO₂ humidified air and experiments were performed within 24 hours of plating.

3.2.4 Calcium Imaging

3.2.4.1 Experimental Set-Up

All additional steps were completed while in a dark room. Cells were incubated in 3 µg/ml Fura-2 AM (Invitrogen Life Technologies, Eugene, OR), a fluorescent intracellular calcium indicator, for 45 minutes and then incubated for 30 minutes in external solution constituting 130 mM NaCl (Sigma-Aldrich), 5 mM KCl (Sigma-

Aldrich), 2 mM CaCl₂ (Sigma-Aldrich), 1 mM MgCl₂ (Sigma-Aldrich), 30 mM Glucose (Sigma-Aldrich), 10 mM HEPES (Sigma-Aldrich). For each recording, a coverslip was placed in a perfusion chamber and perfused with external solution at room temperature at a rate of 2 mL/min. Cells were viewed under an inverted microscope (Olympus Optical, Tokyo, Japan) and images were captured with an Orca camera (Hamamatsu Photonics, Hamamatsu City, Japan). SimplePCI Software (Hamamatsu Photonics) was used to manually draw regions of interest (ROIs) around Fura-loaded neurons prior to recording as shown in Figure 16. The ratio of fluorescence emission at an excitation wavelength of 357 and 380 nm was measured for each ROI.

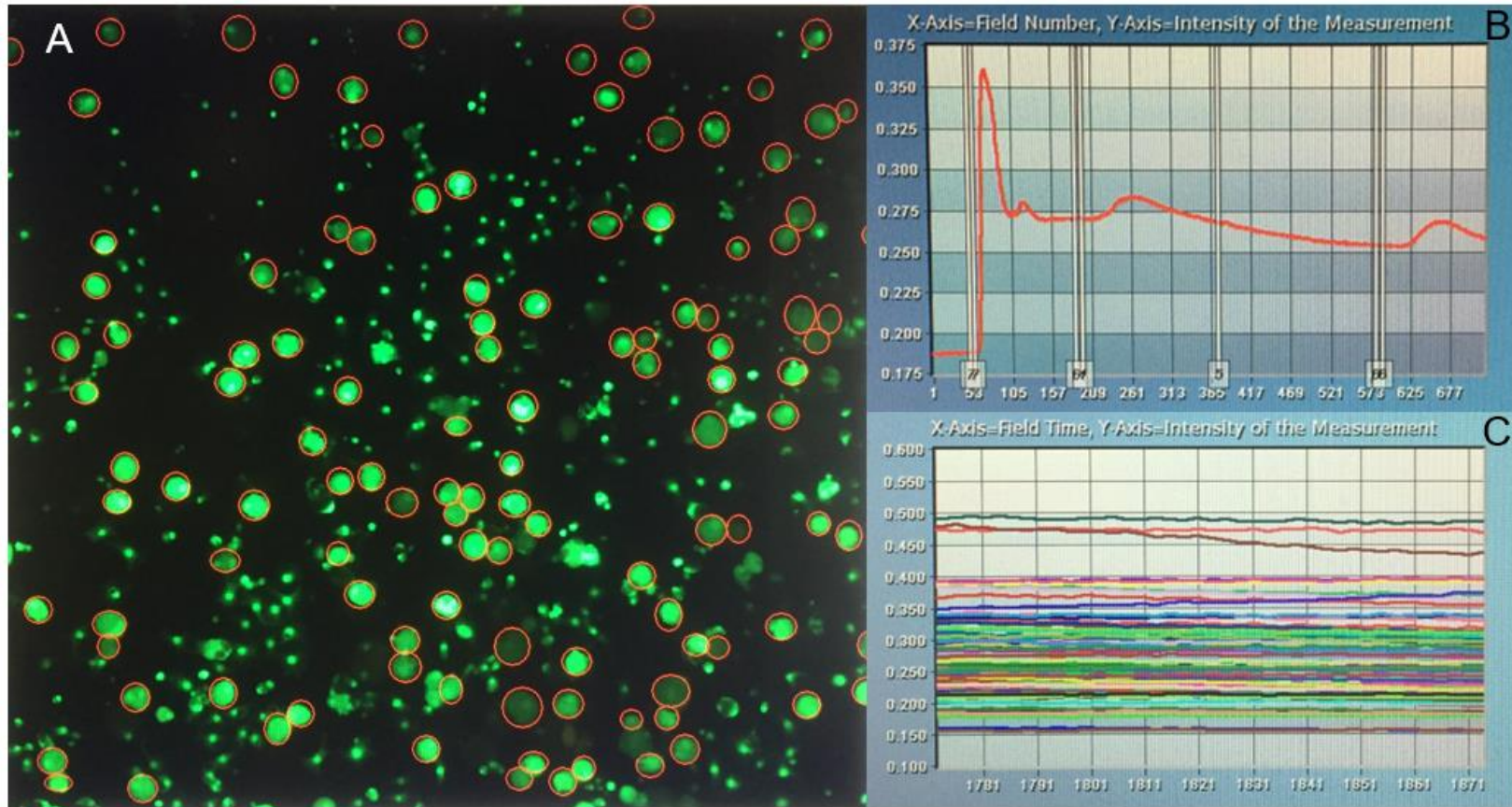


Figure 16: Calcium imaging recording view. Screenshot of neurons identified as ROIs (red circles; A). The ratio of fluorescence emission at an excitation wavelength of 357 and 380 nm (y-axis) averaged over all ROIs. White vertical lines correspond to applications of solutions used during the experimental protocol with external solution washes in between applications (B). The ratio of fluorescence emission at an excitation wavelength of 357 and 380 nm (y-axis) for each individual ROI (C).

3.2.4.2 Experimental Protocol

3.2.4.2.1 High Capsaicin Dose (200 nM) NGF Potentiation Protocol

To determine the percentage of neurons responsive to capsaicin, the experimental protocol recorded a 2 minute baseline with external solution (Sigma-Aldrich), then a 10 second bath application of KCl (50 mM; Sigma-Aldrich) to determine live neurons, followed by external solution wash (>6 minutes; Sigma-Aldrich) to give neurons the opportunity to return to baseline. This was followed by a 20 second application of capsaicin (CAP1; 200 nM; Sigma-Aldrich), >8 minutes of external solution wash (Sigma-Aldrich), 8 minute application of 2.5S NGF (50 ng/mL; Corning, Corning, NY), 20 second application of capsaicin (CAP2; 200 nM; Sigma-Aldrich), and >8 minutes external solution wash.

3.2.4.2.2 Low Capsaicin Dose (100 nM) NGF Potentiation Protocol

To determine the percentage of neurons which were still able to respond to capsaicin after application of CAP1 and NGF incubation, as well as the ratio of CAP2/CAP1 and neurons which responded to CAP2 only, a low capsaicin dose (100 nM) NGF potentiation protocol was used. These studies were done using the same experimental protocol described (section 3.2.4.2.1), but with applications of 100 nM capsaicin for CAP1 and CAP2. A sample recording of 1 neuron is shown in Figure 17.

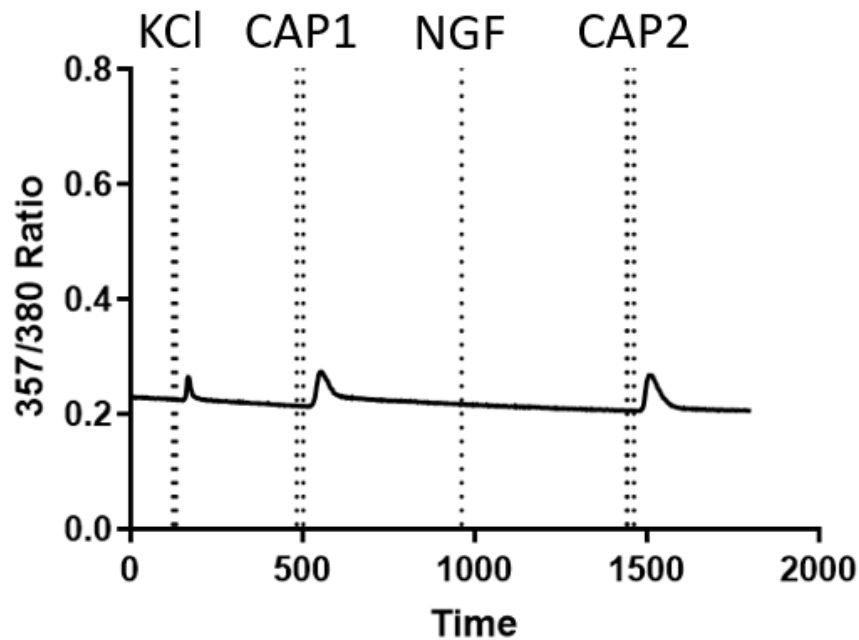


Figure 17: A recording of 1 individual neuron that returned to baseline after every stimulus. Vertical dotted lines correspond to the application and removal of each labeled stimulus with external buffer solution washes. NGF was removed immediately before the application of CAP2.

3.2.5 Data Analysis

3.2.5.1 Determination of Responsive Neurons

Recorded tracings of individual neuron responses over time were plotted using GraphPad Prism (GraphPad Software) to immediately eliminate any non-neuronal cells or cells which did not return to baseline after responding to the application of KCl or CAP1. For the remaining ROIs, the following equation was used to determine the percentage response (PR) to each stimulus:

$$[(\text{Maximum response} / \text{Average Baseline}) - 1] * 100 = PR \quad (2)$$

where the peak amplitude achieved due to the stimulus is compared to the average baseline values of up to 30 seconds before the stimulus was given. A 10% or greater change from the baseline 357 nm/380 nm ratio was considered a positive response. In this way, the total number of alive neurons (positive KCl response) and CAP1-responsive neurons was determined using the high capsaicin dose NGF potentiation protocol. This protocol was used to assess the neuronal response to capsaicin because a dose of 200 nM should elicit a response from every neuron which is able to respond to capsaicin. Differences in the number of CAP1-responsive neurons compared to those which did not respond between the Sham and LDP groups were assessed via Chi-Square tests ($\alpha < 0.05$; GraphPad Software) with ipsilateral and contralateral neurons analyzed separately. Differences in the number of capsaicin-responsive ipsilateral and contralateral neurons within each treatment group were also assessed via Chi-Square tests ($\alpha < 0.05$; GraphPad Software).

3.2.5.1.1 Comparison of CAP1-Responsive Neurons to Prior Work

The percentage of CAP1-responsive neurons at a capsaicin dose of 200 nM from the current study was compared to published raw data from previous studies in rats [79, 169], and the percentage of CAP1-responsive neurons found in these prior studies was also compared via Chi-Square tests ($\alpha < 0.05$; GraphPad Software). These studies stimulated DRG neurons from Naïve adult rats with a capsaicin dose of 1 μ M and

reported the percentage of CAP1-responsive neurons after incubation with 100 [79] and 50 [169] ng/mL NGF.

3.2.5.2 Neurons Responsive to Both CAP1 and CAP2

Neurons which exhibited a positive CAP1 response (section 4.2.5.1) during the low capsaicin dose (100 nM) NGF potentiation protocol experiment were further analyzed for responsiveness to CAP2. Those which showed a positive response to the application of CAP 1 as well as CAP2 were counted and differences between the Sham and LDP groups were assessed via Chi-Square tests ($\alpha < 0.05$; GraphPad Software) with ipsilateral and contralateral neurons analyzed separately. Differences in the number of ipsilateral and contralateral neurons responsive to both doses of capsaicin within each treatment group were also assessed via Chi-Square tests ($\alpha < 0.05$; GraphPad Software).

3.2.5.3 Positive Responses to Only the Second Application of Capsaicin

Many neurons in the low capsaicin dose (100 nM) NGF potentiation protocol experiment showed no response to CAP1, but then a positive response after the application of CAP2. These neurons showing a positive response to only CAP2 (section 4.2.5.1) were counted in a separate analysis and differences between the Sham and LDP groups were assessed via Chi-Square tests ($\alpha < 0.05$; GraphPad Software) with ipsilateral and contralateral neurons analyzed separately. Differences in the number of ipsilateral and contralateral neurons responsive only to the second application of capsaicin within

each treatment group were also assessed via Chi-Square tests ($\alpha < 0.05$; GraphPad Software).

3.2.5.4 CAP2/CAP1 Ratio

All neurons which responded to any application of capsaicin during the low capsaicin dose (100 nM) NGF potentiation protocol experiment were included in the CAP2/CAP1 ratio analysis. CAP2/CAP1 ratio was calculated according to the following formula:

$$PR_{CAP2} / PR_{CAP1} = CAP2 / CAP1 \text{ Ratio} \quad (3)$$

where the PR for each stimulus is calculated based on the peak amplitude relative to baseline as described in section 4.2.5.1 (equation 2). Differences in the ratio of capsaicin responses between the Sham and LDP groups were assessed via unpaired t-tests with Welch's correction ($\alpha < 0.05$; GraphPad Software) with ipsilateral and contralateral neurons analyzed separately. Differences in the ratio of capsaicin responses for ipsilateral and contralateral neurons within each treatment group were also assessed via unpaired t-tests with Welch's correction ($\alpha < 0.05$; GraphPad Software).

3.2.5.4.1 Effect Size Calculation

The effect size (Cohen's *d*) of the difference between Sham and LDP groups at the chronic timepoint was determined for the CAP2/CAP1 ratio. Results were classified as either small (0.20-0.49), medium (0.50-0.79) or large (≥ 0.80) and were entered into

G*Power 3.0.10 (Heinrich Heine University Düsseldorf) to compute the achieved power as described in section 2.2.5.3.1.

3.2.5.4.2 Neurons with CAP2/CAP1 Ratio Greater Than 1

To further characterize the neuronal response to capsaicin, the distribution of CAP2/CAP1 ratio values amongst groups was examined. Differences in the number of neurons with CAP2/CAP1 ratio values of less than 1 and greater than 1 were assessed via Fisher's exact test ($\alpha < 0.05$; GraphPad Software).

3.3 Results

The high capsaicin dose (200 nM) NGF potentiation protocol revealed a significantly increased number of CAP1-responsive neurons in the Sham group compared to the LDP group for both the ipsilateral ($p=0.016$) and contralateral ($p=0.036$) DRG neurons (Figure 18; Table 6). No differences in responsiveness to CAP1 were shown between the ipsilateral and contralateral neurons for any treatment group (Table 6).

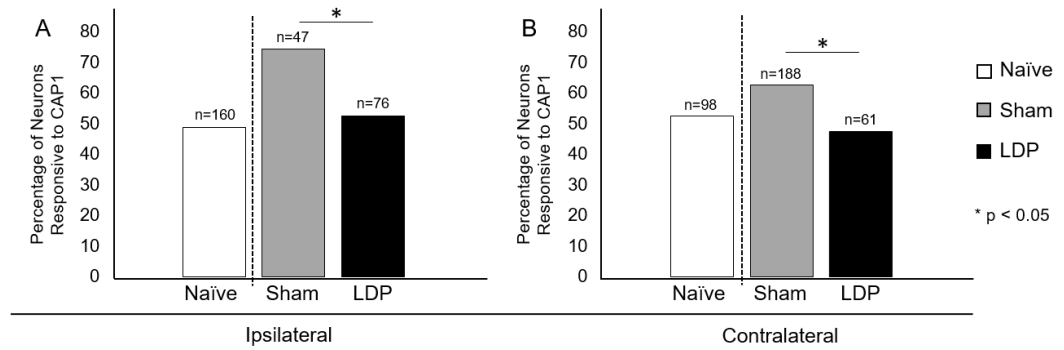


Figure 18: Percentage of neurons responsive to application of CAP1. Responsiveness of the ipsilateral (A) and contralateral (B) L1 and L2 DRG neurons to the high capsaicin dose (200 nM) NGF potentiation protocol. Total number of neurons in each group are given above the corresponding bars and results are expressed as a percentage of those neurons.

Table 6: Calcium Imaging Results. Naïve, Sham, and LDP entries indicate comparison of ipsilateral and contralateral neuronal responses in the corresponding group.

NGF Potentiation Protocol	Measure (Percentage of Neurons)	Comparison	p value
High Capsaicin Dose (200 nM)	Response to CAP1	Sham vs LDP Ipsilateral	0.016
		Sham vs LDP Contralateral	0.036
		Naïve	0.63
		Sham	0.13
		LDP	0.55
Low Capsaicin Dose (100 nM)	Response to CAP1 AND CAP2	Sham vs LDP Ipsilateral	0.21
		Sham vs LDP Contralateral	0.042
		Naïve	0.26
		Sham	0.31
		LDP	0.75
Low Capsaicin Dose (100 nM)	Response to CAP2 Only	Sham vs LDP Ipsilateral	0.014
		Sham vs LDP Contralateral	0.14
		Naïve	0.46
		Sham	0.12
		LDP	0.024
Low Capsaicin Dose (100 nM)	CAP2/CAP1 Ratio	Sham vs LDP Ipsilateral	0.052
		Sham vs LDP Contralateral	0.75
		Naïve	0.35
		Sham	0.20
		LDP	0.16
Low Capsaicin Dose (100 nM)	CAP2/CAP1 Ratio >1	Sham vs LDP Ipsilateral	0.082
		Sham vs LDP Contralateral	0.59
		Naïve	0.44
		Sham	0.73
		LDP	0.012

Previous studies found that 67% [79] and 76% [169] of rat DRG neurons were capsaicin-responsive on electrophysiology and calcium imaging, respectively (Table 7). These results were not significantly different from each other ($p=0.18$). However, results found using the high capsaicin dose (200 nM) protocol were significantly different from

those found by Shu and Mendell ($p=0.048$), as well as Oh and co-workers ($p<0.0001$; Table 7).

Table 7: Comparison of CAP1-Responsive Neurons to that of Prior Studies.

Study	CAP1-Responsive Neurons (%)	Number CAP1-Responsive Neurons	Total Number Alive Neurons	Comparison	p value
High Capsaicin Dose (200 nM)	51	132	258	High Capsaicin Dose (200 nM) vs Shu and Mendell 1999	0.048
Shu and Mendell 1999	67	32	48	High Capsaicin Dose (200 nM) vs Oh and Miller 2001	<0.0001
Oh and Miller 2001	76	120	157	Shu and Mendell 1999 vs Oh and Miller 2001	0.18

Compared to the Sham group, the contralateral LDP group showed a significantly decreased number of CAP2-responsive neurons out of those which had already responded to capsaicin ($p=0.042$; Figure 19B). The ipsilateral neurons showed no differences between groups (Figure 19A), and no differences were detected between the ipsilateral and contralateral neurons for any treatment group (Table 6).

The number of ipsilateral neurons in the LDP group which responded only to CAP2 was significantly decreased compared to that of the Sham group ($p=0.014$), with zero ipsilateral neurons responding for the LDP group (Figure 19C). The contralateral neurons showed no differences between groups (Figure 19D). In addition, the number of ipsilateral LDP neurons which responded to only CAP2 was significantly decreased compared to contralateral LDP neurons ($p=0.024$). No differences were detected between the ipsilateral and contralateral neurons for the Sham and Naïve groups (Table 6).

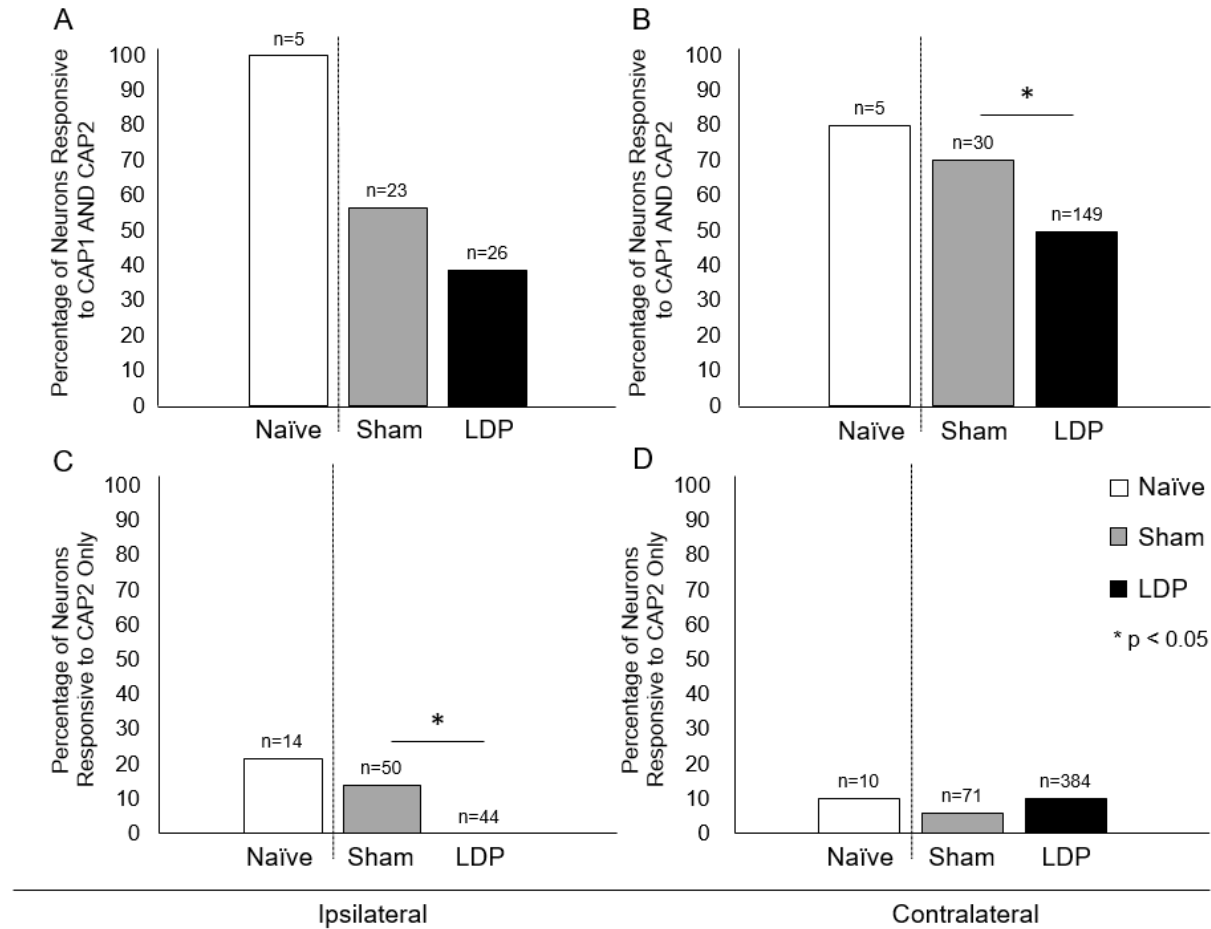


Figure 19: Percentage of L1 and L2 DRG neurons responsive to both applications of capsaicin (A, B) and CAP2 only (C, D) during the low capsaicin dose (100 nM) NGF potentiation protocol. Total number of neurons in each group are given above the corresponding bars and results are expressed as a percentage of those neurons.

The ipsilateral LDP neurons showed a strong trend toward a significant decrease of the CAP2/CAP1 ratio compared to those of the Sham group ($p=0.052$; Figure 20A). No differences were detected in the CAP2/CAP1 ratio between the contralateral Sham and LDP neurons (Figure 20B) or between ipsilateral and contralateral neurons for any treatment group (Table 6).

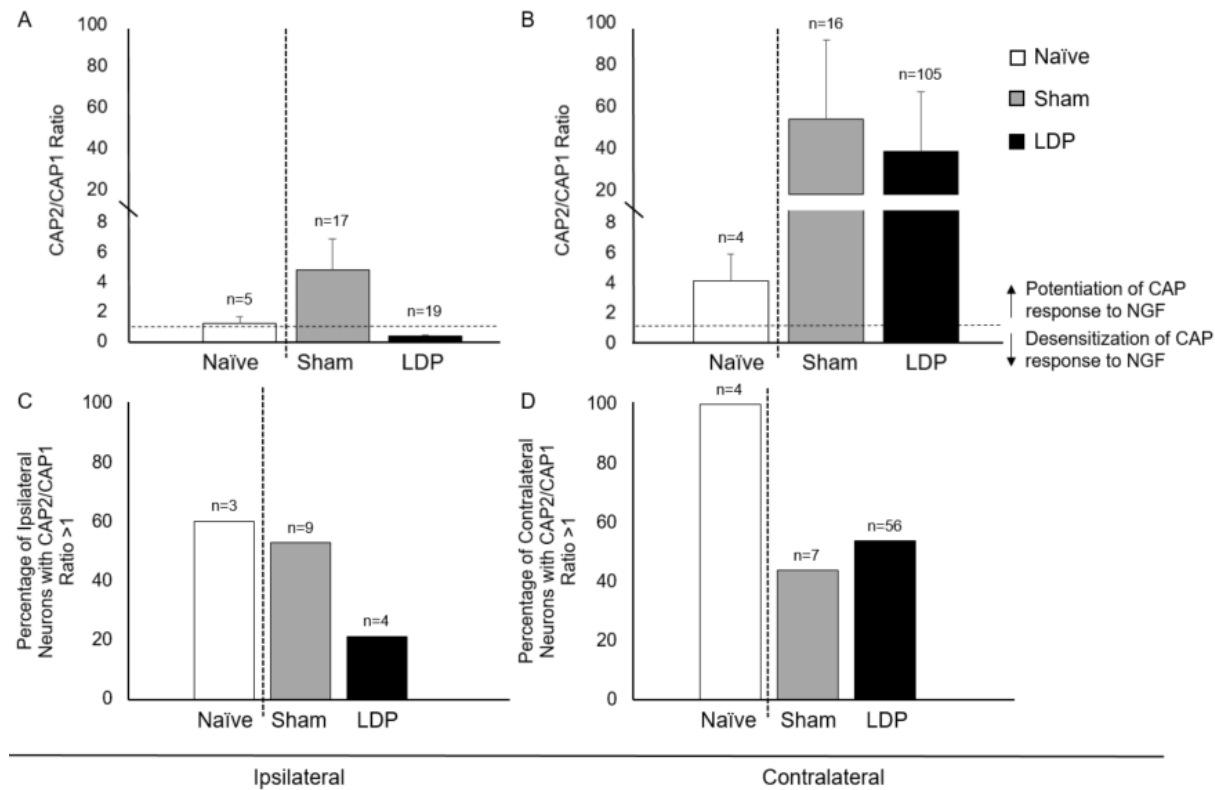


Figure 20: L1 and L2 DRG neuron CAP2/CAP1 ratios (A, B) and the percentage of neurons with a CAP2/CAP1 ratio greater than 1 (C, D) during the low capsaicin dose (100 nM) NGF potentiation protocol. CAP2/CAP1 ratios were calculated from neuronal responses to capsaicin. A CAP2/CAP1 ratio equal to 1 (horizontal dotted line) indicates equivalent neuronal responses to both applications of capsaicin. A CAP2/CAP1 ratio greater than 1 indicates potentiation of the capsaicin response to NGF, meaning that the neuronal response to CAP2 was greater than that to CAP1. A CAP2/CAP1 ratio less than 1 indicates desensitization of the capsaicin response to NGF, meaning that the neuronal response to CAP2 was less than that to CAP1. Error bars represent standard error of the mean (SEM). Total number of neurons in each group are given above the corresponding bar.

The percentage of ipsilateral LDP neurons with a CAP2/CAP1 ratio greater than 1 trended toward a significant decrease compared to those of the Sham group ($p=0.082$; Figure 20C) and was significantly decreased compared to that of the contralateral LDP neurons ($p=0.012$; Table 6). No differences were detected in the percentage of neurons with a CAP2/CAP1 ratio greater than 1 between the contralateral Sham and LDP neurons (Figure 20D) or between ipsilateral and contralateral neurons for the Naïve or Sham treatment groups (Table 6).

3.3.1 Effect Size Calculation

The effect size and corresponding power for the comparison of CAP2/CAP1 ratio between Sham and LDP neurons are presented in Table 8. CAP2/CAP1 ratio showed a medium effect size at the chronic timepoint.

Table 8: CAP2/CAP1 Ratio Effect Size.

Assessment	Effect Size	Power (%)
CAP2/CAP1	0.72	55

3.4 Discussion

Comparison to previous studies. This study was performed at the chronic timepoint to characterize the effects of IVD degeneration on DRG neuron function in vitro. Previous studies stimulated DRG neurons from Naïve adult rats with a capsaicin dose of 1 μ M and found the percentage of capsaicin-responsive neurons on electrophysiology [79] and calcium imaging [169] after incubation with 100 and 50

ng/mL NGF, respectively. Comparing these prior findings revealed no significant differences. However, these results were significantly different from those of the current study, which can be attributed to the 10-fold higher capsaicin dose used in the previous studies.

Neuronal responses to high dose capsaicin. Neuronal responses to CAP1 during the high capsaicin dose (200 nM) protocol revealed a possible sham-effect, where an increased number of both the ipsilateral and contralateral DRG neurons of the Sham group responded compared to those of the LDP group.

Neuronal responses to low dose capsaicin. For neurons which responded to CAP1 with the low capsaicin dose (100 nM) NGF potentiation protocol, their ability to respond to CAP2 was unaffected except for the contralateral LDP neurons (50%) compared to those of the Sham group (70%). However, many contralateral LDP neurons which did not respond to CAP1 were recruited by NGF incubation and responded to CAP2. This was not the case for ipsilateral LDP neurons. Ipsilateral LDP neurons which responded to CAP1 showed no difference in their ability to respond to CAP2, but those which did not respond to CAP1 remained unresponsive even after incubation with acute NGF. This could indicate that the neuron had been exposed to minimal NGF previously and was sensitized by the NGF incubation, meaning that NGF led to the recruitment of TRPV1 receptors to the membrane surface. This would then allow the neuron to achieve a positive response to CAP2. The significant differences in the number of neurons

responding to only CAP2 between the ipsilateral Sham and LDP groups, as well as between the ipsilateral and contralateral LDP neurons can be attributed to zero ipsilateral LDP DRG neurons responding to only CAP2. This means that 100% of the time in this study, if a given ipsilateral LDP neuron did not respond to CAP1, it also did not respond to CAP2. One explanation could be that these cells underwent chronic exposure to NGF in vivo, which altered the ability of TRPV1 to sensitize to further acute NGF. Additional possible explanations for these results are discussed in conjunction with immunostaining results in Chapter 4.

CAP2/CAP1 ratios. The ratio of capsaicin responses was determined for all capsaicin-responsive DRG neurons from data obtained using the low dose capsaicin (100 nM) NGF potentiation protocol. The ipsilateral LDP neuron CAP2/CAP1 ratio showed a strong trend toward being significantly decreased compared to both the ipsilateral Sham neurons and contralateral LDP neurons. In addition, only the ipsilateral LDP group showed desensitization of TRPV1 to capsaicin after incubation with NGF (CAP2/CAP1 < 1). All other groups showed a sensitization response (CAP2/CAP1 > 1). A CAP2/CAP1 ratio of greater than 1 is expected in healthy capsaicin-responsive neurons. The percentage of ipsilateral LDP neurons with a CAP2/CAP1 ratio greater than 1 also showed a strong trend toward being significantly decreased compared to ipsilateral Sham neurons. This indicates that the desensitization response to capsaicin shown by the ipsilateral LDP neurons was representative of the neuronal population, as 79% of

these individual neurons showed a desensitization response. Despite no statistically significant differences, the effect size for the CAP2/CAP1 ratio indicates a substantial difference between the ipsilateral Sham and LDP neurons at this timepoint.

The medium effect size of desensitization of TRPV1 to capsaicin after incubation with NGF in ipsilateral DRG neurons, taken together with the trend toward increased number of neurons responsive to CAP1, pronounced change in the number of neurons responding to CAP2 after responding to CAP1, and zero neurons responding to CAP2 only, show that the ipsilateral LDP DRG neurons are functionally different at this chronic timepoint.

One limitation in this work was the possible bias introduced while identifying the ROIs. A neuron could be missed and not identified until the calcium imaging experimental protocol had started, excluding it from the data collection process. In addition, a small neuron could appear similar to a large satellite cell and therefore not be identified as an ROI. This could lead to a selection bias for larger neurons and brighter fluorescence. The other substantial limitation in this work was the low number of animals included in the Naïve group for the low capsaicin dose (100 nM) NGF potential protocol studies, and a resulting low neuron yield. Increasing the number of rats in the Naïve group would increase the neuron sample size and lead to data from a more representative neuronal population.

3.5 Conclusion

This study identified functional neuronal changes in a surgical model of IVD degeneration in a rat through testing of isolated DRG neurons in vitro. L1 and L2 DRG neurons responded as expected to the NGF potentiation protocols, except for the unilateral DRG neurons in the LDP group. Puncture of the L5-L6 IVD led to unilateral changes in the L1 and L2 DRG neurons as predicted based on the known innervation pattern of the lateral aspect of this IVD. However, some contralateral changes were also detected in the LDP neurons, suggesting that injury to the lateral aspect of the IVD resulted in functional changes to the ipsilateral neurons at 20 weeks post-surgery, with a slower progression of changes to the contralateral neurons. Based on these results, puncture of this single IVD is an adequate model for future studies to further elucidate specific mechanisms of pain in IVD degeneration.

4. Characterization of IVD and DRG Changes in IVD Degeneration Model

4.1 Introduction

The degree of IVD degeneration is often assessed via morphologic changes, which can be seen on histology. However, differentiating between painful IVD degeneration and non-pathologic age-related changes using histologic or imaging methods remains a clinically relevant challenge. Prior studies have focused on developing a histologic classification system to best define the grade of IVD degeneration for comparison to a variety of outcomes, including age-related IVD changes and pain [55, 170-172]. A review of 30 lumbar IVD degeneration grading systems revealed a high degree a variability between them, making comparisons amongst studies difficult [173]. Recommended criteria for a more standardized grading system of IVD degeneration includes a scale of three to five grades starting with the non-degenerate state as grade zero [173]. Such a system has been used in a mouse tail model of IVD degeneration and successfully differentiated between groups [174].

Injured IVDs have elevated levels of NGF [76], which can sensitize primary afferent neurons through TrkA [64] as discussed in Chapters 1 and 3. Nerve fibers expressing TrkA have been shown to innervate painful IVDs in humans [84], and fibers expressing both TrkA and p75NTR innervate non-pathologic IVDs in rats [175]. A study by Pezet and co-workers investigated sensory neuron changes due to elevated NGF in a Freund's adjuvant-induced arthritis model of rat hind paws over 12 weeks. Results

showed an increase in p75NTR during acute inflammation and a subsequent increase in TrkA protein levels via Western blot analysis, which was associated with a long-lasting inflammatory response [77]. These receptors have also been implicated in neuropathic pain as shown by a model of spinal nerve ligation, where nerve injury increased p75NTR expression as well as phosphorylation of TrkA in uninjured sensory neurons. Inhibition of p75NTR led to decreased TRPV1 channel activation and reversal of neuropathic pain [176].

Changes in DRG neurons have been studied extensively in the context of nerve injury and regeneration. DRG avulsion is a brachial plexus injury where the spinal nerve roots are violently pulled away from the spinal cord, resulting in a disrupted connection between it and the affected DRGs. Treatment to restore even partial sensory function requires surgical reimplantation of the avulsed nerve roots and axonal regeneration. Nerve injury in this pathology is characterized by an increased number of TRPV1-positive neurons [177, 178] and altered levels of NGF, GDNF, and the GDNF receptor, Ret [179, 180]. A study by Anand and co-workers cultured neurons from avulsed DRGs with neurotrophic factors such as NGF and determined that these factors lead to neuronal hypertrophy, elevated TRPV1 levels, and enhanced capsaicin responses [181].

DRG neurons also undergo morphologic changes after peripheral nerve injury. Depending on the type of injury, short-term changes after injury include Wallerian axonal degeneration, and possibly apoptosis. Apoptosis is characterized by chromatin

condensation, nuclear fragmentation, and formation of cytoplasmic blebs [182]. The sizes of the nucleolus [183] and mitochondria [184] increase, cellular DNA is degraded, and the cell breaks apart into fragments [185]. However, surviving neurons may begin to show changes associated with axonal regeneration. This includes nuclear and neuronal hypertrophy due to increased metabolic and transcriptional activity [186], as well as collateral sprouting of the axon toward the distal site [187]. An increasing number of genes associated with axon growth are also upregulated during this phase, including IL6, IGF1, FGFR3, NPY, GAP43, and CSF1 [188].

For this study, it was important to confirm IVD degeneration due to the surgical lumbar disc puncture, as well as detect changes to innervating DRG neurons to further explain the described functional changes (Chapter 3). Therefore, IVD sections were stained and graded for severity of degenerative changes and DRG sections were immunostained for TrkA, p75NTR, and TRPV1 to assess NGF-related changes.

4.1.1 Objective

This study was performed to confirm IVD degeneration and assess changes to innervating DRGs 20 weeks after a surgical lumbar disc puncture injury.

4.2 Materials and Methods

4.2.1 Euthanasia, Exsanguination, and Perfusion

At 20-22 weeks post-surgery (age 38-40 weeks), animals were euthanized with euthanasia solution (euthanasia solution with phenytoin; 150 mg/kg; intraperitoneal)

and then exsanguinated via transcardial perfusion with 1X PBS (Gibco) followed by 150 mL of 4% paraformaldehyde (PFA) in PBS, with all procedures using a peristaltic pump (n=3 per group).

4.2.2 Tissue Harvesting and Processing

4.2.2.1 Tissue Harvesting

Tissues were harvested as described in section 3.2.2. The L5-L6 motion segment of each animal was also harvested with intact endplate and some vertebral bone as shown in Figure 15 (n=3 per group).

4.2.2.2 Tissue Processing

4.2.2.2.1 L5-L6 IVDs

L5-L6 IVDs were post-fixed in 4% PFA for 48 hours at 4°C and decalcified using Immunocal (StatLab, McKinney, TX) for 72 hours at 4°C, with solution changes every 24 hours. Then specimens were immersed in a solution containing 30% sucrose for 24 hours at 4°C, and then set in OCT Tissue Tek (Sakura Finetek Japan, Tokyo) overnight at 4°C. Specimens were then placed in fresh OCT Tissue Tek (Sakura Finetek Japan), frozen in liquid nitrogen, and stored at -80°C.

4.2.2.2.2 L1-L2 DRGs

L1-L2 bilateral DRGs were post-fixed in 4% paraformaldehyde for 48 hours at 4°C, immersed in 30% sucrose solution for 24 hours at 4°C, embedded in OCT Tissue Tek (Sakura Finetek Japan), frozen in liquid nitrogen, and stored at -80°C.

4.2.3 Histology & Immunohistochemistry

4.2.3.1 L5-L6 IVD Histology

L5-L6 IVDs were sectioned in the frontal plane at a thickness of 7-9 μ m on a Leica CM1950 cryostat (Leica Microsystems; Wetzlar, Germany), and sections were mounted on glass slides so that 2 consecutive sections were mounted every 28 μ m. One slide from the anterior, mid-section, and posterior aspects of each IVD was post-fixed with 4% PFA and stained with 0.1% safranin-O (Sigma-Aldrich, St. Louis, MO) and 0.02% fast green (Sigma-Aldrich), and then coverslips were mounted with Permount (Fisher Scientific, Chicago, IL) and examined at 5X using the brightfield settings on a confocal microscope (Model DM6; Leica Microsystems).

4.2.3.2 DRG Immunohistochemistry

4.2.3.2.1 Bilateral L1 DRGs

Each L1 DRG was sectioned at 7 μ m thickness on a cryostat (Leica Microsystems). Every L1 DRG section was collected (2 sections per slide; one section for a control antibody and one for the specific target), and mounted on glass slides. One section from each rat (n=3 per treatment group) was randomly selected for immunostaining per target of interest. Sections were washed in 0.1M Tris (pH 7.6), blocked in Tris-BSA (pH 7.6; 0.005% BSA) and then 10% serum in Tris-BSA for 1 hour, washed and blocked again in 0.1M Tris and Tris-BSA, respectively, and then incubated with a primary antibody (Table 9) in Tris-BSA overnight at 4°C. After this first incubation, sections were washed

in 0.1M Tris, incubated with an Alexa Fluor 488 conjugated goat anti-rabbit IgG (5 $\mu\text{g}/\text{mL}$; Abcam; Cambridge, MA) for 2 hours at room temperature, and then stained with propidium iodide (PI; 1:5; Sigma-Aldrich) for cell morphology after subsequent washing in 0.1M Tris. Sections were mounted with ClearMount (Life Technologies; Frederick, MD), and examined at 20X using a confocal microscope (Leica Microsystems).

Table 9: IHC Targets for L1 DRGs.

Target	Primary Antibody	Secondary Antibody
TrkA	rabbit anti-TrkA	Alexa Fluor 488 conjugated goat anti-rabbit
p75NTR	rabbit anti-p75NTR	Alexa Fluor 488 conjugated goat anti-rabbit

4.2.3.2.2 Bilateral L2 DRGs

To obtain *in vivo* neuronal cell counts, one L2 DRG per treatment group was sectioned at 10 μm thickness on a cryostat (Leica Microsystems) and sections were mounted on glass slides. Five sections were used for staining (sections separated by $\geq 110\mu\text{m}$) to ensure that each neuron was counted only once [189]. Staining procedures were followed as described (section 4.2.1.5.1). Sections were incubated overnight at 4°C with a rabbit anti-TRPV1 primary antibody (Table 10) to determine the presence of TRPV1 receptors. After washing, sections were incubated with an Alexa Fluor 488 goat anti-rabbit IgG (5 $\mu\text{g}/\text{mL}$; Abcam) for 2 hours at room temperature and then incubated overnight at 4°C with a mouse anti-PGP9.5 primary antibody (5 $\mu\text{g}/\text{mL}$; Abcam) to identify neurons. After washing, sections were incubated with an Alexa Fluor 633 goat

anti-mouse antibody (5 µg/mL; Abcam; Table 9) for 2 hours at room temperature, and then stained with PI (1:5; Sigma-Aldrich) for cell morphology. Stained sections were mounted with ClearMount (Life Technologies), and imaged at 20X using a confocal microscope (Leica Microsystems).

Table 10: IHC Targets for L2 DRGs.

Target	Primary Antibody	Secondary Antibody
PGP9.5	mouse anti-PGP9.5	Alexa Fluor 633 conjugated goat anti-mouse
TRPV1	rabbit anti-TRPV1	Alexa Fluor 488 conjugated goat anti-rabbit

4.2.4 Data Analysis

4.2.4.1 L5-L6 IVD Histology

Frontal histologic sections (n=3 sections per IVD; anterior, mid-section, posterior) were ordered randomly and graded to consensus by two investigators blinded to treatment group and other identifiers. Grading criteria were modified from Tam and co-workers [174], which focus on morphologic changes to the AF and NP regions of the IVD, as well as the border between them (Table 11). Each section was evaluated for grade of degeneration on a 0-4 scale with grades of 0-1 considered as non-degenerate, 2-3 as moderately degenerate, and 4 as degenerate. The section with the most advanced degeneration was assigned as the grade of degeneration for each individual IVD. Grades were then averaged to obtain one overall measurement per treatment group and the

Wilcoxon rank-sum test was used to determine differences in the severity of degeneration between Sham and LDP treatment groups (GraphPad Software).

Table 11: IVD Histology Grading Criteria. Modified from Tam and co-workers [174].

Grade	Description
0	AF lamellae clearly defined and not disrupted with clear border between AF and NP NP compartment occupied predominantly by large cell mass
1	AF moderately serpentine with/without rupture NP cell mass has honey comb-like structure with fragmentation into smaller cell clusters
2	AF severely serpentine with rupture. Border between AF and NP less defined NP has many small cell clusters
3	AF lamellae indistinct and disorganized NP has few cell clusters with/without minor cleft formation
4	AF has cleft formation with/without lamella fragmentation NP compartment lost and occupied by connective tissue

4.2.4.1.1 Effect Size Calculation

The effect size (Cohen's *d*) of the difference between Sham and LDP groups at the chronic timepoint was determined for grade of IVD degeneration. Results were classified as either small (0.20-0.49), medium (0.50-0.79) or large (≥ 0.80) and were entered into G*Power 3.0.10 (Heinrich Heine University Düsseldorf) to compute the achieved power as described in section 2.2.5.3.1.

4.2.4.2 Correlations Between Pain-Related Behavioral Changes and Histology

Correlation analysis was performed for behavioral changes against grade of IVD degeneration on histology at the 20 week timepoint. This was done using data from each animal that completed the open field and treadmill gait assessments and the

corresponding histology grade for each IVD, which were ranked (GraphPad Software) and then correlated across all groups using the CORREL function in Microsoft Excel to yield Spearman's rank-order correlation coefficient (r_s). Spearman's correlation coefficient was tested for significance against the null hypothesis that $r_s=0$ ($\alpha<0.05$). For these datasets and a two-tailed analysis, significance was declared if $r_s<-0.35$ or >0.35 , or $r_s<-0.39$ or >0.39 [190], respectively as shown in Table 12.

Table 12: Assessments and Critical Values Used for Correlation Analysis.

Assessment Parameter Compared to Histologic Grade	Sample Size (n)	Critical Value for Spearman's Rho (r_s)
Percentage time spent traveling in 30 minutes	32	0.35
Forelimb versus hind limb step frequency	26	0.39
Left hind limb swing duration (s)	26	0.39

4.2.4.3 DRG Immunohistochemistry

4.2.4.3.1 Quantitative Analysis Using ImageJ Software

DRG images were first opened in ImageJ and stitched together using the paired stitching and grid/collection stitching plugins as described by Preibisch and co-workers [191]. The resulting stitched image was duplicated and separated into individual channels, with one channel representing each stain (section 3.2.3.2). Neurons (Figure 21A) were manually segmented into ROIs on the composite image (Figure 21B) based on the PI staining for neuron morphology, and subsequent analyses were performed automatically via ImageJ. ROIs were combined and thresholded using the isodata algorithm [192] to output a binary image (Figure 21C). The percentage of pixels above the threshold (white; Figure 21C) determined the area fraction of positive stain in each

neuron ($area_{cytoplasm}$). The mean intensity of positively stained pixels for each ROI ($I_{cytoplasm}$) was calculated using the green channel, which corresponded to immunostaining for the antibody of interest (TrkA, p75NTR, TRPV1). ROIs were also analyzed for area (μm^2) and maximum diameter (μm).

Background regions were defined as all pixels outside the combined ROIs on the green channel. Huang's fuzzy thresholding method [193] was applied to the image background to identify pixels of background fluorescence (white; Figure 21D). The average background fluorescence was calculated as the mean intensity of these pixels using the green channel ($I_{background}$).

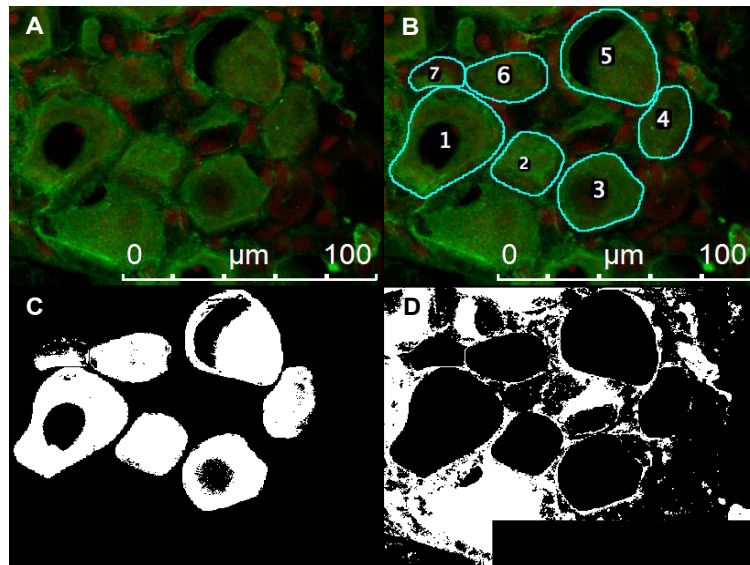


Figure 21: Image processing using ImageJ. DRG neurons with positive antibody stain (green; A). ROIs of manually segmented DRG neurons (B). ROIs thresholded using the isodata algorithm (C). Background region thresholded using Huang's fuzzy thresholding method (D).

4.2.4.3.2 Bilateral L1 DRGs

Sections were analyzed for neuronal cell parameters using ImageJ. Corrected total cell fluorescence (CTCF) was calculated using the following equation:

$$CTCF = (I_{cytoplasm} - I_{background}) * (area_{cytoplasm}) \quad (4)$$

where I is the mean fluorescence intensity (section 4.2.4.3.1) and CTCF values are expressed in fluorescence units*microns² (FLU* μm^2). The overall CTCF mean and standard deviation were calculated and used to convert individual CTCF values to z-scores using the following equation:

$$Z = (CTCF - Mean\ CTCF) / SD \quad (5)$$

where Z is an individual z-score and Mean CTCF and SD are the mean corrected total cell fluorescence and standard deviation, respectively. Resulting z-scores were averaged to give one overall measurement per treatment group and graphed to show qualitative differences between groups. Z-test statistics were performed using raw data and compared a z-statistic table [194] to determine differences between Sham and LDP groups ($\alpha < 0.05$).

4.2.4.3.3 Bilateral L2 DRGs

Sections were analyzed for neuronal parameters using ImageJ as described. CTCF for PGP9.5 was calculated for each ROI, and those with a positive value were defined as neurons (PGP9.5+). These PGP9.5+ cells were counted to determine the total number of neurons present per DRG and were included in all subsequent L2 DRG

analyses. CTCF for TRPV1 was calculated for PGP9.5+ cells and converted to z-scores. A positive CTCF z-score was chosen as criteria for an ROI to be considered TRPV1-positive (TRPV1+). TRPV1+ cells were counted and the percentage of TRPV1+ cells out of PGP9.5+ cells was calculated for each DRG. Statistical analyses were done via Chi-Square tests for differences between the number of TRPV1+ cells for Sham and LDP groups, as well as between ipsilateral and contralateral DRGs within treatment groups, ($\alpha < 0.05$, GraphPad Software).

TRPV1+ cells were further analyzed for differences in fluorescence intensity between groups. . CTCF z-scores were averaged to give one overall measurement per treatment group and graphed to show qualitative differences between groups. Z-test statistics were performed to determine differences between Sham and LDP groups, as well as between ipsilateral and contralateral DRGs within treatment groups ($\alpha < 0.05$).

The maximum diameter of PGP9.5+ cells was analyzed for differences in size between treatment groups via unpaired t-test with Welch's correction ($\alpha < 0.05$, GraphPad Software). Then these ROIs were grouped into small ($< 30 \mu\text{m}$), medium (30-40 μm), and large ($> 40 \mu\text{m}$) diameter neurons and the number of neurons in each group was obtained. Differences in neuron size distribution between the Sham and LDP groups, as well as between ipsilateral and contralateral DRGs within treatment groups, was determined via Chi-Square tests ($\alpha < 0.017$, GraphPad Software). This procedure was

repeated for TRPV1+ cells to investigate differences in size distribution of between treatment groups.

Qualitative observation of IHC images revealed circular, unstained nuclei within neurons. We therefore determined the percentage of neuron area which stained positive for TRPV1 (TRPV1+ Area) as an indirect measure of nucleus size, as TRPV1 immunostaining was not present in the nucleus. This parameter was determined for PGP9.5+ cells, and compared between and within treatment groups via unpaired t-tests with Welch's correction ($\alpha < 0.05$, GraphPad Software). This analysis was repeated for TRPV1+ cells as well as PGP9.5+ cells with a negative CTCF z-score for TRPV1 (TRPV1-). Differences in this parameter between TRPV1+ and TRPV1- cells were determined via unpaired t-tests with Welch's correction ($\alpha < 0.05$, GraphPad Software).

4.2.4.3.4 Effect Size Calculation

The effect size (Cohen's d) of the difference between Sham and LDP groups at the chronic timepoint was determined for p75NTR, TrkA, and TRPV1 corrected total cell fluorescence as the difference between z-scores. Results were classified as either small (0.20-0.49), medium (0.50-0.79) or large (≥ 0.80) and were entered into G*Power 3.0.10 (Heinrich Heine University Düsseldorf) to compute the achieved power as described in section 2.2.5.3.1.

4.3 Results

4.3.1 L5-L6 IVD Histology

Safranin-O/fast green staining of the L5-L6 IVD confirmed bilateral morphological changes associated with degeneration in the LDP group, including an indistinct AF-NP border, replacement of NP with connective tissue, and disorganized AF lamellae (Figure 22). The LDP group also showed significantly increased IVD degeneration compared to the Sham group ($p=0.019$; Figure 23).



Figure 22: Safranin-O/Fast Green histology stain for IVD grade of degeneration 20 weeks post-surgery. The LDP IVD shows decreased NP with infiltration of connective tissue.

Table 14: Spearman’s Correlation Coefficients for Comparisons Between Behavioral and Histologic Changes.

Assessment Parameter Compared to Histologic Grade	Spearman’s Correlation Coefficient	Critical Value (+) for Spearman’s Rho (r_s)
Percentage time spent traveling in 30 minutes	-0.047	0.35
Forelimb versus hind limb step frequency	0.27	0.39
Left hind limb swing duration (s)	0.11	0.39

4.3.3 DRG Immunohistochemistry

4.3.3.1 Bilateral L1 DRGs

At 20 weeks post-surgery, L1 DRG neurons from the LDP group showed qualitative changes such as increased fluorescence intensity of TrkA staining compared to the Sham and Naïve groups (Figure 24). On analysis, these changes showed significantly increased TrkA staining intensity of the contralateral L1 DRG neurons compared to the Sham group ($p=0.0019$; Figure 25B). Within groups comparisons showed a significant increase in TrkA CTCF for the ipsilateral Sham ($p<0.001$) and LDP neurons ($p=0.0093$) compared to corresponding contralateral neurons. No differences were detected in TrkA staining intensity between the ipsilateral Sham and LDP neurons (Figure 25A) or between ipsilateral and contralateral neurons for the Naïve group (Table 15). Effect sizes of these comparisons are shown in Table 15.

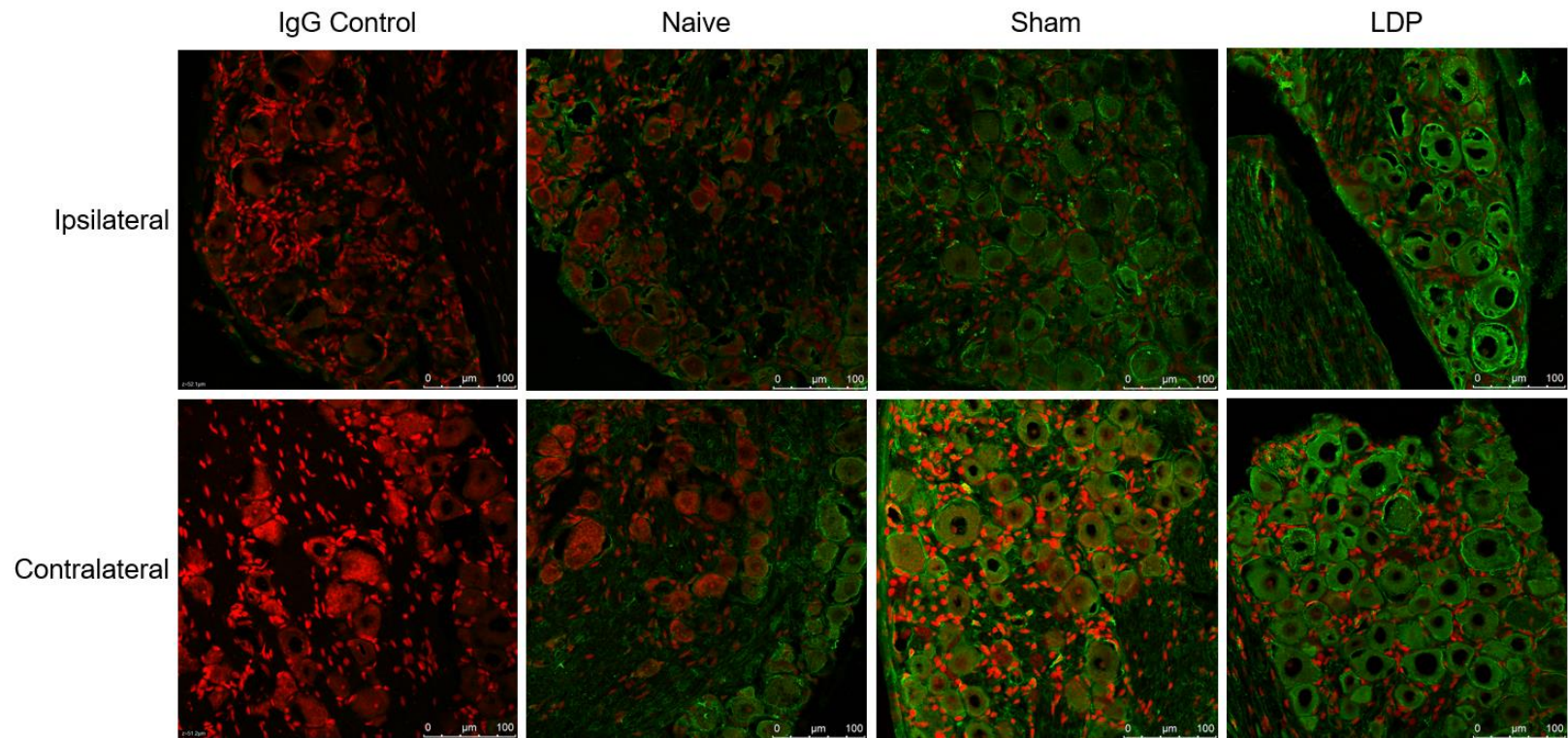


Figure 24: Bilateral L1 DRG sections immunostained for TrkA. Satellite cell nuclei and neuron somas stained with propidium iodide (PI; red); primary antibodies conjugated to an Alexa Fluor 488 secondary antibody (green).

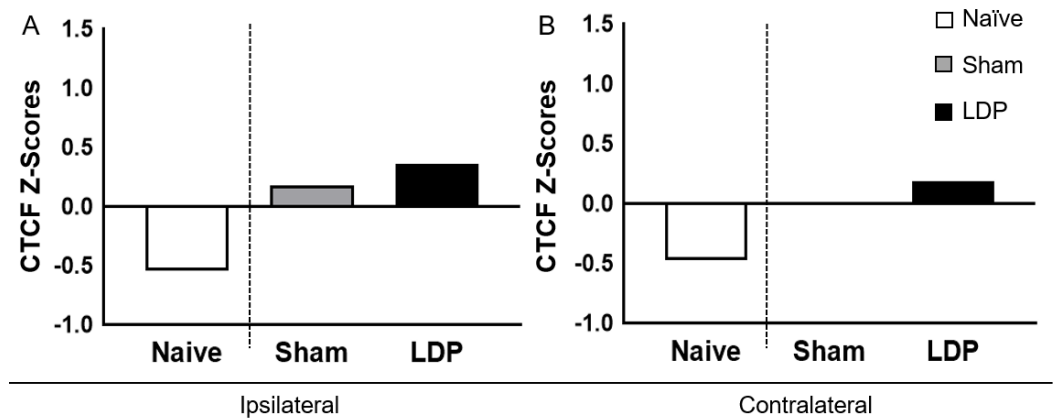


Figure 25: Corrected total cell fluorescence z-scores of TrkA staining for ipsilateral (A) and contralateral (B) L1 DRG neurons.

Table 15: TrkA CTCF Z-Statistic and Effect Size. Naïve, Sham, and LDP entries indicate comparison of ipsilateral and contralateral neuronal responses in the corresponding group.

Comparison	Z-Statistic	p value	Effect Size	Power (%)
Sham vs LDP Ipsilateral	1.4	0.16	0.18	78
Sham vs LDP Contralateral	3.1	0.0019	0.20	86
Naïve	1.0	0.32	-0.066	15
Sham	3.6	<0.001	0.18	70
LDP	2.6	0.0093	0.17	82

Ipsilateral L1 DRG neurons from the LDP group also showed qualitative increased fluorescence intensity of p75NTR staining compared to the Sham and Naïve groups (Figure 26), and analysis revealed significantly increased p75NTR staining intensity (CTCF) of the ipsilateral neurons compared to the Sham group ($p < 0.0001$) and no difference between groups for the contralateral neurons ($p = 0.56$; Figure 27). Within groups comparisons showed a significant increase in p75NTR CTCF for the contralateral

Sham neurons compared to corresponding ipsilateral neurons ($p < 0.0001$), and no difference between ipsilateral and contralateral LDP DRG neurons ($p = 0.90$; Table 16). Effect sizes of these comparisons are shown in Table 16.

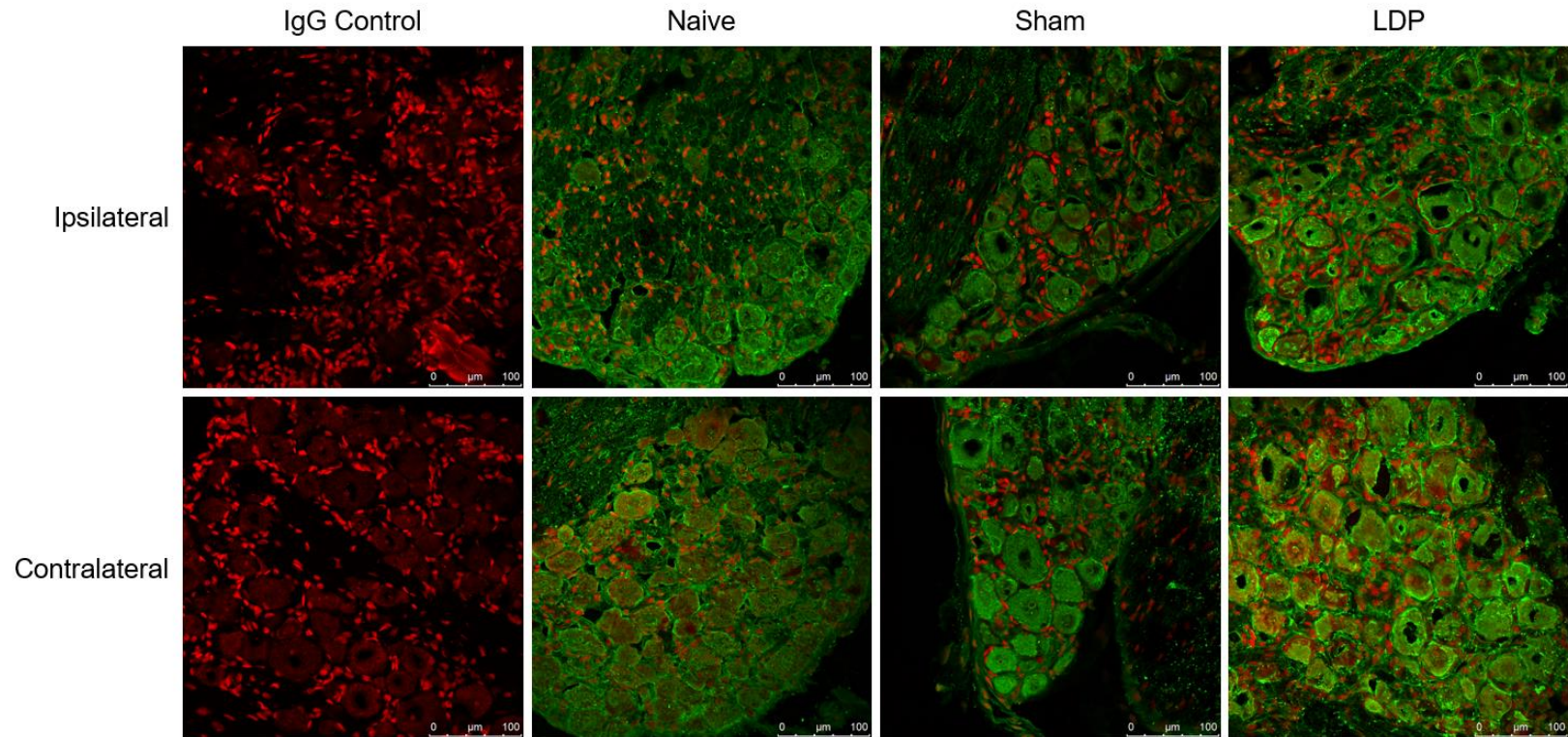


Figure 26: Bilateral L1 DRG sections immunostained for p75NTR. Satellite cell nuclei and neuron somas stained with propidium iodide (PI; red); primary antibodies conjugated to an Alexa Fluor 488 secondary antibody (green).

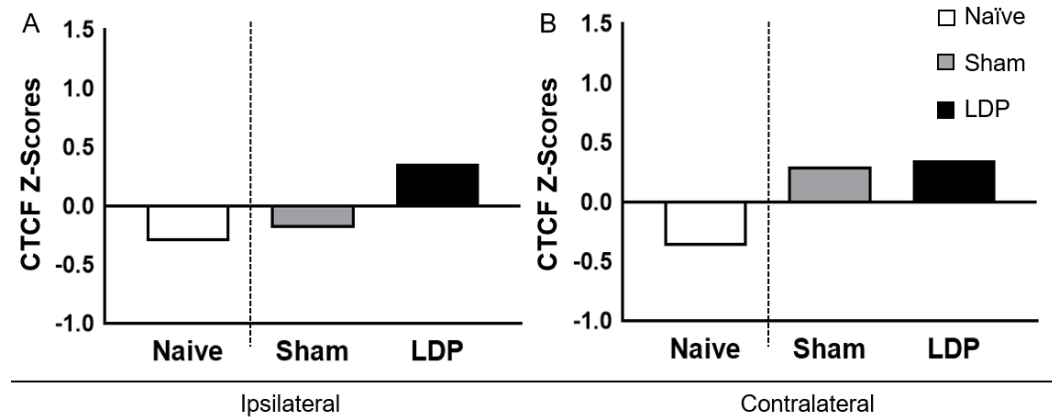


Figure 27: Corrected total cell fluorescence z-scores of p75NTR staining for ipsilateral (A) and contralateral (B) L1 DRG neurons.

Table 16: p75NTR CTCF Z-Statistic and Effect Size. Naïve, Sham, and LDP entries indicate comparison of ipsilateral and contralateral neuronal responses in the corresponding group.

Comparison	Z-Statistic	p value	Effect Size	Power (%)
Sham vs LDP Ipsilateral	4.8	<0.0001	0.55	98
Sham vs LDP Contralateral	0.54	0.56	0.052	9.4
Naive	1.0	0.32	0.031	6.8
Sham	4.2	<0.0001	0.062	7.7
LDP	0.12	0.13	0.90	26

4.3.3.2 Bilateral L2 DRGs

4.3.3.2.1 DRG Neuron Counts

Ipsilateral Sham and LDP DRGs appeared to contain a similar number of neurons (Figure 28A). The contralateral LDP DRG appeared to show an increased number of neurons compared to the Sham DRG (Figure 28B). The percentage of TRPV1+ cells in bilateral LDP DRGs was increased compared to those of the Sham group

($p < 0.0001$; Figure 28C, D) as described in Table 17. This parameter was also increased in contralateral L2 DRG neurons for the Sham ($p < 0.0001$) and LDP ($p < 0.0001$) groups compared to ipsilateral neurons (Table 17).

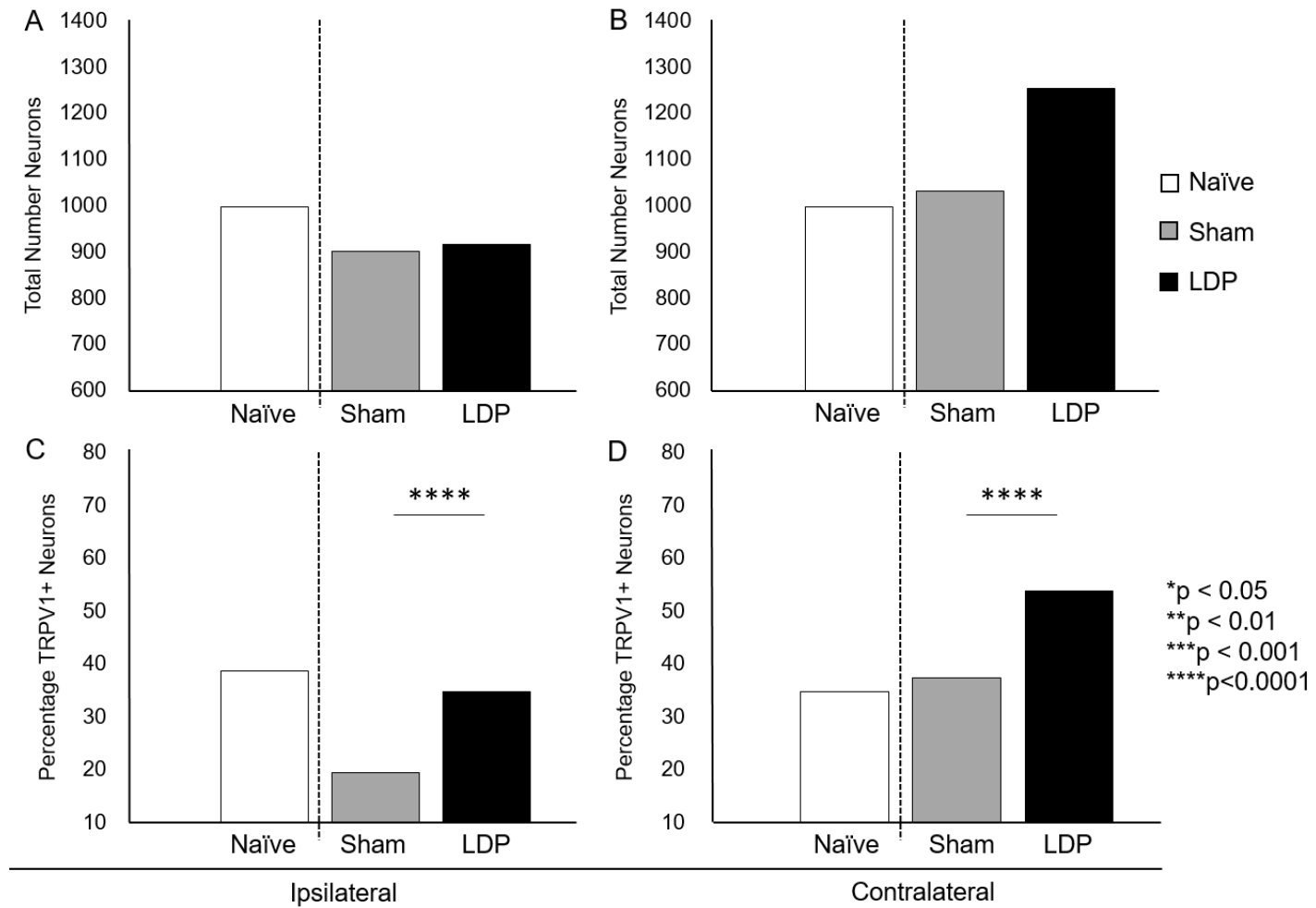


Figure 28: DRG neuron counts. Total number of PGP9.5+ cells for the ipsilateral (A) and contralateral (B) L2 DRG neurons, and the percentage of TRPV1+ cells for the ipsilateral (C) and contralateral (D) L2 DRG neurons.

Table 17: Number of TRPV1+ cells. Naïve, Sham, and LDP entries indicate comparison of ipsilateral and contralateral neuronal responses in the corresponding group.

Parameter	Comparison	p value
	Sham vs LDP Ipsilateral	<0.0001
	Sham vs LDP Contralateral	<0.0001
TRPV1+ Cell Number	Naïve	0.077
	Sham	<0.0001
	LDP	<0.0001

The LDP group also showed qualitative increased fluorescence intensity of TRPV1 staining of the ipsilateral (Figure 29) and contralateral (Figure 30) L2 DRG neurons compared to the Sham group. Staining intensity of TRPV1+ cells in the LDP group was significantly increased for the ipsilateral ($p=0.0027$; Figure 31A) and contralateral ($p=0.021$; Figure 31B) L2 DRG neurons compared to the Sham group (Table 18). This parameter was also significantly increased in the contralateral L2 DRG neurons of the Sham ($p<0.0001$) and LDP ($p<0.0001$) groups compared to the ipsilateral neurons (Table 18). The effect sizes for these comparisons are presented in Table 18.

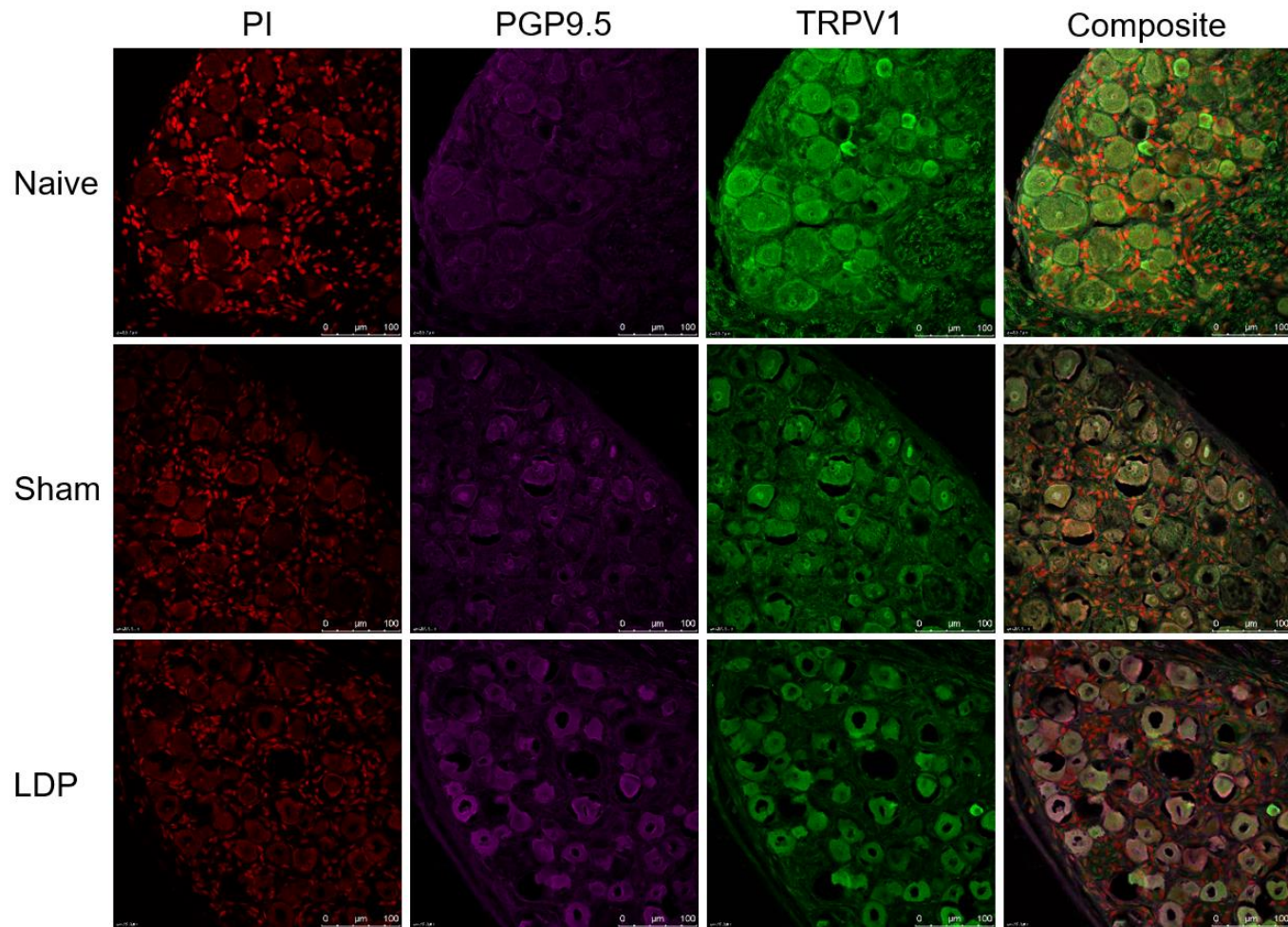


Figure 29: Ipsilateral L2 DRG neurons co-stained for PGP9.5 and TRPV1. Satellite cell nuclei and neuron somas stained with propidium iodide (PI; red); primary antibodies conjugated to an Alexa Fluor 488 secondary antibody (green).

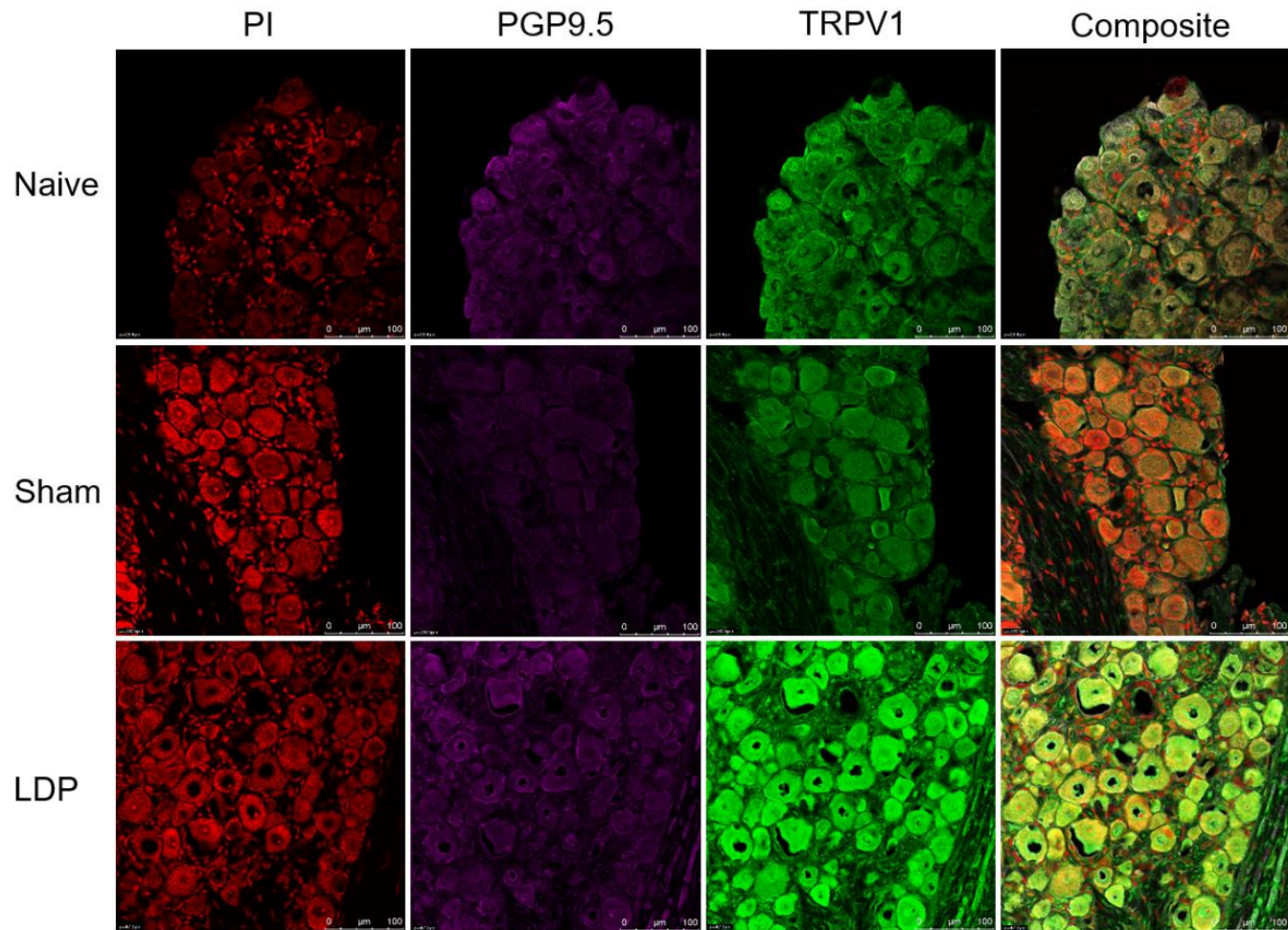


Figure 30: Contralateral L2 DRG neurons co-stained for PGP9.5 and TRPV1. Satellite cell nuclei and neuron somas stained with propidium iodide (PI; red); primary antibodies conjugated to an Alexa Fluor 488 secondary antibody (green).

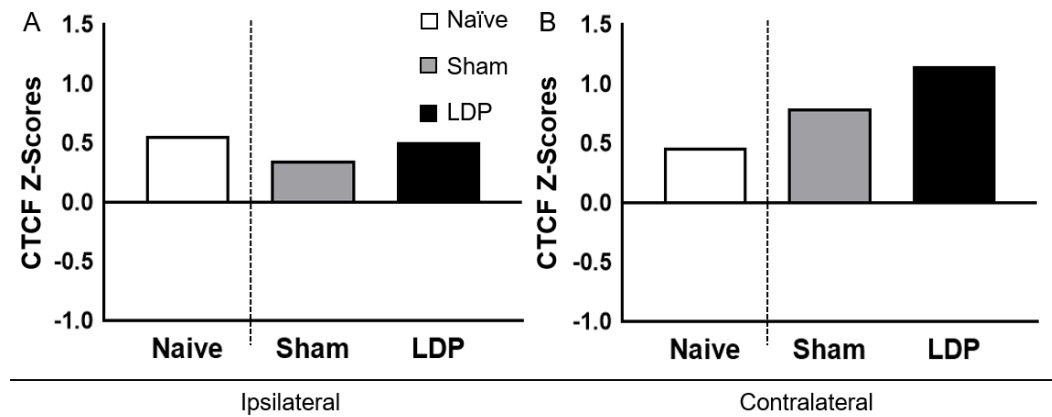


Figure 31: Corrected total cell fluorescence z-scores of TRPV1 staining for ipsilateral (A) and contralateral (B) L2 DRG neurons.

Table 18: TRPV1 CTCF Z-Statistic and Effect Size. Naïve, Sham, and LDP entries indicate comparison of ipsilateral and contralateral neuronal responses in the corresponding group.

Comparison	Z-Statistic	p value	Effect Size	Power (%)
Sham vs LDP Ipsilateral	3.0	0.0027	0.19	52
Sham vs LDP Contralateral	2.3	0.021	0.18	80
Naïve	1.5	0.13	0.088	22
Sham	6.5	<0.0001	0.49	100
LDP	7.2	<0.0001	0.47	100

Ipsilateral LDP neurons showed an increased maximum diameter compared to the Sham group ($p=0.00010$; Figure 32A). No difference was detected between the Sham and LDP groups for maximum diameter of contralateral L2 DRG neurons ($p=0.74$; Figure 32B). Differences in neuronal size distribution revealed that the proportions of ipsilateral medium and large neurons in the LDP group relative to the Sham group were significantly increased ($p=0.0046$ and $p=0.0094$, respectively) compared to that of small

L2 DRG neurons. Similarly, the proportions of contralateral small and medium-sized neurons in the LDP group were significantly decreased ($p=0.013$) and trended toward a significant decrease ($p=0.017$), respectively, compared to large L2 DRG neurons.

Neuronal maximum diameter was also significantly increased in the contralateral L2 DRG neurons of the Sham group ($p=0.012$) compared to the ipsilateral neurons (Table 19). Comparison of neuronal size distributions for ipsilateral and contralateral Sham DRGs showed a trend toward a significantly increased proportion of medium-sized neurons compared to small neurons in the contralateral L2 DRG ($p=0.023$). This analysis for LDP DRGs showed a trend toward a significantly increased proportion of large neurons compared to medium neurons in the contralateral L2 DRG ($p=0.079$; Table 19).

The effect sizes for these comparisons are shown in Table 20.

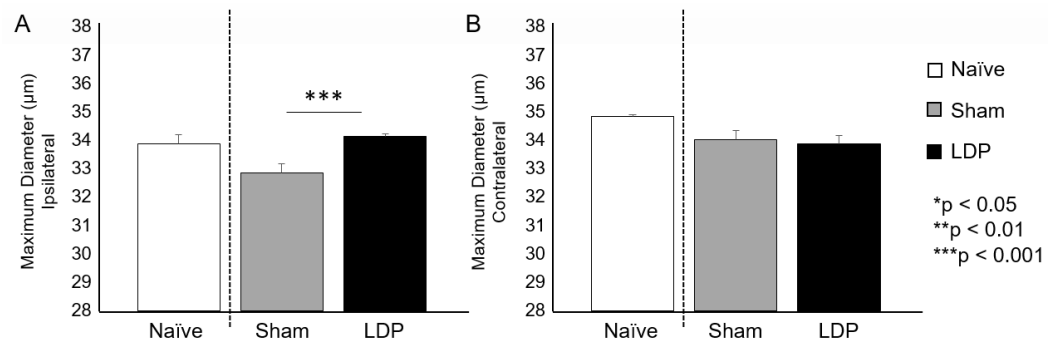


Figure 32: Maximum diameter of PGP9.5+ cells of the ipsilateral (A) and contralateral (B) L2 DRGs.

Table 19: Maximum Diameter for PGP9.5+ Cells. Naïve, Sham, and LDP entries indicate comparison of ipsilateral and contralateral neuronal responses in the corresponding group.

Group	Comparison	p value
PGP9.5+ Cells	Sham vs LDP Ipsilateral	0.0010
	Sham vs LDP Contralateral	0.74
	Naïve	0.0039
	Sham	0.012
	LDP	0.36
PGP9.5+ Cells By Size (Ipsilateral)	Small vs Medium	0.0046
	Small vs Large	0.0094
	Medium vs Large	0.74
PGP9.5+ Cells By Size (Contralateral)	Small vs Medium	0.85
	Small vs Large	0.013
	Medium vs Large	0.017
PGP9.5+ Cells By Size (Sham)	Small vs Medium	0.023
	Small vs Large	0.11
	Medium vs Large	0.85
PGP9.5+ Cells By Size (LDP)	Small vs Medium	0.63
	Small vs Large	0.20
	Medium vs Large	0.079

Table 20: Effect Size of Maximum Diameter for PGP9.5+ Cells. Naïve, Sham, and LDP entries indicate comparison of ipsilateral and contralateral neuronal responses in the corresponding group.

Comparison	Effect Size	Power (%)
Sham vs LDP Ipsilateral	0.18	97
Sham vs LDP Contralateral	0.014	6.3
Naïve	0.13	83
Sham	0.11	67
LDP	0.037	14

No differences in maximum neuron diameter were detected for ipsilateral (Figure 33A) or contralateral (Figure 33B) TRPV1-positive neurons between the Sham

and LDP groups. However, neuronal maximum diameter was significantly decreased in the contralateral L2 DRG TRPV1-positive neurons of both the Sham ($p=0.0038$) and LDP ($p=0.015$) groups compared to the corresponding ipsilateral neurons (Table 21). Ipsilateral LDP neurons showed a trend toward a significantly decreased proportion of large neurons compared to medium neurons relative to the Sham group ($p=0.085$; Figure 33C, D). No differences were detected in the neuron size distribution of contralateral LDP and Sham DRG neurons (Figure 33E, F; Table 21). The neuronal size distribution of the contralateral Sham and LDP DRGs relative to the corresponding ipsilateral DRGs showed a significantly decreased proportion of large neurons compared to small (Sham $p=0.0015$; LDP $p=0.0045$) and medium-sized (Sham $p=0.0061$; LDP $p=0.0019$) neurons (Table 21). Effect sizes for these comparisons are shown in Table 22.

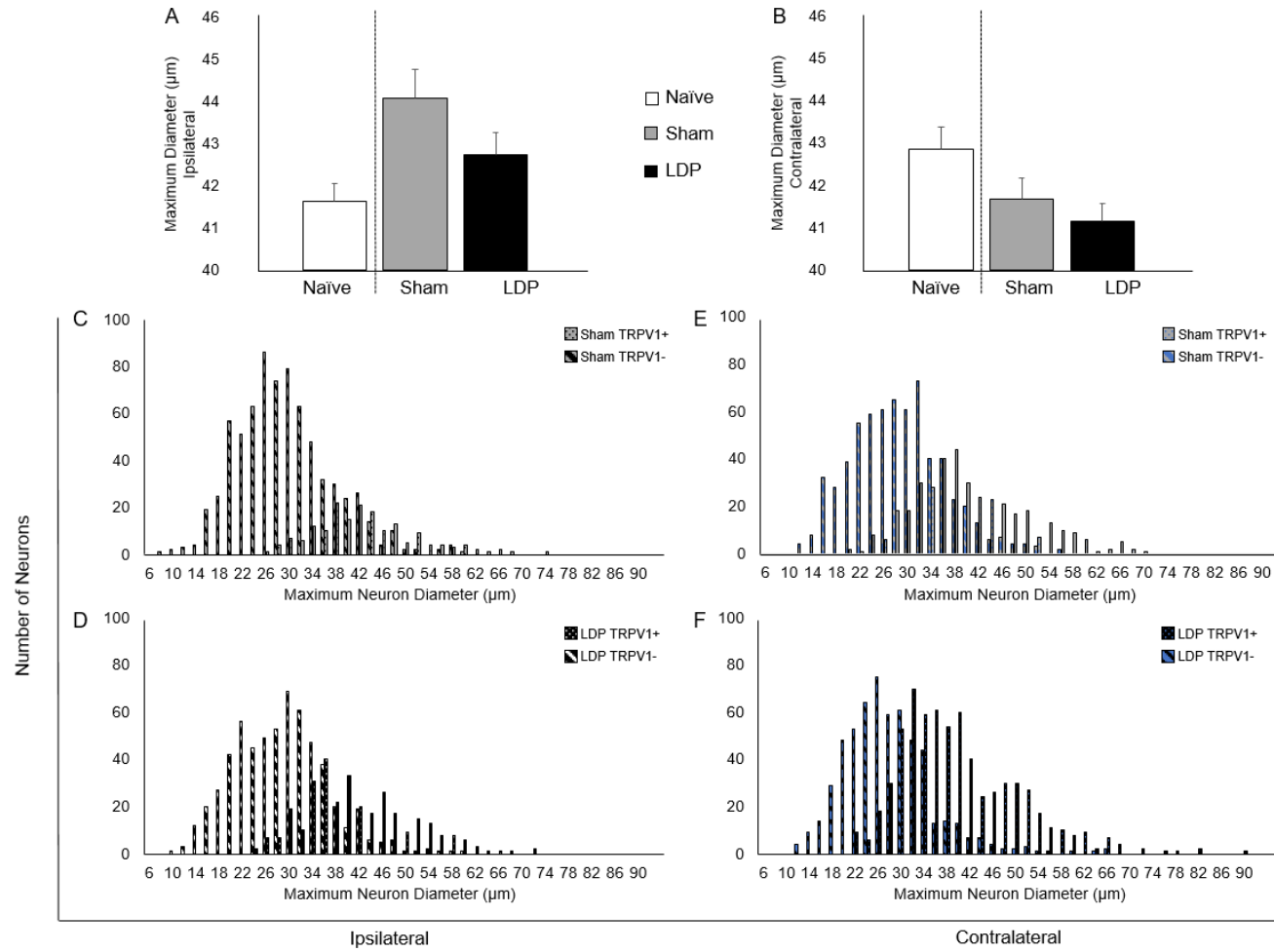


Figure 33: Maximum diameter of the ipsilateral (A) and contralateral (B) TRPV1+ cells. Neuronal size distribution of ipsilateral and contralateral Sham (C, E) and LDP (D, F) TRPV1+ and TRPV1- cells.

Table 21: Maximum Diameter for TRPV1+ Cells. Naïve, Sham, and LDP entries indicate comparison of ipsilateral and contralateral neuronal responses in the corresponding group.

Group	Comparison	p value
TRPV1+ Cells	Sham vs LDP Ipsilateral	0.11
	Sham vs LDP Contralateral	0.41
	Naïve	0.080
	Sham	0.0038
	LDP	0.015
TRPV1+ Cells By Size (Ipsilateral)	Small vs Medium	0.45
	Small vs Large	0.14
	Medium vs Large	0.085
TRPV1+ Cells By Size (Contralateral)	Small vs Medium	0.89
	Small vs Large	0.57
	Medium vs Large	0.26
TRPV1+ Cells By Size (Sham)	Small vs Medium	0.062
	Small vs Large	0.0015
	Medium vs Large	0.0061
TRPV1+ Cells By Size (LDP)	Small vs Medium	0.11
	Small vs Large	0.0045
	Medium vs Large	0.019

Table 22: Effect Size of Maximum Diameter for TRPV1+ Cells. Naïve, Sham, and LDP entries indicate comparison of ipsilateral and contralateral neuronal responses in the corresponding group.

Comparison	Effect Size	Power (%)
Sham vs LDP Ipsilateral	0.15	36
Sham vs LDP Contralateral	0.052	13
Naïve	0.13	42
Sham	0.26	81
LDP	0.16	65

For PGP9.5+ cells, both ipsilateral and contralateral LDP neurons showed a significant decrease in the percentage of TRPV1+ Area compared to the corresponding Sham groups ($p < 0.0001$; Figure 34A, B) as shown in Table 23. Ipsilateral DRG neurons showed a significant decrease in this parameter compared to the contralateral neurons for both the Sham ($p < 0.0001$) and LDP ($p = 0.0027$) groups. These results extended to analyses of TRPV1+ cells (Figure 34C, D, E; Table 23), as well as TRPV1- cells with one exception: contralateral TRPV1- cells showed a significant decrease compared to ipsilateral neurons in the LDP group ($p = 0.0003$; Figure 34E). Effect sizes for these comparisons are also shown in Table 23, and show medium and large effect sizes at the chronic timepoint.

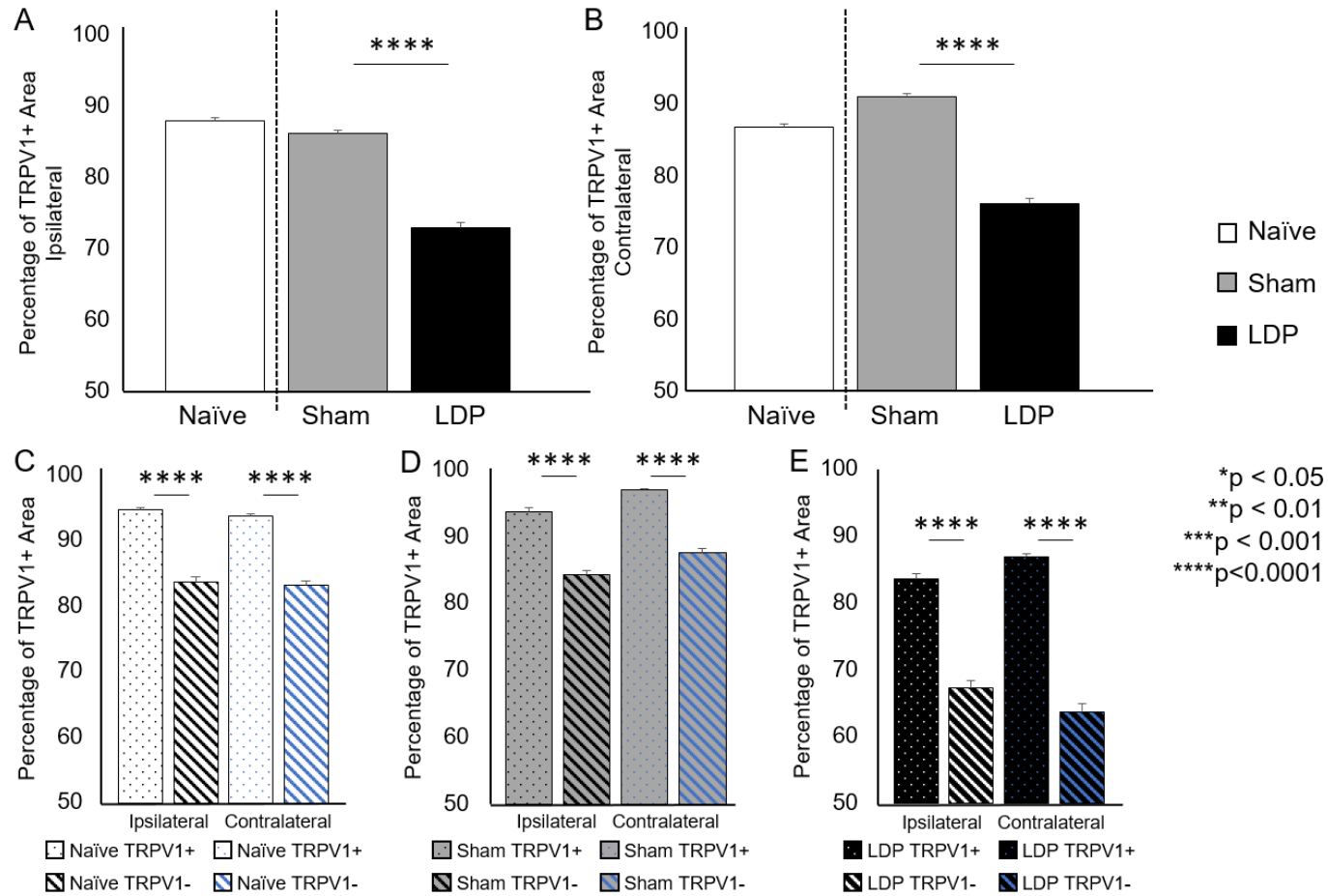


Figure 34: Percentage of TRPV1+ Area in L2 DRG neurons. Percentage of TRPV1+ Area for PGP9.5+ cells grouped into ipsilateral (A) and contralateral (B) neurons. Percentage of TRPV1+ Area of ipsilateral and contralateral TRPV1+ and TRPV1- cells for the Naive (C), Sham (D) and LDP (E) groups.

Table 23: Percentage of TRPV1+ Area with Effect Sizes. Naïve, Sham, and LDP entries indicate comparison of ipsilateral and contralateral neuronal responses in the corresponding group.

Group	Comparison	p value	Effect Size	Power
PGP9.5+ Cells	Sham vs LDP Ipsilateral	<0.0001	0.62	100
	Sham vs LDP Contralateral	<0.0001	0.75	100
	Naïve	0.12	0.070	34
	Sham	<0.0001	0.34	100
	LDP	0.0027	0.13	85
TRPV1+ Cells	Sham vs LDP Ipsilateral	<0.0001	0.85	100
	Sham vs LDP Contralateral	<0.0001	0.97	100
	Naïve	0.053	0.14	47
	Sham	<0.0001	0.47	100
	LDP	0.0003	0.26	97
TRPV1- Cells	Sham vs LDP Ipsilateral	<0.0001	0.74	100
	Sham vs LDP Contralateral	<0.0001	1.0	100
	Naïve	0.61	0.029	8.1
	Sham	0.0001	0.21	97
	LDP	0.034	0.12	54
TRPV1+ vs TRPV1- Cells	Naive Ipsilateral	<0.0001	0.78	100
	Naïve Contralateral	<0.0001	0.70	100
	Sham Ipsilateral	<0.0001	0.68	100
	Sham Contralateral	<0.0001	0.85	100
	LDP Ipsilateral	<0.0001	0.75	100
	LDP Contralateral	<0.0001	1.0	100

4.4 Discussion

Histologic changes. This study was performed to confirm IVD degeneration and assess changes to innervating DRGs 20 weeks after a surgical lumbar disc puncture injury. Degenerative changes were seen in all groups via histology, but more severe degeneration was found in the LDP group. This is supported by the large effect size for grade of IVD degeneration at this timepoint, and is consistent with expected outcomes

of our surgical intervention. However, correlation analyses revealed no relationship between grade of IVD degeneration and open field or treadmill gait parameters at the chronic timepoint. Because animals in every treatment group developed degenerative changes and not every rat in the LDP group developed severe IVD degeneration (section 3.3.1), this suggests a more complex relationship between onset of symptoms and degenerative IVD changes that would be predicted by correlation.

Changes to ipsilateral DRG neurons. Early in the calcium imaging experiments, it became apparent that these ipsilateral LDP DRG neurons were different. The final step of the cell isolation process was to spin down the isolated cells to obtain a cell pellet, and then resuspend the cells in the correct volume of media for plating. The qualitative volume of every ipsilateral LDP cell pellet was greatly reduced compared to the contralateral LDP cell pellet, with a resulting decrease in neuronal cell number on calcium imaging. This was possibly due to cell death at any of three distinct points in the study:

1. Neuronal degeneration in vivo.
2. Neuronal changes in vivo such that they were unable to survive the enzymatic digestion of the DRG for cell isolation.
3. Neuronal changes in vivo such that they became increasingly unhealthy during the cell isolation, and were ultimately unable to survive on the coverslip in a co-culture with satellite cells.

The third hypothesis was deemed the least likely due to observing the decreased cell pellet volume before plating. The first and second hypotheses were tested by systematically sectioning and staining L2 DRGs to count neuronal cell bodies as described in section 3.2.4.3.2 and by counting cells after resuspending the cells, respectively. However, the number of resuspended ipsilateral cells from the LDP animals was only 10% of what was needed to accurately calculate the total cell number using a hemocytometer. Results of DRG neuron cell counts via IHC did not reveal in vivo degeneration. Instead, the LDP group showed a similar or increased number of neurons in the ipsilateral and contralateral DRG, respectively, compared to the corresponding Sham DRG. These results suggest that ipsilateral DRG neurons had undergone phenotypic changes in vivo and were unable to survive enzymatic digestion of the DRG for cell isolation at this timepoint. However, this analysis was limited by counting neurons in only one ipsilateral and contralateral DRG per treatment group.

The composition of NGF receptors on LDP DRG neurons provides one possible explanation for apoptosis of these cells during enzymatic digestion. TrkA and p75NTR were increased in the contralateral and ipsilateral LDP neurons, respectively, compared to those of the Sham group. NGF binding to TrkA promotes cell survival and collateral nerve sprouting, while binding to p75NTR leads to expression of additional pro-inflammatory cytokines or apoptosis (section 1.3.2.1). Therefore, the increased presence of p75NTR on ipsilateral DRG neurons of the LDP group suggests cellular changes that

contribute to inflammation in vivo and an inability to survive enzymatic digestion for cell isolation. This analysis was limited by fluorescence intensity data from only one ipsilateral and contralateral DRG section per animal.

Numbers of TRPV1-positive neurons. This study also revealed increased numbers of TRPV1-positive neurons in bilateral DRGs 20 weeks after lumbar disc puncture, with more TRPV1-positive neurons present in the contralateral DRG of both the Sham and LDP groups compared to the corresponding ipsilateral DRG. These results suggest that the number of TRPV1-positive neurons present in a DRG is dependent on treatment group as well as the site of injury.

Neuron size distributions. Findings of neuron proliferation or neurogenesis in the peripheral nervous system have been controversial due to variability of methods for sectioning tissue and counting neurons. However, recent evidence of neurogenesis in adult rat DRGs has been shown after capsaicin treatment [195] and after peripheral nerve damage and regeneration [196]. Prior studies have also shown hypertrophy of NGF-dependent neurons in sensory ganglion in distal organ pathologies with increased levels of NGF such as urethral [197] and intestinal [198] obstruction. The current study revealed an increased proportion of medium-sized and large neurons compared to small neurons in the ipsilateral LDP DRG relative to the Sham group without a change in the total number of neurons present. However, the proportions of large TRPV1-positive neurons in this DRG were decreased compared to that of medium neurons and the

neuronal size distribution in the ipsilateral Sham DRG, suggesting hypertrophy of TRPV1-negative neurons. The contralateral LDP DRG showed an increased number of neurons compared to the Sham group and trended toward an increased proportion of large neurons compared to both the contralateral Sham and ipsilateral LDP neurons. However, the contralateral DRG for both Sham and LDP groups showed decreased proportions of TRPV1-positive large neurons compared to small and medium-sized neurons relative to that of the corresponding ipsilateral DRG. These results suggest hypertrophy of TRPV1-negative neurons, as well as proliferation of small and medium-sized TRPV1-positive neurons in the contralateral LDP L2 DRG. However, this analysis was limited to sections from one ipsilateral and contralateral DRG per treatment group.

Changes to TRPV1 receptors of DRG neurons. Increased TRPV1 corrected total cell fluorescence revealed that not only are the numbers of TRPV1-positive neurons increased in bilateral LDP DRGs, but that these neurons express an increased number of TRPV1 receptors compared to the Sham group. The contralateral DRGs showed increased TRPV1 CTCF compared to the ipsilateral DRGs within groups, again suggesting that TRPV1 expression is dependent on treatment group and the site of injury. Increased neuronal TRPV1 expression has been associated with clinical chronic pain pathologies such as rectal hypersensitivity [199], inflamed bowel [200], and vulvodynia [201].

These findings seem to contradict the calcium imaging results at this chronic timepoint. An increased number of TRPV1-positive neurons, each with more TRPV1 receptors, should result in more neurons responding to application of capsaicin (CAP1). However, the LDP neuronal response to the high capsaicin dose (200 nM), a dose where every neuron presenting TRPV1 receptors should respond, was decreased bilaterally compared to the Sham group. This suggests that the functionality of TRPV1 receptors present on bilateral LDP neurons was impaired. In addition, ipsilateral LDP neurons were unable to potentiate the function of TRPV1 after NGF incubation (CAP2/CAP1). These results indicate a problem with two pathways after NGF binds to TrkA (section 4.1) in the ipsilateral DRG neurons after lumbar disc puncture:

1. The signaling cascade and phosphorylation of existing TRPV1.
2. Rapid insertion of new TRPV1 receptors into the neuronal cell membrane.

However, contralateral neurons also showed a decreased CAP1 response, but remained able to potentiate the function of TRPV1 after NGF incubation. These results indicate alterations in the biochemical signaling cascades regulating TRPV1 function.

Altered function of existing TRPV1 receptors indicates possible changes to the PKC pathway, including phosphorylation of the TrkA residue Y794, PLC γ , PKC ϵ , or TRPV1 residues S800, S502, or T704 [160, 202]. Rapid insertion of new TRPV1 receptors into the neuronal cell membrane to potentiate TRPV1 function via TrkA may be explained by a non-transcriptional mechanism involving phosphorylation of a single

residue, as this could occur in sensory terminals independent of the nucleus [79, 165]. One possible mechanism involves autophosphorylation of the Y760 residue on TrkA to activate phosphoinositide 3-kinase (PI3 kinase), and the downstream element Src phosphorylates TRPV1 at residue Y200 to promote TRPV1 insertion into the cell membrane [165]. Therefore, alterations of the PKC and IP3 kinase pathways may play a role in impaired TRPV1 receptor function as well as insertion into the cell membrane and resulting desensitization, respectively. However, the data sets used to draw these conclusions were subject to their own limitations, as discussed in this section and previously (section 3.4).

Percent area of TRPV1-positive staining. The percentage of TRPV1-positive area corresponds to the neuronal membrane and cytoplasmic staining of TRPV1, which excludes the unstained nuclear region. Therefore, the percentage of TRPV1-positive area decreases as the area of the unstained nuclear region increases. In analyses of all neurons and of TRPV1-positive neurons only, the percentage of TRPV1-positive area was decreased in bilateral DRGs 20 weeks after lumbar disc puncture compared to the Sham group. However, the greatest change was the decreased percentage of TRPV1-positive area in TRPV1-negative neurons of bilateral LDP DRGs compared to that of the Sham DRGs. These changes suggest nuclear hypertrophy in TRPV1-positive and TRPV1-negative neurons in bilateral DRGs 20 weeks after lumbar disc puncture, with the greatest changes seen in the TRPV1-negative neurons. Taken together with the neuronal

size distribution results, this suggests that both nuclear and cytoplasmic hypertrophy occur in TRPV1-negative neurons in bilateral innervating DRGs. Similar plastic changes have been reported as corresponding to axonal regeneration in models of peripheral nerve injury at a distal location, such as amputation of a lizard tail [186, 203], where these changes are thought to be a response to increased metabolic and transcriptional activity due to outward growth. However, the data sets used to draw these conclusions were limited to sections from one ipsilateral and contralateral DRG per treatment group.

4.5 Conclusion

This study confirmed IVD degeneration in this model and identified molecular changes of sensory neurons in a rat 20 weeks after lumbar disc puncture through immunostaining of L1 and L2 DRG tissue sections. Degenerative pathology in this model provided one explanation of the pain-related behavioral changes described in Chapter 2. However, the lack of correlation between grade of IVD degeneration and these parameters suggested a more complex relationship between onset of symptoms and degenerative IVD changes that would be predicted by correlation.

Based on results from Chapter 3, neurons in the contralateral DRG were expected to have undergone minimal changes at the 20 week timepoint. However, the contralateral DRG neurons showed changes suggesting proliferation of small and medium-sized TRPV1-positive neurons, as well as changes indicating impaired functionality of TRPV1 receptors and increased transcriptional activity of both TRPV1-

positive and TRPV1-negative neurons. Immunostaining results also revealed that ipsilateral neurons were not able to survive the enzymatic digestion for cell isolation during the calcium imaging study with a possible role for p75NTR, as well as increased transcriptional activity of both TRPV1-positive and TRPV1-negative neurons. Results also showed changes suggesting impaired functionality of TRPV1 receptors as well as impaired TRPV1 receptor insertion into the cell membrane, which could explain the neuronal desensitization observed in Chapter 3.

Therefore, puncture of this single IVD provides a model of painful IVD degeneration which can be used to further elucidate mechanisms of discogenic pain and related changes associated with this degenerative pathology.

5. Conclusion and Future Directions

5.1 Conclusion

In summary, painful IVD degeneration due to a disc injury is likely the result of a chronic inflammatory process leading to an increased expression of NGF and associated changes to innervating DRG neurons. Prior studies have confirmed the presence of nerve fibers expressing TrkA, the high affinity NGF receptor, innervating painful human IVDs [84], suggesting a role for NGF in the development of discogenic pain. However, there is a limited understanding of this mechanism of pain generation in the IVD.

Motivated by a lack of targeted and effective therapeutic treatments to help patients better manage their low back pain, the overarching goal of this dissertation was to characterize NGF-related molecular and functional neuronal changes in a model of painful IVD degeneration. Results of the studies performed in this dissertation produced several key findings:

1. Timeline of pain-related behavioral changes. Rats do not fully recover from the soft tissue trauma and acute pain induced by lumbar disc puncture surgery until 4-6 weeks post-surgery, and develop evidence of LDP-related behavioral and gait changes at 16-18 weeks post-surgery.
2. Clinically relevant behavioral changes. This model produced a phenotype of pain-related bilateral behavioral changes characterized by decreased overall activity as well as decreased hind limb stride frequency.

3. Behavioral changes are not correlated to grade of IVD degeneration.

Degenerative changes were seen in all groups via histology, but more severe degeneration was found in the LDP group. However, correlation analyses revealed no relationship between grade of IVD degeneration and open field or treadmill gait parameters at the chronic timepoint.

4. DRG neurons are functionally different 20 weeks after lumbar disc puncture.

- Contralateral DRG neurons showed proliferation of small TRPV1-positive neurons, as well as impaired functionality of TRPV1 receptors and increased transcriptional activity of both TRPV1-positive and TRPV1-negative neurons.
- Many ipsilateral DRG neurons were unable to survive enzymatic digestion of the DRG for cell isolation at this timepoint. TrkA and p75NTR was increased in contralateral and ipsilateral DRGs, respectively. Results also showed increased transcriptional activity of both TRPV1-positive and TRPV1-negative neurons. Impaired functionality of TRPV1 receptors and impaired TRPV1 receptor insertion into the cell membrane could explain the desensitization response to capsaicin exhibited by surviving neurons via calcium imaging studies.

5.2 Future Directions

This model of painful IVD degeneration after puncture of a single IVD could be used to further elucidate pain-related mechanisms and understand the role of key mediators in the development and maintenance of discogenic pain. The findings presented in this dissertation suggest a number of areas for future study:

1. While pain-related behavioral changes were described for each timepoint in this study out to 20 weeks post-surgery, molecular and functional neuron data is only provided for the chronic 20 week timepoint. Repeating this study for both an acute and intermediate timepoint would reveal a timeline of the described changes and increase our understanding of the role of potential therapeutic targets in this pathology. Not only are these timepoints important for understanding changes which contribute to the development of chronic pain, but identifying the earliest changes could lead to beneficial therapies for patients who present with acute onset low back pain without IVD herniation or vertebral fracture.
2. While pain-related behavioral changes were detected in Chapter 2 and NGF-related changes were detected and in Chapters 3 and 4, this dissertation did not describe studies to definitively prove that the described behavioral changes were due to only pain. Therefore, future studies should include additional groups receiving treatment to restore the pain-related behaviors to

the pre-surgical baseline. These groups could include 1) pain medication starting pre-surgery and continuing throughout the duration of the study, 2) pain medication starting immediately post-surgery and continuing throughout the duration of the study, and 3) pain medication starting at 20 weeks post-surgery corresponding to the development of behavioral changes and continuing through out the duration of the study.

3. This study also did not definitively prove that upregulated NGF with nerve fiber infiltration is the dominant mechanism of pain in this model. Therefore, future studies should include additional groups receiving NGF-inhibitor treatment to investigate the development of pain-related behavioral changes. However, systemic NGF treatment has failed clinical trials for treatment of osteoarthritis pain [204]. An alternative method for anti-NGF treatment would be local delivery via the lumbar disc puncture surgery. This would allow for delivery of NGF-inhibitor concurrent with the surgery to induce IVD degeneration.
4. This study did not elucidate the specific roles of TrkA or p75NTR in this model, or directly link their increased expression in DRG neurons to pain-related behaviors. This could be accomplished by repeating the described behavioral assessments with a p75NTR knockout rat (Horizon Discovery Group, St. Louis, MO) with the addition of pain medication-treated groups.

Similar immunohistochemical and calcium imaging analyses would also determine the role of p75^{NTR} in neuronal apoptosis in vivo or during enzymatic digestion for cell isolation.

5. Results in Chapter 4 indicated impaired functionality of TRPV1 receptors and increased transcriptional activity of both TRPV1-positive and TRPV1-negative neurons. A possible explanation for these results is activation of growth-associated protein 43 (GAP43), marker of neuronal growth which shows increased gene expression during the regeneration phase after axonal injury [188]. GAP43 facilitates actin polymerization and therefore regulates neuronal structure [205]. NGF binding to TrkA can activate GAP43 and allow phosphatidylinositol 4,5-bisphosphate (PIP₂) to promote filopodia extension and branching [206]. However, TRPV1 activation is inhibited by PIP₂ [167], resulting in a competing mechanism. To determine if GAP43 and axonal growth is the dominant mechanism at this chronic timepoint, immunostaining for GAP43 and subsequent analyses could be done in the same manner as described for that of TRPV1 in Chapter 4. Future studies could also investigate the percentage of TRPV1 positive neurons out of those that are GAP43 positive via co-staining for both targets.

6. Results in Chapters 3 and 4 could be more specific to individual neurons innervating the injured IVD via a second surgery where a neurotracer and fluorescent lipophilic membrane stain, 1,1'-Dioctadecyl-3,3,3',3'-Tetramethylindocarbocyanine Perchlorate (DiI_{C18}(3); DiI), is injected into the L5-L6 IVD at 20 weeks post-surgery. Animal sacrifice could be delayed one week for adequate DiI uptake by innervating nerve fibers and retrograde transport to the cell bodies in the DRGs. DiI can be detected on immunohistochemical studies as well as calcium imaging, as it has excitation and emission wavelengths of 549 and 565 nm, respectively, which does not interfere with that of the Fura-2 AM fluorescence. Therefore, repeated calcium imaging and immunohistochemical studies with only DiI-positive neurons would yield more specific results.

In summary, this dissertation showed that surgical puncture of a single lumbar IVD produces a model of painful IVD degeneration with a discrete timeline of phenotypic changes which could be used for future studies investigating the development and maintenance of discogenic pain, or therapeutic interventions. This dissertation also demonstrated the importance of including DRG neuron changes in future studies using models of painful musculoskeletal pathology. Both of these conclusions will be necessary components of future studies to further elucidate pain-

related mechanisms and understand the role of key mediators in the development and maintenance of discogenic pain.

References

- [1] Zhang YG, et al. Clinical diagnosis for discogenic low back pain. *Int J Biol Sci* 2009; 5(7):647-658.
- [2] Andersson GB. Epidemiological features of chronic low-back pain. *Lancet* 1999; 354(9178):581-585.
- [3] Vos T, et al. Years lived with disability (YLDs) for 1160 sequelae of 289 diseases and injuries 1990-2010: a systematic analysis for the Global Burden of Disease Study 2010. *Lancet* 2012; 380(9859):2163-2196.
- [4] Dagenais S, et al. A systematic review of low back pain cost of illness studies in the United States and internationally. *Spine J* 2008; 8(1):8-20.
- [5] Druss BG, et al. The most expensive medical conditions in America. *Health Aff* 2002; 21(4):105-111.
- [6] Luo X, et al. Estimates and patterns of direct health care expenditures among individuals with back pain in the United States. *Spine* 2004; 29(1):79-86.
- [7] Ricci JA, et al. Back pain exacerbations and lost productive time costs in United States workers. *Spine* 2006; 31(26):3052-3060.
- [8] Rizzo JA, et al. The labor productivity effects of chronic backache in the United States. *Med Care* 1998; 1471-1488.
- [9] Luoma K, et al. Low back pain in relation to lumbar disc degeneration. *Spine*, 2000; 25(4):487-492.
- [10] Molinos M, et al. Inflammation in intervertebral disc degeneration and regeneration. *J Royal Soc Interface* 2015; 12(104):20141191.
- [11] Urban J & Roberts S. Degeneration of the intervertebral disc. *Arthritis Res Ther* 2003; 5(3):120-138.
- [12] Wheeler SG, et al. Evaluation of low back pain in adults. Atlas SJ (Ed), *UpToDate* 2017. Retrieved August 31, 2017, from <https://www.uptodate.com/contents/evaluation-of-low-back-pain-in-adults>.

- [13] Raj PP. Intervertebral disc: anatomy-physiology-pathophysiology-treatment. *Pain Pract* 2008; 8(1):18-44.
- [14] Roberts S, et al. Histology and pathology of the human intervertebral disc. *J Bone Joint Surg Am* 2006; 88 Suppl 2:10-14.
- [15] Haefeli M, et al. The course of macroscopic degeneration in the human lumbar intervertebral disc. *Spine* 2006; 31(14):1522-1531.
- [16] Buckwalter JA. Aging and degeneration of the human intervertebral disc. *Spine* 1995; 20(11):1307-1314.
- [17] García-Cosamalón J, et al. Intervertebral disc, sensory nerves and neurotrophins: who is who in discogenic pain? *J Anat* 2010; 217(1):1-15.
- [18] Aoki Y, et al. Disc inflammation potentially promotes axonal regeneration of dorsal root ganglion neurons innervating lumbar intervertebral disc in rats. *Spine* 2004; 29(23):2621-2626.
- [19] Wallach D, et al. How are the regulators regulated? The search for mechanisms that impose specificity on induction of cell death and NF-kappaB activation by members of the TNF/NGF receptor family. *Arthritis Res* 2002; 4(Suppl 3):S189-S196.
- [20] Zhou XF, et al. Satellite-cell-derived nerve growth factor and neurotrophin-3 are involved in noradrenergic sprouting in the dorsal root ganglia following peripheral nerve injury in the rat. *Eur J Neurosci* 1999; 11(5):1711-1722.
- [21] Bogduk N, et al. The nerve supply to the human lumbar intervertebral discs. *J Anat* 1981; 132(Pt 1):39-56.
- [22] Fagan A, et al. ISSLS prize winner: the innervation of the intervertebral disc: a quantitative analysis. *Spine* 2003; 28(23):2570-2576.
- [23] Johnson WE, et al. Immunohistochemical detection of Schwann cells in innervated and vascularized human intervertebral discs. *Spine* 2001; 26(23):2550-2557.
- [24] Luschka H. Die nerven des menschlichen Wirbelkanals. *Laupp* 1850.
- [25] Roberts S, et al. Mechanoreceptors in Intervertebral Discs: Morphology, Distribution, and Neuropeptides. *Spine* 1995; 20(24):2645-2651.

- [26] Paxinos G (Ed). The rat nervous system. *Academic press* 2014.
- [27] Nakamura S-i, et al. Origin of nerves supplying the posterior portion of lumbar intervertebral discs in rats. *Spine* 1996; 21(8):917-924.
- [28] Fagan A, et al. ISSLS prize winner: The innervation of the intervertebral disc: a quantitative analysis. *Spine* 2003; 28(23):2570-2576.
- [29] Cavanaugh JM, et al. Innervation of the rabbit lumbar intervertebral disc and posterior longitudinal ligament. *Spine* 1995; 20(19):2080-2085.
- [30] Kojima Y, et al. Nerve supply to the posterior longitudinal ligament and the intervertebral disc of the rat vertebral column as studied by acetylcholinesterase histochemistry. I. Distribution in the lumbar region. *J Anat* 1990; 169:237.
- [31] Moneta G, et al. Reported Pain During Lumbar Discography As a Function of Anular Ruptures and Disc Degeneration: A Re-analysis of 833 Discograms. *Spine* 1994; 19(17):1968-1974.
- [32] Greene EC. Anatomy of the Rat. *Am J Med Sci* 1936; 191(6):858.
- [33] Morinaga T, et al. Sensory innervation to the anterior portion of lumbar intervertebral disc. *Spine* 1996; 21(16):1848-1851.
- [34] Ohtori S, et al. Sensory innervation of the dorsal portion of the lumbar intervertebral disc in rats. *Spine* 1999; 24(22):2295.
- [35] Aoki Y, et al. Sensory innervation of the lateral portion of the lumbar intervertebral disc in rats. *Spine J* 2004; 4(3):275-280.
- [36] Aoki Y, et al. Distribution and immunocytochemical characterization of dorsal root ganglion neurons innervating the lumbar intervertebral disc in rats: a review. *Life Sci* 2004; 74(21):2627-2642.
- [37] Bear MF, Connors BW, Paradiso MA (Eds). Neuroscience. Vol. 2. *Lippincott Williams & Wilkins* 2007.
- [38] Snider WD & McMahon SB. Tackling pain at the source: new ideas about nociceptors. *Neuron* 1998; 20(4):629-632.

- [39] Averill S, et al. Immunocytochemical localization of trkA receptors in chemically identified subgroups of adult rat sensory neurons. *Eur J Neurosci* 1995; 7(7):1484-1494.
- [40] Silverman J & Kruger L. Selective neuronal glycoconjugate expression in sensory and autonomic ganglia: relation of lectin reactivity to peptide and enzyme markers. *J Neurocytol* 1990; 19(5):789-801.
- [41] Molliver D, et al. IB4-binding DRG neurons switch from NGF to GDNF dependence in early postnatal life. *Neuron* 1997; 19(4):849-861.
- [42] Ohtori S, et al. Existence of brain-derived neurotrophic factor and vanilloid receptor subtype 1 immunoreactive sensory DRG neurons innervating L5/6 intervertebral discs in rats. *J Orthop Sci* 2003; 8(1):84-87.
- [43] Averbek B, et al. Inflammatory mediators release calcitonin gene-related peptide from dorsal root ganglion neurons of the rat. *Neuroscience* 2000; 98(1):135-140.
- [44] Hayashi Y, et al. Direct single injection of p38 mitogen-activated protein kinase inhibitor does not affect calcitonin gene-related peptide expression in dorsal root ganglion neurons innervating punctured discs in rats. *Spine* 2009; 34(26):2843-2847.
- [45] Molliver DC, et al. Presence or absence of TrkA protein distinguishes subsets of small sensory neurons with unique cytochemical characteristics and dorsal horn projections. *J Comp Neurol* 1995; 361(3):404-416.
- [46] Malmberg AB, et al. Preserved acute pain and reduced neuropathic pain in mice lacking PKC γ . *Science* 1997; 278(5336):279-283.
- [47] Aoki Y, et al. Innervation of the lumbar intervertebral disc by nerve growth factor-dependent neurons related to inflammatory pain. *Spine* 2004; 29(10):1077-1081.
- [48] Ozawa T, et al. The dorsal portion of the lumbar intervertebral disc is innervated primarily by small peptide-containing dorsal root ganglion neurons in rats. *Neurosci Lett* 2003; 344(1):65-67.
- [49] Stucky CL & Lewin GR. Isolectin B4-positive and-negative nociceptors are functionally distinct. *J Neurosci* 1999; 19(15):6497-6505.
- [50] Matsuda Y, et al. Tetrodotoxin sensitivity and Ca component of action potentials of mouse dorsal root ganglion cells cultured in vitro. *Brain Res* 1978; 154(1):69-82.

- [51] Segond von Banchet G, et al. Acute and long-term effects of IL-6 on cultured dorsal root ganglion neurones from adult rat. *J Neurochem* 2005; 94(1):238-248.
- [52] Valtcheva MV, et al. Protein kinase C δ mediates histamine-evoked itch and responses in pruriceptors. *Mol Pain* 2015; 11(1):1.
- [53] Egeland NG, et al. Spinal nociceptive hyperexcitability induced by experimental disc herniation is associated with enhanced local expression of Csf1 and FasL. *Pain* 2013; 154(9):1743-1748.
- [54] Cuellar JM, et al. Application of nucleus pulposus to L5 dorsal root ganglion in rats enhances nociceptive dorsal horn neuronal windup. *J Neurophysiol* 2005; 94(1):35-48.
- [55] Boos N, et al. Classification of age-related changes in lumbar intervertebral discs: 2002 Volvo Award in basic science. *Spine* 2002; 27(23):2631-2644.
- [56] Bernick S, et al. Age changes to the annulus fibrosus in human intervertebral discs. *Spine* 1991; 16(5):520-524.
- [57] Trout JJ, et al. Ultrastructure of the human intervertebral disc: II. Cells of the nucleus pulposus. *Anat Rec* 1982; 204(4):307-314.
- [58] McNally DS, et al. In vivo stress measurement can predict pain on discography. *Spine* 1996; 21(22):2580-2587.
- [59] Maroudas A. Biophysical chemistry of cartilaginous tissues with special reference to solute and fluid transport. *Biorheology* 1975; 12(3-4):233.
- [60] Johnson WE, et al. Human intervertebral disc aggrecan inhibits nerve growth in vitro. *Arthritis Rheum* 2002; 46(10):2658-2664.
- [61] Melrose J, et al. Increased nerve and blood vessel ingrowth associated with proteoglycan depletion in an ovine annular lesion model of experimental disc degeneration. *Spine* 2002; 27(12):1278-1285.
- [62] Freemont A, et al. Nerve ingrowth into diseased intervertebral disc in chronic back pain. *Lancet* 1997; 350(9072):178-181.

- [63] Weiler C, et al. Expression and distribution of tumor necrosis factor alpha in human lumbar intervertebral discs: a study in surgical specimen and autopsy controls. *Spine* 2005; 30(1):44-53.
- [64] Burke J, et al. Intervertebral discs which cause low back pain secrete high levels of proinflammatory mediators. *J Bone Joint Surg Br* 2002; 84(2):196-201.
- [65] Takahashi H, et al. Inflammatory cytokines in the herniated disc of the lumbar spine. *Spine* 1996; 21(2):218-224.
- [66] Ahn S-H, et al. mRNA expression of cytokines and chemokines in herniated lumbar intervertebral discs. *Spine* 2002; 27(9):911-917.
- [67] Lee S, et al. Comparison of growth factor and cytokine expression in patients with degenerated disc disease and herniated nucleus pulposus. *Clin Biochem* 2009; 42(15):1504-1511.
- [68] Le Maitre CL, et al. Catabolic cytokine expression in degenerate and herniated human intervertebral discs: IL-1beta and TNFalpha expression profile. *Arthritis Res Ther* 2007; 9(4):R77.
- [69] Shamji MF, et al. Proinflammatory cytokine expression profile in degenerated and herniated human intervertebral disc tissues. *Arthritis Rheum* 2010; 62(7):1974-1982.
- [70] Heumann R, et al. Differential regulation of mRNA encoding nerve growth factor and its receptor in rat sciatic nerve during development, degeneration, and regeneration: role of macrophages. *Proc Natl Acad Sci* 1987; 84(23), 8735-8739.
- [71] Safieh-Garabedian B, et al. Contribution of interleukin-1 β to the inflammation-induced increase in nerve growth factor levels and inflammatory hyperalgesia. *Br J Pharmacol* 1995; 115(7):1265-1275.
- [72] Woolf C, et al. Cytokines, nerve growth factor and inflammatory hyperalgesia: the contribution of tumour necrosis factor α . *Br J Pharmacol* 1997; 121(3):417-424.
- [73] Abe Y, et al. Proinflammatory cytokines stimulate the expression of nerve growth factor by human intervertebral disc cells. *Spine* 2007; 32(6):635.

- [74] Richardson SM, et al. Increased expression of matrix metalloproteinase-10, nerve growth factor and substance P in the painful degenerate intervertebral disc. *Arthritis Res Ther* 2009; 11(4):1-8.
- [75] Miyagi M, et al. Disk injury in rats produces persistent increases in pain-related neuropeptides in dorsal root ganglia and spinal cord glia but only transient increases in inflammatory mediators: pathomechanism of chronic diskogenic low back pain. *Spine* 2011; 36(26):2260-2266.
- [76] Woolf C, et al. Nerve growth factor contributes to the generation of inflammatory sensory hypersensitivity. *Neuroscience* 1994; 62(2):327-331.
- [77] Pezet S, et al. Differential regulation of NGF receptors in primary sensory neurons by adjuvant-induced arthritis in the rat. *Pain* 2001; 90(1):113-125.
- [78] Dmitrieva N & McMahon SB. Sensitisation of visceral afferents by nerve growth factor in the adult rat. *Pain* 1996; 66(1):87-97.
- [79] Shu X & Mendell LM. Nerve growth factor acutely sensitizes the response of adult rat sensory neurons to capsaicin. *Neurosci Lett* 1999; 274(3):159-162.
- [80] Priestley J, et al. Regulation of nociceptive neurons by nerve growth factor and glial cell line derived neurotrophic factor. *Can J Physiol Pharmacol* 2002; 80(5):495-505.
- [81] Segal RA. Selectivity in neurotrophin signaling: theme and variations. *Ann Rev Neurosci* 2003; 26(1):299-330.
- [82] Diamond J, et al. Endogenous NGF and nerve impulses regulate the collateral sprouting of sensory axons in the skin of the adult rat. *J Neurosci* 1992; 12(4):1454-1466.
- [83] Chung K, et al. Sympathetic sprouting in the dorsal root ganglia of the injured peripheral nerve in a rat neuropathic pain model. *J Comp Neurol* 1996; 376(2):241-252.
- [84] Freemont A, et al. Nerve growth factor expression and innervation of the painful intervertebral disc. *J Pathol* 2002; 197(3):286-292.
- [85] Lever IJ, et al. Brain-derived neurotrophic factor is released in the dorsal horn by distinctive patterns of afferent fiber stimulation. *J Neurosci* 2001; 21(12):4469-4477.

- [86] Walker SM, et al. Release of immunoreactive brain-derived neurotrophic factor in the spinal cord of the rat following sciatic nerve transection. *Brain Res* 2001; 899(1):240-247.
- [87] Salio C, et al. Costorage of BDNF and neuropeptides within individual dense-core vesicles in central and peripheral neurons. *Dev Neurobiol* 2007; 67(3):326-338.
- [88] Mannion R, et al. Neurotrophins: peripherally and centrally acting modulators of tactile stimulus-induced inflammatory pain hypersensitivity. *Proc Natl Acad Sci* 1999; 96(16):9385-9390.
- [89] Bennett GJ. Are the complex regional pain syndromes due to neurogenic inflammation? *Neurology* 2001; 57(12):2161-2162.
- [90] Pezet S & McMahon SB. Neurotrophins: mediators and modulators of pain. *Annu Rev Neurosci* 2006; 29:507-538.
- [91] Merighi A, et al. BDNF as a pain modulator. *Prog Neurobiol* 2008; 85(3):297-317.
- [92] Purmessur D, et al. Expression and regulation of neurotrophins in the nondegenerate and degenerate human intervertebral disc. *Arthritis Res Ther* 2008; 10(4):1-9.
- [93] Skene JP & Willard M. Axonally transported proteins associated with axon growth in rabbit central and peripheral nervous systems. *J Cell Biol* 1981; 89(1):96-103.
- [94] Benowitz LI & Routtenberg A. A membrane phosphoprotein associated with neural development, axonal regeneration, phospholipid metabolism, and synaptic plasticity. *Trends Neurosci* 1987; 10(12):527-532.
- [95] Skene JP. Axonal growth-associated proteins. *Annu Rev Neurosci* 1989; 2(1):127-156.
- [96] Edgar M & Ghadially J. Innervation of the lumbar spine. *Clin Orthop Relat Res* 1976; 115:35-41.
- [97] Coppes MH, et al. Innervation of "painful" lumbar discs. *Spine* 1997; 22(20):2342-2349.

- [98] Aoki Y, et al. Axonal growth potential of lumbar dorsal root ganglion neurons in an organ culture system: response of nerve growth factor-sensitive neurons to neuronal injury and an inflammatory cytokine. *Spine* 2007; 32(8):857-863.
- [99] Costello KE, et al. Locomotor activity and gait in aged mice deficient for type IX collagen. *J Appl Physiol* 2010; 109(1):211-218.
- [100] Millecamps M, et al. Lumbar intervertebral disc degeneration associated with axial and radiating low back pain in ageing SPARC-null mice. *Pain* 2012; 153(6):1167-1179.
- [101] Olmarker K. Puncture of a lumbar intervertebral disc induces changes in spontaneous pain behavior: an experimental study in rats. *Spine* 2008; 33(8):850-855.
- [102] Lai A, et al. Assessment of functional and behavioral changes sensitive to painful disc degeneration. *J Orthop Res* 2015; 33(5):755-764.
- [103] Kim JS, et al. The rat intervertebral disk degeneration pain model: relationships between biological and structural alterations and pain. *Arthritis Res Ther* 2011; 13(5):R165.
- [104] Kiester DP, et al. The dose-related effect of intradiscal chymopapain on rabbit intervertebral discs. *Spine* 1994; 19(7):747-751.
- [105] Sanders GP, et al. Identifying the Early Effects of Mechanical Loading on the Lumbar Spine Using a Novel In Vivo Animal Model. *Spine J* 2010; 10(9):S75-S76.
- [106] Osti OL, et al. 1990 Volvo Award in Experimental Studies: Anulus Tears and Intervertebral Disc Degeneration: An Experimental Study Using an Animal Model. *Spine* 1990; 15(8):762-767.
- [107] Oehme D, et al. Radiological, morphological, histological and biochemical changes of lumbar discs in an animal model of disc degeneration suitable for evaluating the potential regenerative capacity of novel biological agents. *J Tissue Sci Eng* 2015; 6(2):1.
- [108] Hoogendoorn R, et al. Molecular changes in the degenerated goat intervertebral disc. *Spine* 2008; 33(16):1714-1721.
- [109] Zhang Y, et al. Histological features of the degenerating intervertebral disc in a goat disc-injury model. *Spine* 2011; 36(19):1519.

- [110] Nuckley DJ, et al. Intervertebral disc degeneration in a naturally occurring primate model: radiographic and biomechanical evidence. *J Orthop Res* 2008; 26(9):1283-1288.
- [111] Stern W, et al. Effects of collagenase upon the intervertebral disc in monkeys. *J Neurosurg* 1976; 44(1):32-44.
- [112] Daly C, et al. A review of animal models of intervertebral disc degeneration: pathophysiology, regeneration, and translation to the clinic. *BioMed Res Int* 2016.
- [113] Lotz JC. Animal models of intervertebral disc degeneration: lessons learned. *Spine* 2004; 29(23):2742-2750.
- [114] Horii M, et al. Direct application of the tumor necrosis factor- α inhibitor, etanercept, into a punctured intervertebral disc decreases calcitonin gene-related peptide expression in rat dorsal root ganglion neurons. *Spine* 2011; 36(2):E80-E85.
- [115] Rousseau MAA, et al. Stab incision for inducing intervertebral disc degeneration in the rat. *Spine* 2007; 32(1):17-24.
- [116] Takahashi Y, et al. Capsaicin applied to rat lumbar intervertebral disc causes extravasation in the groin skin: a possible mechanism of referred pain of the intervertebral disc. *Neurosci Lett* 1993; 161(1):1-3.
- [117] Takahashi Y, et al. Neural connection between the ventral portion of the lumbar intervertebral disc and the groin skin. *J Neurosurg* 1996; 85(2):323-328.
- [118] Takahashi Y, et al. Regional correspondence between the ventral portion of the lumbar intervertebral disc and the groin mediated by a spinal reflex: a possible basis of discogenic referred pain. *Spine* 1998; 23(17): 1853-1858.
- [119] Ohtori S, et al. Sensory innervation of the dorsal portion of the lumbar intervertebral disc in rats. *Spine* 1999; 24(22):2295.
- [120] Ohtori S, et al. Substance P and calcitonin gene-related peptide immunoreactive sensory DRG neurons innervating the lumbar intervertebral discs in rats. *Ann Anat* 2002; 184(3):235-240.
- [121] Takahashi Y, et al. Dorsoventral organization of sensory nerves in the lumbar spine as indicated by double labeling of dorsal root ganglion neurons. *J Orthop Sci* 2010; 15(4):578-583.

- [122] Aoki Y, et al. Expression and co-expression of VR1, CGRP, and IB4-binding glycoprotein in dorsal root ganglion neurons in rats: differences between the disc afferents and the cutaneous afferents. *Spine* 2005; 30(13):1496-1500.
- [123] Onda A, et al. Nerve growth factor content in dorsal root ganglion as related to changes in pain behavior in a rat model of experimental lumbar disc herniation. *Spine* 2005; 30(2):188-193.
- [124] Murata Y, et al. Distribution and appearance of tumor necrosis factor- α in the dorsal root ganglion exposed to experimental disc herniation in rats. *Spine* 2004; 29(20):2235-2241.
- [125] Murata Y, et al. Effects of selective tumor necrosis factor-alpha inhibition to pain-behavioral changes caused by nucleus pulposus-induced damage to the spinal nerve in rats. *Neurosci Lett* 2005; 382(1):148-152.
- [126] Onda A, et al. Infliximab attenuates immunoreactivity of brain-derived neurotrophic factor in a rat model of herniated nucleus pulposus. *Spine* 2004; 29(17):1857-1861.
- [127] Li D, et al. Lumbar intervertebral disc puncture under C-arm fluoroscopy: a new rat model of lumbar intervertebral disc degeneration. *Exp Anim Tokyo* 2014; 63(2):227-234.
- [128] Stevenson GW, et al. Targeting pain-suppressed behaviors in preclinical assays of pain and analgesia: effects of morphine on acetic acid-suppressed feeding in C57BL/6J mice. *J Pain* 2006; 7(6):408-416.
- [129] Matson DJ, et al. Inflammation-induced reduction of spontaneous activity by adjuvant: A novel model to study the effect of analgesics in rats. *J Pharmacol Exp Ther* 2007; 320(1):194-201.
- [130] Andrews N, et al. Novel, nonreflex tests detect analgesic action in rodents at clinically relevant concentrations. *Ann N Y Acad Sci* 2011; 1245(1):11-13.
- [131] Rice ASC, et al. Animal models and the prediction of efficacy in clinical trials of analgesic drugs: a critical appraisal and call for uniform reporting standards. *Pain* 2008; 139(2):243-247.

- [132] Mogil JS. Animal models of pain: progress and challenges. *Nature Rev Neurosci* 2009; 10(4).
- [133] Peng MT, et al. Changes in running-wheel activity, eating and drinking and their day/night distributions throughout the life span of the rat. *J Gerontol* 1980; 35(3):339-347.
- [134] Haskell-Luevano C, et al. Voluntary exercise prevents the obese and diabetic metabolic syndrome of the melanocortin-4 receptor knockout mouse. *FASEB J* 2009; 23(2):642-655.
- [135] Novak CM, et al. The use of a running wheel to measure activity in rodents: relationship to energy balance, general activity, and reward. *Neurosci Biobehav Rev* 2012; 36(3):1001-1014.
- [136] Tappe-Theodor A & Kuner R. Studying ongoing and spontaneous pain in rodents—challenges and opportunities. *Eur J Neurosci* 2014; 39(11):1881-1890.
- [137] Rutten K, et al. Burrowing as a non-reflex behavioural readout for analgesic action in a rat model of sub-chronic knee joint inflammation. *Eur J Pain* 2014; 18(2):204-212.
- [138] Deacon RMJ. Burrowing: a sensitive behavioural assay, tested in five species of laboratory rodents. *Behav Brain Res* 2009; 200(1):128-133.
- [139] Andrews N, et al. Spontaneous burrowing behaviour in the rat is reduced by peripheral nerve injury or inflammation associated pain. *Eur J Pain* 2012; 16(4):485-495.
- [140] Lalonde R, et al. Spatial learning, exploration, anxiety, and motor coordination in female APP23 transgenic mice with the Swedish mutation. *Brain Res* 2002; 956:36-44.
- [141] Allen KD, et al. Kinematic and dynamic gait compensations in a rat model of lumbar radiculopathy and the effects of tumor necrosis factor-alpha antagonism. *Arthritis Res Ther* 2011; 13(4):R137.
- [142] Allen KD, et al. Decreased physical function and increased pain sensitivity in mice deficient for type IX collagen. *Arthritis Rheum* 2009; 60(9):2684-2693.
- [143] Farasyn A & Meeusen R. The influence of non-specific low back pain on pressure pain thresholds and disability. *Eur J Pain* 2005; 9(4):375-375.

- [144] Adams MA, et al. Healing of a painful intervertebral disc should not be confused with reversing disc degeneration: implications for physical therapies for discogenic back pain. *Clin Biomech* 2010; 25(10):961-971.
- [145] Crawley JN. What's wrong with my mouse?: behavioral phenotyping of transgenic and knockout mice. *Wiley-Liss*, New York, NY 2009.
- [146] Scholz J, et al. A novel tool for the assessment of pain: validation in low back pain. *PLoS Med* 2009; 6(4):e1000047.
- [147] Kim JS, et al. Development of an Experimental Animal Model for Lower Back Pain by Percutaneous Injury-Induced Lumbar Facet Joint Osteoarthritis. *J Cell Physiol* 2015; 230(11):2837-2847.
- [148] Porsolt RD, et al. Behavioural despair in rats: a new model sensitive to antidepressant treatments. *Eur J Pharmacol* 1978; 47(4):379-391.
- [149] Carli MC, et al. Effect of 5-HT 1A agonists on stress-induced deficit in open field locomotor activity of rats: evidence that this model identifies anxiolytic-like activity. *Neuropharmacology* 1989; 28(5):471-476.
- [150] Parent AJ, et al. Increased anxiety-like behaviors in rats experiencing chronic inflammatory pain. *Behav Brain Res* 2012; 229(1):160-167.
- [151] United States National Health Survey. Limitation of Activity Due to Chronic Conditions. *US Department of Health, Education, and Welfare* 1974; 10(111): DHEW Publication No. (H RA) 77-1537.
- [152] Fordyce W, et al. Pain complaint-exercise performance relationship in chronic pain. *Pain* 1981; 10(3):311-321.
- [153] Ek CJ, et al. Spatio-temporal progression of grey and white matter damage following contusion injury in rat spinal cord. *PLoS One* 2010; 5(8):e12021.
- [154] Mixter WJ, et al. Rupture of the intervertebral disk with involvement of the spinal canal. *New Engl J Med* 1934; 211:210-215.
- [155] de Souza Grava AL, et al. Cytokine inhibition and time-related influence of inflammatory stimuli on the hyperalgesia induced by the nucleus pulposus. *Eur Spine J* 2012; 21(3):537-545.

- [156] Shamji MF, et al. Gait abnormalities and inflammatory cytokines in an autologous nucleus pulposus model of radiculopathy. *Spine* 2009; 34(7):648.
- [157] Hwang PY, et al. Changes in midbrain pain receptor expression, gait and behavioral sensitivity in a rat model of radiculopathy. *Open Orthop J* 2012; 6:383.
- [158] Egeland NG, et al. Spinal nociceptive hyperexcitability induced by experimental disc herniation is associated with enhanced local expression of Csf1 and FasL. *Pain* 2013; 154(9):1743-1748.
- [159] Bibel M, et al. Biochemical and functional interactions between the neurotrophin receptors trk and p75 NTR. *EMBO J* 1999; 18(3):616-622.
- [160] Bhawe G, et al. Protein kinase C phosphorylation sensitizes but does not activate the capsaicin receptor transient receptor potential vanilloid 1 (TRPV1). *Proc Natl Acad Sci* 2003; 100(21):12480-12485.
- [161] Bhawe G, et al. cAMP-dependent protein kinase regulates desensitization of the capsaicin receptor (VR1) by direct phosphorylation. *Neuron* 2002; 35(4):721-731.
- [162] Mohapatra DP & Nau C. Desensitization of capsaicin-activated currents in the vanilloid receptor TRPV1 is decreased by the cyclic AMP-dependent protein kinase pathway. *J Biol Chem* 2003; 278(50):50080-50090.
- [163] Bonnington JK & McNaughton PA. Signalling pathways involved in the sensitisation of mouse nociceptive neurones by nerve growth factor. *J Physiol* 2003; 551(2):433-446.
- [164] Zhuang ZY, et al. Phosphatidylinositol 3-kinase activates ERK in primary sensory neurons and mediates inflammatory heat hyperalgesia through TRPV1 sensitization. *J Neurosci* 2004; 24(38):8300-8309.
- [165] Zhang X, et al. NGF rapidly increases membrane expression of TRPV1 heat-gated ion channels. *EMBO J* 2005; 24(24):4211-4223.
- [166] Puntambekar P, et al. Essential role of Rac1/NADPH oxidase in nerve growth factor induction of TRPV1 expression. *J Neurochem* 2005; 95(6):1689-1703.
- [167] Prescott ED & Julius D. A modular PIP2 binding site as a determinant of capsaicin receptor sensitivity. *Science* 2003; 300(5623):1284-1288.

- [168] Langhofer M, et al. The matrix secreted by 804G cells contains laminin-related components that participate in hemidesmosome assembly in vitro. *J Cell Sci* 1993; 105(3):753-764.
- [169] Oh SB, et al. Chemokines and glycoprotein120 produce pain hypersensitivity by directly exciting primary nociceptive neurons. *J Neurosci* 2001; 21(14):5027-5035.
- [170] Thompson JP, et al. Preliminary evaluation of a scheme for grading the gross morphology of the human intervertebral disc. *Spine* 1990; 15(5):411-415.
- [171] Elliott DM, et al. The effect of relative needle diameter in puncture and sham injection animal models of degeneration. *Spine* 2008; 33(6):588-596.
- [172] Gries NC, et al. Early histologic changes in lower lumbar discs and facet joints and their correlation. *Eur Spine J* 2000; 9(1):23-29.
- [173] Kettler A & Wilke HJ. Review of existing grading systems for cervical or lumbar disc and facet joint degeneration. *Eur Spine J* 2006; 15(6):705-718.
- [174] Tam V, et al. A comparison of intravenous and intradiscal delivery of multipotential stem cells on the healing of injured intervertebral disk. *J Orthop Res* 2014; 32(6):819-825.
- [175] Sugiura A, et al. Existence of nerve growth factor receptors, tyrosine kinase a and p75 neurotrophin receptors in intervertebral discs and on dorsal root ganglion neurons innervating intervertebral discs in rats. *Spine* 2008; 33(19):2047-2051.
- [176] Obata K, et al. Suppression of the p75 neurotrophin receptor in uninjured sensory neurons reduces neuropathic pain after nerve injury. *J Neurosci* 2006; 26(46):11974-11986.
- [177] Smith GD, et al. TRPV3 is a temperature-sensitive vanilloid receptor-like protein. *Nature* 2002; 418(6894):186-191.
- [178] Facer P, et al. Differential expression of the capsaicin receptor TRPV1 and related novel receptors TRPV3, TRPV4 and TRPM8 in normal human tissues and changes in traumatic and diabetic neuropathy. *BMC Neurol* 2007; 7(1):11.
- [179] Anand P. Neurotrophic factors and their receptors in human sensory neuropathies. *Prog Brain Res* 2004; 146:477-492.

- [180] Bär KJ, et al. GDNF and its receptor component Ret in injured human nerves and dorsal root ganglia. *Neuroreport* 1998; 9(1):43-47.
- [181] Anand U, et al. The effect of neurotrophic factors on morphology, TRPV1 expression and capsaicin responses of cultured human DRG sensory neurons. *Neurosci Lett* 2006; 399(1):51-56.
- [182] Horký M, et al. Nucleolus and apoptosis. *Ann N Y Acad Sci* 2002; 973(1):258-264.
- [183] Pannese E. Investigations on the ultrastructural changes of the spinal ganglion neurons in the course of axon regeneration and cell hypertrophy. I. Changes during axonal regeneration. *Z Zellforsch Mikrosk Anat* 1963; 61(4):561-586.
- [184] Skulachev VP, et al. Thread-grain transition of mitochondrial reticulum as a step of mitoptosis and apoptosis. *Molec Cell Biochem* 2004; 256(1):341-358.
- [185] Kalinichenko SG & Matveeva NY. Morphological characteristics of apoptosis and its significance in neurogenesis. *Neurosci Behav Physiol* 2008; 38(4), 333-344.
- [186] Pannese E. Investigations on the ultrastructural changes of the spinal ganglion neurons in the course of axon regeneration and cell hypertrophy. II. Changes during cell hypertrophy and comparison between the ultrastructure of nerve cells of the same type under different functional conditions. *Z Zellforsch Mikrosk Anat* 1963; 61:561-586.
- [187] Diamond J, et al. Evidence that endogenous beta nerve growth factor is responsible for the collateral sprouting, but not the regeneration, of nociceptive axons in adult rats. *Proc Natl Acad Sci* 1987; 84(18):6596-6600.
- [188] Li S, et al. The transcriptional landscape of dorsal root ganglia after sciatic nerve transection. *Sci Rep* 2015; 5.
- [189] Bullock CM, et al. Peripheral Calcitonin Gene-Related Peptide Receptor Activation and Mechanical Sensitization of the Joint in Rat Models of Osteoarthritis Pain. *Arthritis Rheumatol* 2014; 66(8):2188-2200.
- [190] Ramsey PH. Critical values for Spearman's rank order correlation. *J Educ Behav Stat* 1989; 14(3):245-253.
- [191] Preibisch S, et al. Globally optimal stitching of tiled 3D microscopic image acquisitions. *Bioinformatics* 2009; 25(11):1463-1465.

- [192] Ridler TW & Calvard S. Picture thresholding using an iterative selection method. *IEEE Trans SMC* 1978; 8:630-632.
- [193] Huang LK & Wang MJJ. Image thresholding by minimizing the measures of fuzziness. *Pattern Recognit* 1995; 28(1):41-51.
- [194] Janicak CA. Applied statistics in occupational safety and health. Government Institutes; 2007; 125-126.
- [195] Gallaher ZR, et al. Neural proliferation in the dorsal root ganglia of the adult rat following capsaicin-induced neuronal death. *J Comp Neurol* 2014; 522(14):3295-3307.
- [196] Muratori L, et al. Generation of new neurons in dorsal root ganglia in adult rats after peripheral nerve crush injury. *Neural Plast* 2015.
- [197] Steers WD, et al. Nerve growth factor in the urinary bladder of the adult regulates neuronal form and function. *J Clin Investig* 1991; 88(5):1709.
- [198] Williams TH, et al. Hypertrophy of rat sensory ganglion neurons following intestinal obstruction. *Gastroenterology* 1993; 105(1):8-14.
- [199] Chan CLH, et al. Sensory fibres expressing capsaicin receptor TRPV1 in patients with rectal hypersensitivity and faecal urgency. *Lancet* 2003, 361(9355):385-391.
- [200] Yiangou Y, et al. ATP-gated ion channel P2X3 is increased in human inflammatory bowel disease. *Neurogastroenterol Motil* 2001; 13(4):365-369.
- [201] Tympanidis P, et al. Increased vanilloid receptor VR1 innervation in vulvodynia. *Eur J Pain* 2004; 8(2):129-133.
- [202] Numazaki M, et al. Direct phosphorylation of capsaicin receptor VR1 by protein kinase C ϵ and identification of two target serine residues. *J Biol Chem* 2002; 277(16):13375-13378.
- [203] Geuna S, et al. Morphological and morphometrical changes in dorsal root ganglion neurons innervating the regenerated lizard tail. *Int J Dev Neurosci* 1998; 16(2):85-95.
- [204] Ekman EF, et al. Efficacy and safety of intravenous tanezumab for the symptomatic treatment of osteoarthritis: 2 randomized controlled trials versus naproxen. *J Rheumatol* 2014; jrheum-131294.

[205] Benowitz LI & Routtenberg A. GAP-43: an intrinsic determinant of neuronal development and plasticity. *Trends Neurosci* 1997; 20(2):84-91.

[206] Denny JB. Molecular mechanisms, biological actions, and neuropharmacology of the growth-associated protein GAP-43. *Curr Neuropharmacol* 2006; 4(4):293-304.

Biography

Elizabeth M. Leimer was born on May 18, 1989 in Wichita, Kansas to Paul M. and Joy M. Leimer. Elizabeth received her Bachelors of Science degree in Biomedical Engineering from Rensselaer Polytechnic Institute (RPI) in May of 2011. Her first research experience was as the undergraduate summer intern in the Orthopaedic Surgery Department at The University of Kansas School of Medicine, where she worked under the mentorship of Terence McIff, PhD and tested scapholunate dissociation fixation methods for arthrodesis. She subsequently joined the Musculoskeletal Mechanics Laboratory under the direction of Eric Ledet, PhD in the Department of Biomedical Engineering at RPI as an undergraduate research assistant. She remained active in this laboratory during her first years in medical school, and through this experience she received her first outstanding poster award. Elizabeth graduated from RPI and attended medical school at Albany Medical College, where she received the Haskell Marsh Scholarship and The Arnold and Olga Pohl Scholarship. She took a leave of absence between her third and fourth years to pursue a PhD under the mentorship of Lori Setton, PhD in the Department of Biomedical Engineering at Duke University. One year after starting her PhD at Duke University, the research laboratory relocated to Washington University in St. Louis, where Elizabeth completed her dissertation research. During her tenure as a PhD candidate, she gave many invited lectures, attended clinical spine workshops, and was nominated for many outstanding podium

and poster presentation awards at both clinical spine and biomedical engineering-related conferences. Additionally, she has been active as a bassoonist in the Durham Medical Orchestra and as a member of the Animal Management and Protocol Systems Steering Committee at Washington University in St. Louis, where she represents the interests of the users on the undergraduate Danforth Campus and in the Department of Biomedical Engineering. Her publications include:

Leimer EM, Elkhayat AI, Gayoso MG, Jing L, Setton LA, Gupta MC. Behavioral and Functional Measures of Chronic Discogenic Pain in a Rodent Model of Intervertebral Disc Degeneration. *The Spine Journal* 2017; 17(10):S126.

Adams SB, **Leimer EM**, Setton LA, Bell RD, Easley ME, Huebner JL, TV Stabler, Kraus VB, Olson SA, Nettles DL. Inflammatory Cytokine Profile in Human Synovial Fluid 6 Months After Intra-Articular Ankle Fracture. *Foot & Ankle International* 2017; 38(5):479-484.

Leimer EM, Pappan KL, Nettles DM, Bell RD, Easley ME, Olson SA, Setton LA, Adams SB. Lipid Signature of Human Synovial Fluid Following Intra-Articular Ankle Fracture. *Journal of Orthopaedic Research* 2017; 35(3):657-666.

Adams SB, Setton LA, Bell RD, Easley ME, Huebner JL, TV Stabler, Kraus VB, **Leimer EM**, Olson SA, Nettles DL. Inflammatory Cytokines and Matrix Metalloproteinases in the Synovial Fluid after Intra-Articular Ankle Fracture. *Foot & Ankle International* 2015; 36(11):1264-1271.

Sanders GP; Linley S; McCallum S; Brule E; Vandeventer E; **Leimer E**; VanEtten B; Colloggi K; Puzas JE; Sowa GA; Lotz JC; Vanderzanden J; Glennon JC; DiRisio DJ; Lawrence JP; Ledet EH. Identifying the Early Effects of Mechanical Loading on the Lumbar Spine Using A Novel *In Vivo* Animal Model. *The Spine Journal* 2010; 10(9S):75S.

Sanders GP; Linley SE; Sowa GA; Glennon JC; DiRisio DJ; Lawrence JP; Vanderzanden J; **Leimer E**; Lotz JC; Ledet EH. *In Vivo* Effects of Cyclic Compression on the Intervertebral Disc and Endplates of the Lumbar Spine: A Pilot Study With a Novel Animal Model. *The Albany Orthopaedic Journal* 2010; 2:48-59.